

Solid bitumen in calcite veins from the Oman Mountains. A structural, microstructural and geochemical study on hydrocarbon migration in the Natih.

Master Thesis Applied Geosciences

by

Reinhard Fink

submitted to the

Faculty of Georesources and Materials Engineering

of RWTH Aachen University

Energy and Mineral Resources Group - Structural Geology, Tectonics, Geomechanics

January 2013

supervised by:

Prof. Dr. Janos L. Urai & Prof. Dr. rer. nat. Ralf Littke

Simon Virgo & Max Arndt

Communicated by Prof. Dr. Janos. L. Urai

RWTH Aachen University

Geologie-Endogene Dynamik

Lochnerstrasse 4-20

52056 Aachen, Germany

Declaration

I hereby declare that I have created this work completely on my own and used no other sources or tools than the ones listed, and that I have marked any citations accordingly.

Hiermit versichere ich, dass ich die vorliegende Masterarbeit selbstständig verfasst habe und keine anderen als die angegebenen Quellen und Hilfsmittel benutzt habe.

Aachen, Datum

Abstract

Fractures are important pathways for hydrocarbon migration in the Earth's crust. This study shows that there was hydrocarbon migration in the Oman mountains, which has not been recognized until now. Solid bitumen in calcite veins from Natih limestone on the southern flank of the Jebel Akhdar Anticline, situated in the Oman Mountains, are remnants of fossil petroleum migration pathways. To understand the role of Natih veins during migration, field work was combined with microscopic analysis including cathodoluminescense, transmitted, and reflected light microscopy. For this purpose, highly polished thin sections were prepared to simultaneously examine solid bitumen in reflected light and its microstructural context in transmitted light.

Straight and en échelon arranged, black impregnated, bedding-normal Natih A calcite veins strike 120° and are cross-cut by all other veins. They contain solid bitumen as small (<10 μm) intracrystal inclusions arranged as trails, high-reflective intracrystal mosaic type particles and angular low reflective particles at pressure solution sites. Solid bitumen formed in multiple events after the first vein growth and was most likely derived from the now highly overmature Natih B source rock. During the first event, intracrystal solid bitumen inclusion trails formed by micro-cracking of the existing vein. Simultaneously or later, mosaic type solid bitumen formed in reactivations. Solid bitumen reflectance (BR_r) of mosaic type solid bitumen (BR_r = 3.40 - 3.76 %) give evidence for high temperatures (T = 317 - 325 °C) which only affect the veins. These temperatures exceed maximum burial temperatures (T = 206 - 238 °C) derived from BR_r measurements of the Natih B source rock.

Formation of low reflective solid bitumen (BR_r = 0.86 - 0.92 %) along pressure solution sites postdates all events. They may be important hydrocarbon migration pathways and may not only affect veins, but the whole Natih sequence.

Contents

1 Introduction **2**

1.1 Motivation and Study Intentions 2

1.2 Geological Setting 3

1.2.1 Stratigraphy 5

1.3 Vein Research in the Jebel Akhdar 7

1.4 Solid bitumen as a Geothermometer 8

1.5 The Natih Petroleum System 9

2 Field Work **11**

2.1 Study Area 11

2.2 Observations 12

2.3 Sampling 24

3 Methodology **26**

3.1 Sample Preparation for Microscopic Study 26

3.1.1 Highly Polished Thin Sections 26

3.1.2 Polished Blocks 27

3.2 Microscopic Study 28

3.2.1 Solid Bitumen Reflectance (BR_r) Measurements 28

3.2.2 Microstructural Analysis 28

3.2.3 Cathodoluminescence Microscopy 30

3.3 Geochemical Study 30

3.3.1 Total Organic Carbon (TOC) Measurements 30

3.3.2 Rock-Eval Pyrolysis 30

3.4 Residual Analysis of Fault Samples with Scanning Electron Microscope (SEM) 31

4 Results **32**

4.1 Microscopic Analysis 32

4.1.1 Solid Bitumen Types under Immersion Oil 32

4.1.2 Microstructural Description 33

4.1.3 Summary of Microscopic Observations 66

4.2 Solid Bitumen Reflectance 70

4.3 Paleaotemperatures 73

4.4 Total Organic Carbon Content 73

4.5 Rock-Eval Pyrolysis 74

4.6 Residual Analysis with Scanning Electron Microscope 76

5 Discussion **78**

5.1 Palaeotemperatures 78

5.2 Model for Vein Development 79

5.3 Faults 82

5.4 Kinematics of Natih A Vein Formation 83

5.5 Palaeotemperatures During Regional Fracture Network Evolution 84

5.6 Natih B Bedding Confined Veins 86

5.7 Hydrocarbon Migration Pathways 86

5.8 Outlook 87

6 Conclusions **89**

Bibliography **91**

List of abbreviations

BSE	*Back-scattered electron*
BR_r	*Bitumen reflectance*
cts	*Counts: number of measuring points*
dol	*Dolomite*
EDX	*Energy dispersive X-ray*
ee(s)	*En échelon set of veins with sinistral sense of shear*
ee(d)	*En échelon set of veins with dextral sense of shear*
fa	*Fault*
HRI	*Host rock inclusion bands*
hr	*Host rock*
low refl.	*Low reflective solid bitumen*
mosaic	*Intracrystal mosaic type solid bitumen*
n_e	*Refraction index of immersion oil*
qz	*Quartz*
SE	*Secondary electron*
SEM	*Scanning electron microscopy*
sc	*Small scale calcite reactivation which is only visible under the microscope*
sig	*Sigmoidal vein*
svA	*Straight vein from Natih A*
svB	*Straight vein from Natih B*
TOC	*Total organic carbon*
trails	*Lined up solid bitumen inclusions*
VR_r	*Vitrinite reflectance*
σ	*Standard deviation*

Chapter 1

Introduction

1.1 Motivation and Study Intentions

The rocks on the southern flank of the Jebel Akhdar anticlinal structure offer world class outcrop conditions to study veins. Usually, these calcite veins are white coloured and form complex networks (fig. 1.1) with a high vein density. At some places, however, there are black impregnated veins. These can be easily overlooked, because they do not show sharp contrasts to the grey carbonates as white veins do. Black impregnated structures were realized in fault calcites by Holland and Urai (2010) and in veins by Virgo (2012) who took a plug from a black impregnated vein in Wadi Ghul during a field trip in 2010. It was found out that the sample contains solid bitumen, which was the start of this Master project.

The presence of solid bitumen as a remnant of oil in veins is an indicator for hydrocarbon migration



Figure 1.1: Calcite vein network from Al Raheba, Jebel Akhdar Anticline in the Oman Mountains. Width is approximately 6 m. Looking down on bedding. North is at the top of the photograph.

which has not been recognised in the Oman Mountains, yet. The Natih formation, where the black impregnated veins were found, is part of a known petroleum system 130 km south which has been

produced by Petroleum Development Oman (PDO) in the Natih and Fahud fields since 1963. Therefore, the black impregnated veins in the Jebel Akhdar might be used as an analogue to understand hydrocarbon migration in northern Oman.

This thesis is a pilot study which should verify the presence of hydrocarbons in structural elements in the Oman Mountains. Therefore, the most fundamental aim of this study is to find, measure the orientation, and describe black impregnated veins and other structures in the field, which are thought to contain solid bitumen. With this, it might be possible to understand, if solid bitumen occurs in a particular vein system, which might give evidence for relative timing of oil migration.

Samples are needed to analyse solid bitumen incorporation at the micro-scale. This can only be done with a combination of different techniques. Therefore, a microscopic method using polarised and reflected light at the same time is used. To achieve this, highly polished thin sections have to be produced (Littke et al., 2012). Polarised light is used for microstructural analysis whereas reflected light is used for the identification of solid bitumen. With this, it is possible to see if solid bitumen is found in distinct microstructures, which may give evidence of migration pathways within the structure and relative timing of oil migration in comparison to the structure.

Solid bitumen reflectance measurements are performed for palaeotemperature estimation. If solid bitumen was incorporated into the vein before maximum temperature, it can be used similar to vitrinite reflectance for maximum temperature determination.

1.2 Geological Setting

The study area is situated at the southern flank of the Jebel Akhdar Anticline in the center of the Oman Mountains (fig. 1.2). They reach over 700 km from the Musandam Peninsula in the north of the Sultanate of Oman to the Batain coast in the southeast. The Jebel Akhdar Anticline is a 70 km wavelength domal structure which is cross-cut by several Wadis. Along these Wadis, especially in Wadi Nakhr, a more than 1 km thick carbonate succession can be studied. These rocks were derived from shelf carbonate platform deposition at a passive margin of the Neo-Thetys Ocean which formed due to the breakup of Gondwana. At this passive continental margin, the mid-Permian to Late Cretaceaous Hajar Unit (Autochthon B) formed (Glennie et al., 1974; Searle, 2007).

At the end of the Cretaceaous, starting in the Cenomonian, intra oceanic, north east directed subduction of the Arabian plate under the European plate started due to the opening of the Atlantic ocean (Glennie et al., 1974). This led to the obduction of the allochthonous Semail ophiolite (fig. 1.3), the Hawasina nappes and Oman exotics (continental margin deep water sediments) from NE to SW, often called the first alpine event. The autochtonos units were metamorphosed from upper anchizone

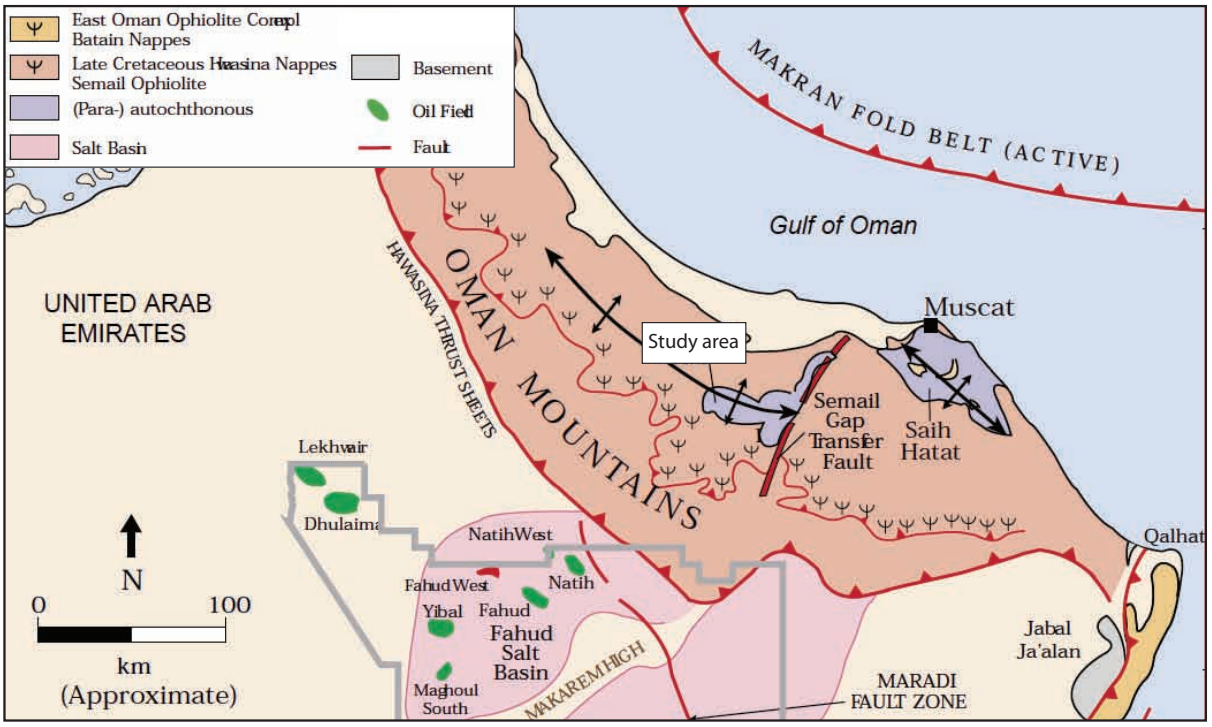


Figure 1.2: Simplified geological map with principal structural elements and location of oil fields in north Oman. The study area is situated at the southern flank of the Jebel Akhdar tectonic window. Modified after Filbrandt et al. (2006).

facies (2-4 kb, <200 ° C) on the southwestern flank of the Jebel Akhdar to eclogite facies in the Saih Hatat tectonic window (Breton et al., 2004).

The ongoing subduction and thrust stacking led to bending of the plate and a peripheral bulge resulting in erosion of the uppermost Natih formation as well as the development of a foredeep basin (Turonian-Santonian) which was filled by carbonaceous breccias of the Muti formation and thick Fiqa shales of the Aruma group. These sediments, which were partly overridden by the allochthonos units, document the migration of the depocenter from north to south due to the obduction. (Breton et al., 2004; Searle, 2007). Moreover, NW-SE tending normal faults in the Natih formation which die out in the Muti could be a result of extensional tectonics during pulling down of the continental plate (Loosveld et al., 1996).

Simultaneously to Semail ophiolite emplacement, the Masirah ophiolite emplacement in eastern Oman which was induced by an oblique collision of the Indian with the Arabian plate, took place. After Filbrandt et al. (2006), this affected the foreland region, so that maximum horizontal stress is NW-SE which contrasts maximum horizontal stress from Semail ophiolite emplacement which is thought to have been NE-SW during Campanian.

Following this, a new subduction zone developed in the north which led to stable conditions with

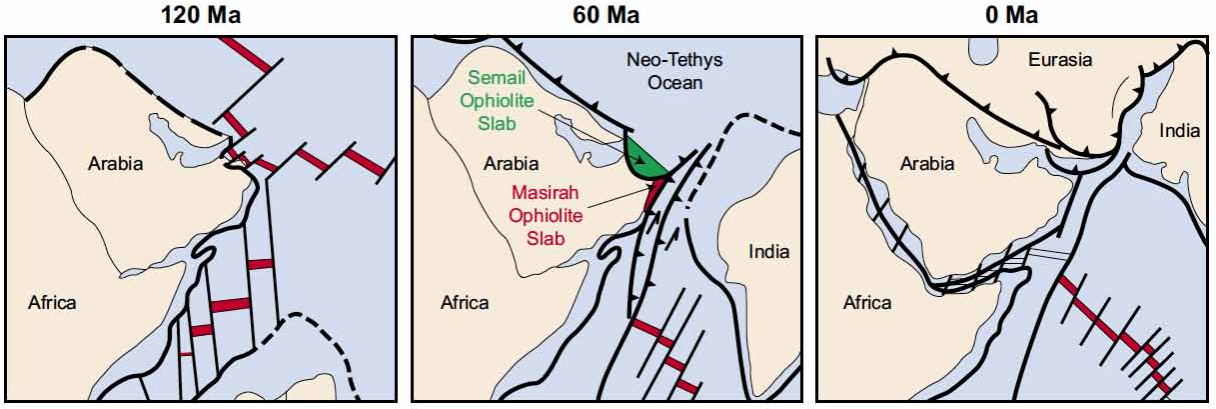


Figure 1.3: Simplified plate tectonic evolution from Early Cretaceous to present-day (Filbrandt et al. (2006) after Loosveld et al. (1996))

uniform shallow marine early Tertiary carbonate deposition (Loosveld et al. (1996)).
Continent-continent collision in the Oligocene at the Zagros, the second alpine event, is thought to have caused the main uplift of the Jebel Akhdar Anticline. This lead to erosion of the overlying allochthonos sequences (Searle, 2007).

1.2.1 Stratigraphy

The studied Natih A and B members shown in figure 1.4 are part of the Permian-Cretaceous Hajar unit (Autochthon B) (Breton et al., 2004). A simplified stratigraphic column of the Hajar unit and

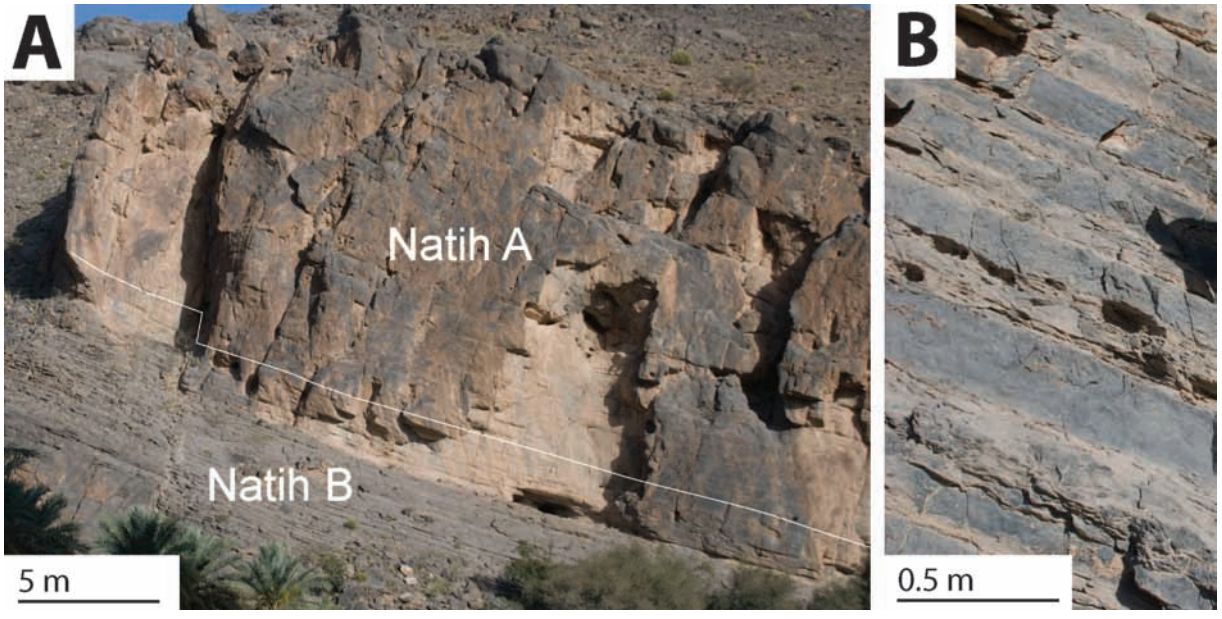


Figure 1.4: Outcrop photograph of Natih A and B at the entrance of Wadi Nakhr. A: Natih A is forming a massive cliff on bedded Natih B. B: Close-up of Natih B layers. Grey layers are more competent and contain oyster shells whereas brown layers are organic rich and shaly.

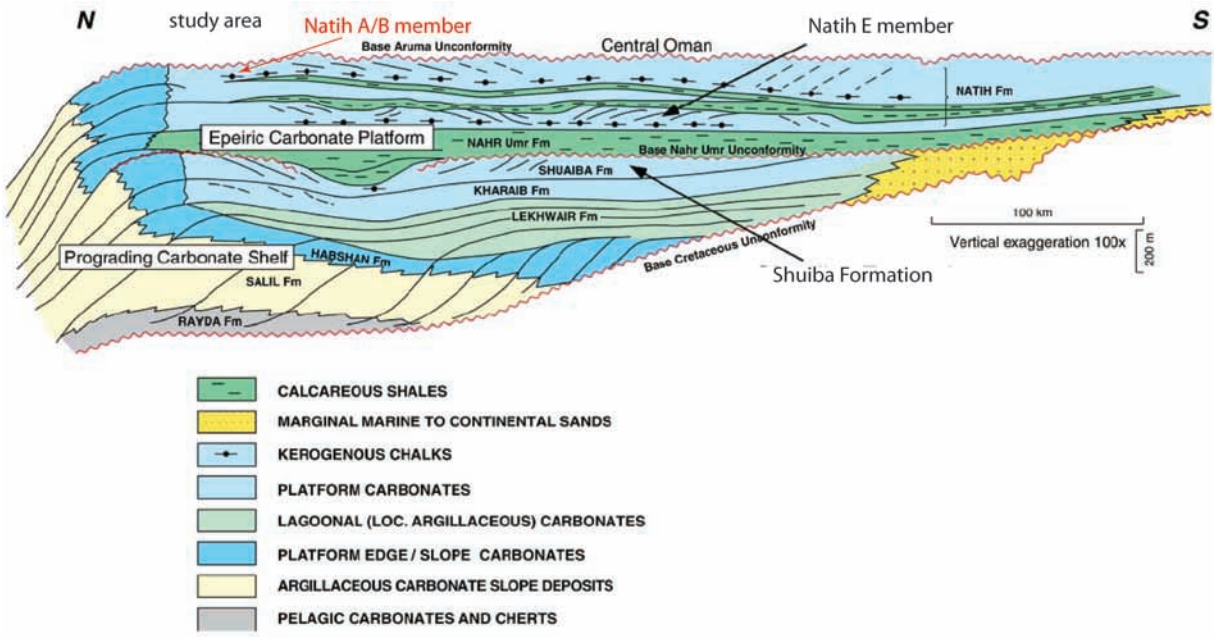


Figure 1.5: Geological cross-section through the North-Oman Cretaceous carbonate platform. Modified after Droste (2010).

overlaying Late Cretaceous and Tertiary sediments are shown in figure 1.6. The late Albian to early Turonian Natih formation has been studied in outcrops on the southern flank of Jebel Akhdar and Adam Foothills by numerous authors (e.g. Homewood et al., 2008). It is part of the Wasia group which is subdivided after Clarke (1988) into seven members from G to A (from oldest to youngest). Authors, e.g. van Buchem et al. (1996), proposed three longterm sequences Natih A/B, Natih C/D and the Natih E member. Between these 3rd order sequences, the depositional environments changed through time between a shallow water broad platform (especially D and C members), and moderately deeper-water intra-shelf basins with anoxic conditions which led to the deposition of source rocks. Due to prograding banks of high-energy intra shelf platform margin sediments, these intra-shelf basins of the Natih E and A-B members became smaller (van Buchem et al., 2002). The Natih forms the top of a Cretaceous carbonate platform system (fig. 1.5) with deposition of source rocks in the Natih B, Natih E and Shuiba formation. Note that during Natih deposition, the Jebel Akhdar region was located at the northern part of the Cretaceous carbonate platform, close to the Thetys-facing platform margin (Grélaud et al., 2006). Natih and shelf carbonate platform deposition ended in Turonian times due to uplift and erosion, the so called Wasia-Aruma break (Robertson, 1987).

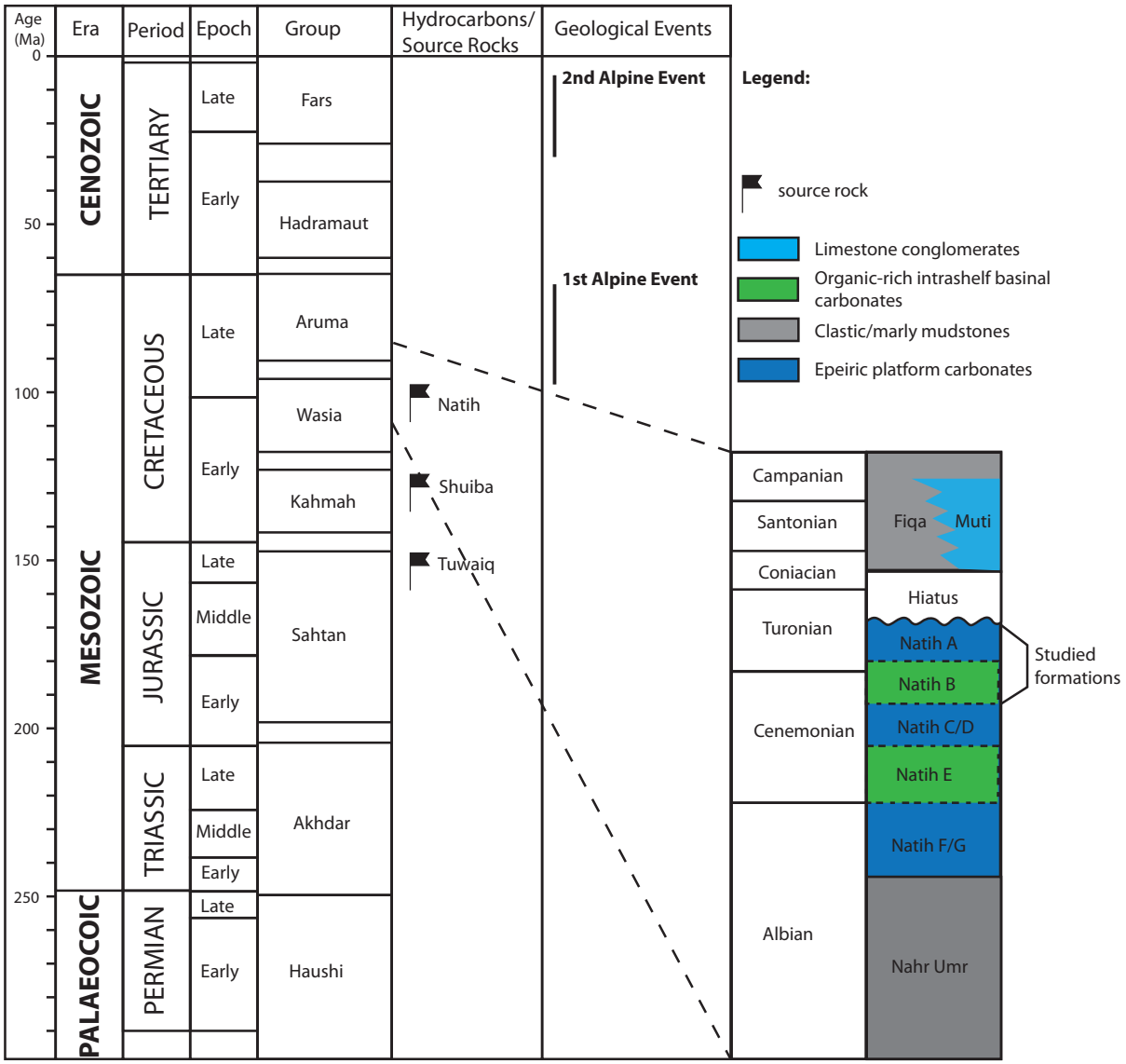


Figure 1.6: Simplified stratigraphic column with a close-up view to the Late Cretaceous. The stratigraphic column was modified after Filbrandt et al. (2006); van Buchem et al. (2002); Terken (1999) and Terken et al. (2001).

1.3 Vein Research in the Jebel Akhdar

Hilgers et al. (2006) first studied veins in the Jebel Akhdar. They identified seven vein and fracture generations in various outcrops on the Jebel Akhdar and their relative timing. The oldest veins are stylolite veins (1) followed by bedding-normal veins (2), pinch-and-swell veins (3), bedding-parallel veins (4), normal faults and associated veins (5 and 6), and thrust veins (7). Generation (2)-(5) formed due to supra-hydrostatic fluid pressure which might have been caused by various processes such as disequilibrium compaction, gas generation or calcite cementation (Hilgers et al., 2006). After the authors, fluid pressure decreased during uplift when normal faults developed which drained the

system, forming a more open system which allowed external fluids to infiltrate the system. This led to precipitation of the youngest vein sets (6) and (7). All veins are filled with quartz and calcite.
Holland et al. (2009b) focused on structures on the southern flank of Jebel Shams. They subdivided the stage (2) bedding-normal veins (Hilgers et al., 2006) into four vein generations which formed due to an anticlockwise rotation of the stress field during burial extension in a high-pressure environment. Calcite cement healed fractures before the next sets were formed. The overpressure was released due to normal faulting accordingly to Hilgers et al. (2006).
Gomez-Riveras et al. (unpuplished) use vein, fault, stylolite and fracture data sets from the southern flank of the Jebel Akhdar to correlate the results with the main tectonic events of the Northeast Arabian plate. The oldest structures consist of diagenetic, layer parallel stylolites and unsystematic veins which formed during subsidence. Obduction of the Semail ophiolite led to top-to-the-South layer-parallel shearing which was followed by seismic- and subseismic-scale, normal (dip-slip) to oblique-slip faults and veins due to crustal loading of the obducted nappes. Exhumation of the autochthonous led to top-to-the-Northeast layer parallel shearing. Gomez-Riveras et al. (unpuplished) show that these events are overprinted by at least three events of strike-slip structures which show an anticlockwise rotation of the principal compressive stress from NW-SE, to E-W and finally to N-S or NE-SW. They correlate this to oblique transpression between Arabia and Indian Plates at the end of the Cretaceous.
Virgo et al. (unpuplished) have collected an extensional structural data set from the dip slope of Jebel Shams to test satellite-based interpretations of structural elements. Their interpretation is consistent with Holland et al. (2009b), except they interpret the anticlockwise rotation of vein strike to start before and end after normal faulting. These WNW-ESE striking faults are the most prominent structures and were rotated together with bedding during folding of the Jebel Akhdar.

1.4 Solid bitumen as a Geothermometer

Palaeotemperatures of a rock can be estimated by various methods. Most important are illite crystallinity, fluid inclusion homogenisation temperatures and vitrinite reflectance, which is widely used as a maturity parameter in sedimentary basin modelling for calibration. However, vitrinites do not occur in Pre-Devonian rocks and are often rare in marine carbonates. If solid bitumen is present in these cases, it can be used instead of vitrinite as a maturity parameter. This has been shown by Jacob (1989) who found a strong correlation between vitrinite reflectance and solid bitumen reflectance:

$$VR_r = 0.618 \cdot BR_r + 0.4 \tag{1.4.1}$$

A similar linear relationship with a larger number of samples in the VRr range of 0.5% - 5% was found by Landis and Castaño (1995) with:

$$VR_r = \frac{BR_r + 0.41}{1.09} \tag{1.4.2}$$

Schoenherr et al. (2007) used a combined dataset from Jacob (1989) and Landis and Castaño (1995) with 82 datapoints. The equation is given by:

$$VR_r = \frac{BRr + 0.2443}{1.0495} \tag{1.4.3}$$

The obtained vitrinite reflectance can then be used to estimate peak temperatures (T_{peak}) as proposed by Barker and Pawlewicz (1994). They subdivided datasets into hydrothermal and burial environments for a more accurate prediction with:

$$T_{peak \quad hydrothermal} = \frac{ln(VR_r) + 1.19}{0.00782} \tag{1.4.4}$$

$$T_{peak \quad burial} = \frac{ln(VR_r) + 1.68}{0.0124} \tag{1.4.5}$$

In general, solid bitumens change their optical characteristics from low to higher reflection during burial due to an increase in aromaticity. Moreover, they can have different optical textures, such as granular, homogeneous or mosaic. Under high temperatures, solid bitumen is becoming more anisotropic and develops into coke-like types with mosaic or flow structure (Hwang et al., 1998; Goodarzi et al., 1992).

1.5 The Natih Petroleum System

The Natih Petroleum System is a small, but extremely efficient petroleum system above the Fahud salt basin, which is located 150 km SW of the study area. Most of the recoverable oils are produced in the giant, fault bound Natih and Fahud fields (for location see fig. 1.2).

The Natih B and E source rocks are Type I/II with TOC values of Natih B up to 15%. A, C/D and E units are the main reservoirs intervalls (Terken, 1999). They form a dual porosity/permeability system with dense fractures crossing the rock matrix. Porosities can be up to 40% due to meteoric water leaching (Terken, 1999). The sequence is overlain by thick sealing Fiqa shales.

Thermal modelling shows that the Natih source rocks in the foreland basin started oil generation 70 ma ago, and have been continually producing until today. The active Natih kitchen is situated north of the Natih and Fahud fields and extends under the Oman mountain frontal thrust which is located 100 km SW of the study area (Terken et al., 2001). Within the study area, the Natih as part of the petroleum system is almost not investigated, because the rocks underwent a different structural,

diagenetic and burial history compared to the rocks in the foreland region. Thermal maturation of the source rocks in the study is assumed to have started earlier induced by the Semail ophiolite obduction, and eased during uplift of the Oman Mountains. Deposition of sealing Fiqa shales has not taken place in the study area. Therefore, the Natih petroleum system, if it extends into the Oman Mountains, works differently compared to the foreland region.

Chapter 2

Field Work

Field work has taken place on the Jebel Akhdar Anticline on the south west flank of the Jebel Shams which is the highest peak in Oman with 3005 m. This area offers exceptional outcrop conditions which is a result of recent arid climate conditions with little vegetation and occasional flash floods. The higher erosion of soft rocks leads to the exposure of more competent beds on the surface. Therefore, the surface mostly consists of the competent Natih A member whereas the Natih B member, especially the soft clay-rich beds, are mainly exposed at wadi walls.
The term "black impregnated" is used in this study to differentiate between structures with white calcite and calcite structures which appear black or, if the impregnation is weaker, grey. Field work focuses on black impregnated structures, which are assumed to contain solid bitumen or other hydrocarbons which may cause the impregnation.

2.1 Study Area

The study area shown in figure 2.1 is located at the southern flank of the Jebel Akhdar Anticline located 20 km northwest of the city Nizwa, Sultanate of Oman. Black impregnated structures were searched at promising places where previous workers had studied Natih veins (Virgo, 2012). The locations of the main outcrops are marked with red dots in figure 2.1. Outcrops where no black impregnated veins within the Natih A member were found are marked with a red cross. At Al Raheba and Wadi Ghul, Natih A is exposed at the surface. At the entrance of Wadi Nakhr Natih A and B are exposed as cliffs at the wadi walls. At Ghul ramps Natih B is exposed at the surface and in small wadis.

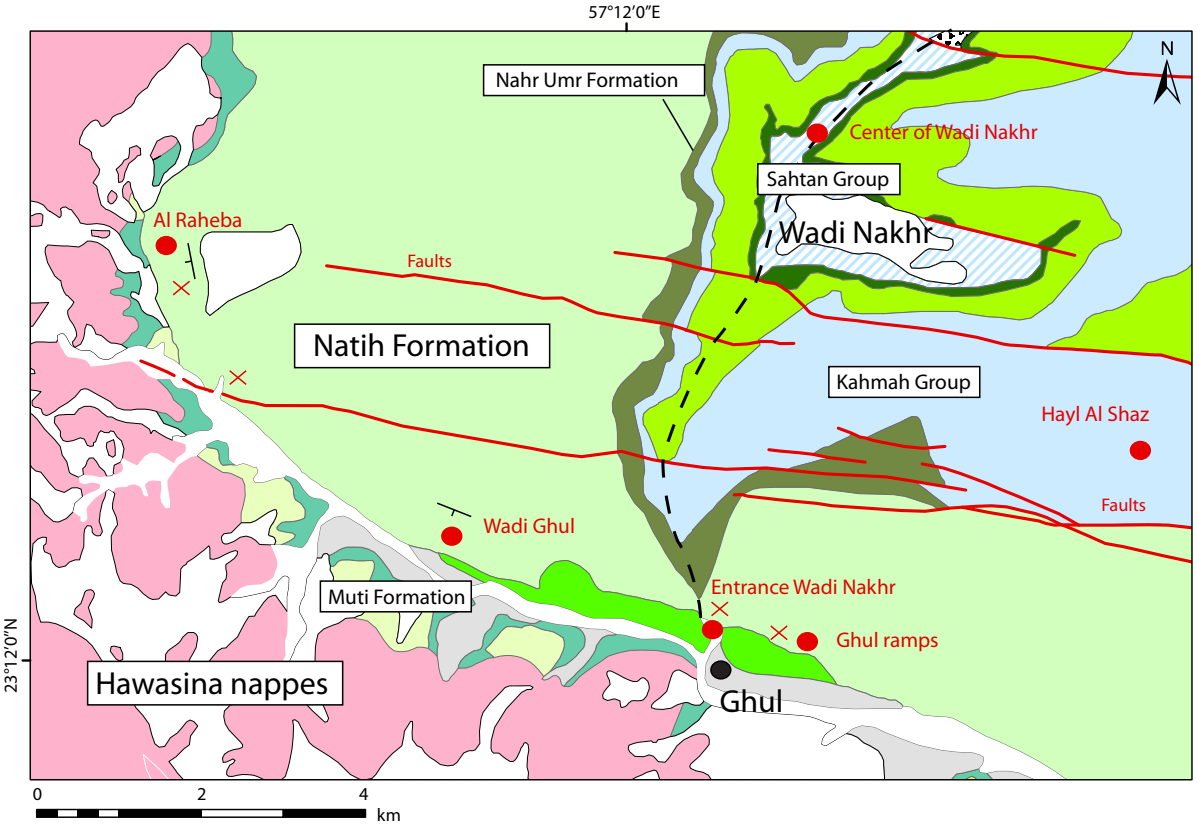


Figure 2.1: Basic geological map of the study area at the southern flank of the Jebel Akhdar Anticline. Main outcrop locations where numerous black impregnated structures within the Natih have been found are Ghul ramps, the entrance of Wadi Nakhr, Wadi Ghul and Al Raheba. At Hayl Al Shaz and the center of Wadi Nakhr, black impregnated faults from other formations were found. From the mentioned locations, structures were sampled, measured and described. Red crosses indicate outcrop locations in Natih A where no black impregnated veins have been found. Modified after Beurrier et al. (1986).

2.2 Observations

Black impregnated structures

Black impregnated structures were searched at numerous promising places and we found four types of black impregnated structures which occur at distinct outcrops:

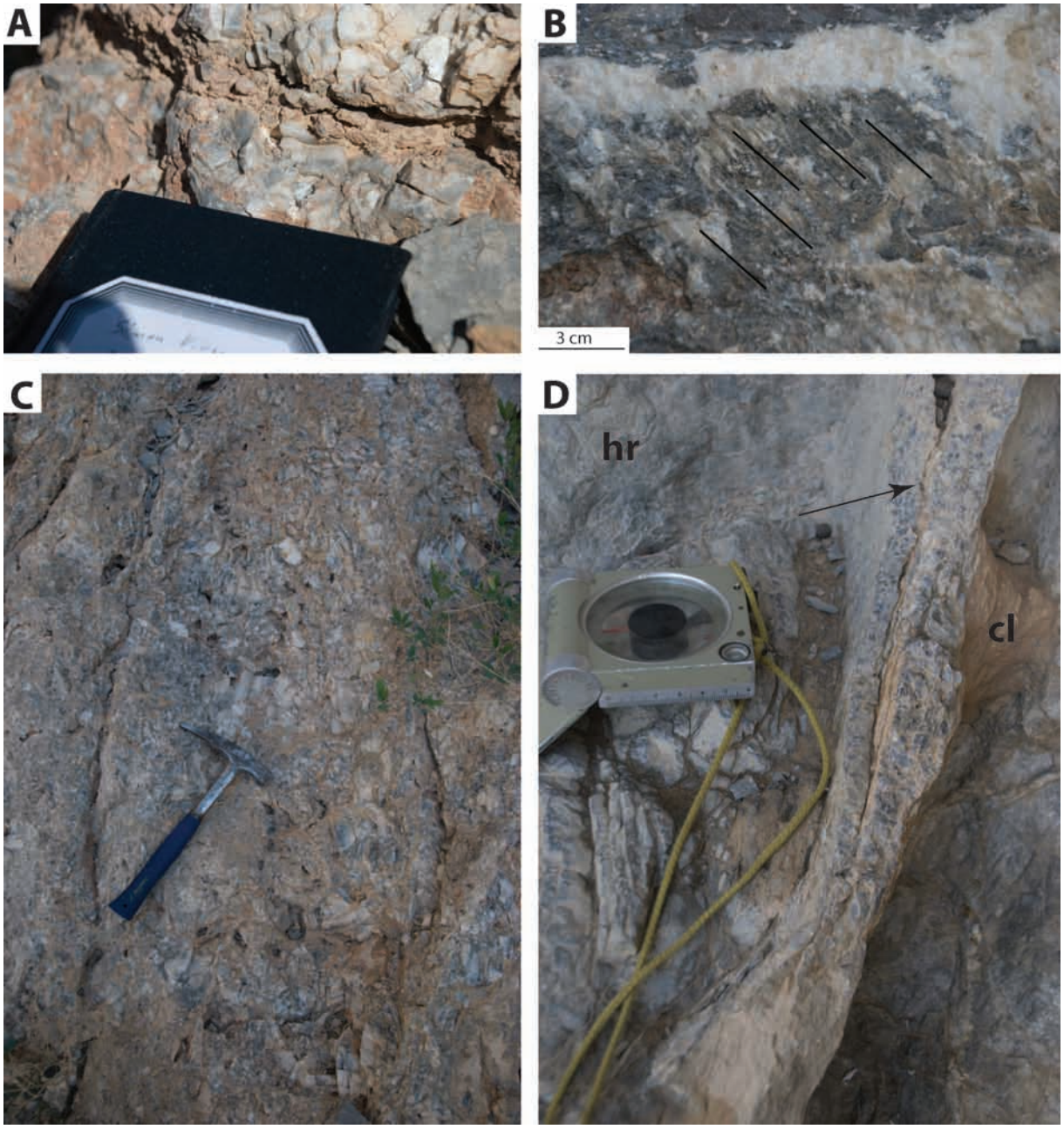
- Faults at the entrance and center of Wadi Nakhr, Ghul ramps and Hayl Al Shaz.
- En échelon arrays of veins in Natih A at Al Raheba and Wadi Ghul.
- Straight veins in Natih A at Al Raheba And Wadi Ghul.
- Veins in Natih B at Ghul ramps.

The characteristics of each black impregnated structural element will be briefly described in the following.

Faults

Black impregnated faults have been found in the center of Wadi Nakhr within the Sahtan group, at Hayl al Shaz within the Kahmah group, at the entrance of Wadi Nakhr and at Ghul ramps within the Natih formation. All of these faults, except at Ghul ramps, are interpreted to be normal faults striking approximately WNW-ESE with high dip angles. They show a complex history with oblique slickensides, some of them indicating strike-slip components (Holland et al., 2009b). The fault at Ghul ramps (orientation 045/15) is a thrust related structure forming a topographic high. Figure 2.2 shows exemplary outcrop photographs of studied faults. All fault cores have a homogeneous grey colour. Close examination of the blocky calcite cementing the cores reveals colour zoning between black, white and grey of individual calcite cleavage rhombohedra. Calcite cleavage rhombohedra within fault cores and branches of faults have sizes up to several centimetres.

Figure 2.2 ***(facing page)*****:** Outcrop photographs of fault structures: ***A*****:** Fault gouge of thrust fault (orientation 045/15) from Ghul ramps. It consists of blocky calcite which shows clear colour zoning between black/grey and white. Cleavage rhombohedra can be >1 cm (book for scale). View is to the north. Sample location of OM12 B16. ***B*****:** Slicken fibres, indicated by black lines (orientation 287/46, linear) from a branch (orientation 022/84) of a fault (orientation 030/80) at the entrance of Wadi Nakhr. The striations show the direction of movement along the fault. Note that there are also striations with different orientation (304/45, 314/65 and 118/05, all linear) which indicate that the direction of movement changed through time. View is to the south. Sample location of OM12 B28. ***C*****:** Fault core of normal fault at the entrance of Wadi Nakhr. The fault core is approximately 1 m in width and consists of blocky calcite which shows clear colour zonations between black/grey and white as in A. The size of the calcite cleavage rhombohedra can be >2 cm. Note that the fault core itself does not show colour zoning. The fault has an vertical offset of approximately 3 m and an orientation of 016/75. Hammer for scale. View is to the east. Sample location of OM12 B06. ***D*****:** Location is 3 m uphill from C. The photograph shows at least two branches of the same fault as C. The branches (orientation 011/70) are cemented with black impregnated blocky calcite (calcite cleavage rhombohedra < 0.5 cm). The branches are separated from the main fault gouge (0.5 m to the right hand side) by a brown coloured band (cl) which is part of the damage zone. To the left hand side the Natih A massive carbonate host rock (hr) shows only minor deformation. Compass is for scale. View is to the east. Sample location of OM12 B07-09.


A
B
3 cm
C
D
hr
cl

En échelon arrays of veins in Natih A

Black impregnated en échelon arrays of veins have been found at Al Raheba and at Wadi Ghul within the Natih A member. Most of the arrays have a sinistral sense of shear. The length of en échelon arrays of veins can reach more than 10 metres with apertures of individual veins up to 10 centimetres. The veins and arrays of veins are oriented $\pm$ normal to bedding. Figure 2.3 shows an en échelon array of black impregnated veins. The veins are cemented by a mixture of black and white calcite crystals. At Al Raheba a sinistral black impregnated en échelon set of veins has been found with a straight black impregnated vein in the center (fig. 2.4).

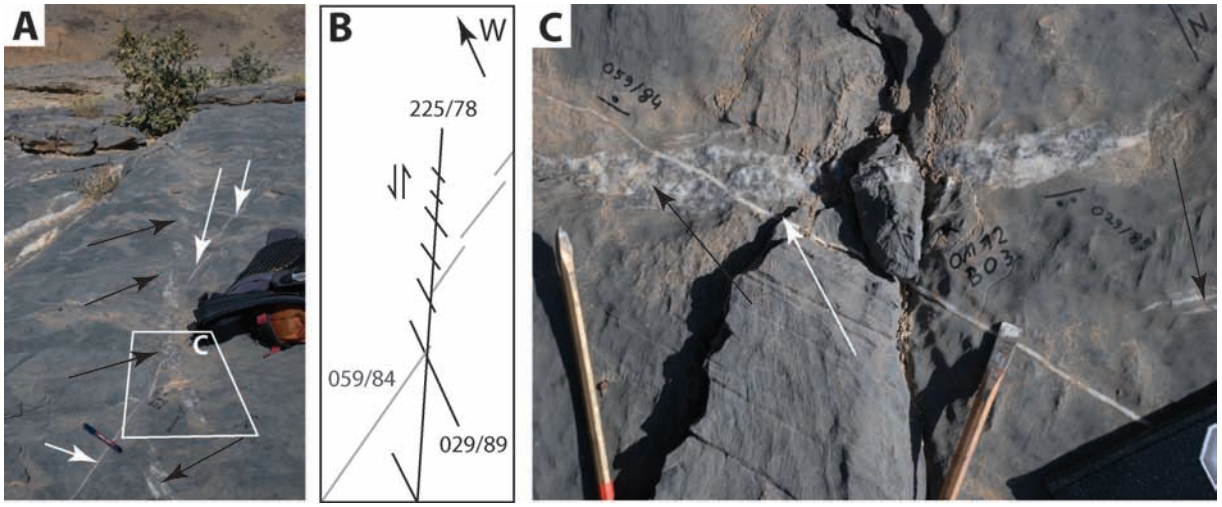


Figure 2.3: ***A*:** Outcrop photograph showing a sinistral, approximately 6 m long en échelon array of black impregnated veins (black arrows) at Al Raheba. The black impregnated veins do overlap each other less than 1 cm and are less than 30 cm in length and 2-3 cm in width. The set is cross-cut by a white vein en échelon array (white arrows). Backpack is for scale and view is to the west. Sample location of OM12 B03. ***B*:** Sketch illustrating main features of photograph A. ***C*:** Detail photograph of the black impregnated vein array (white box in A) showing two black impregnated veins (black arrow) from which one is cross-cut by a white vein (white arrow). The black impregnated vein is cemented by a mixture of black and white calcite which is evenly distributed over the black impregnated vein. Book for scale. View is to the north.

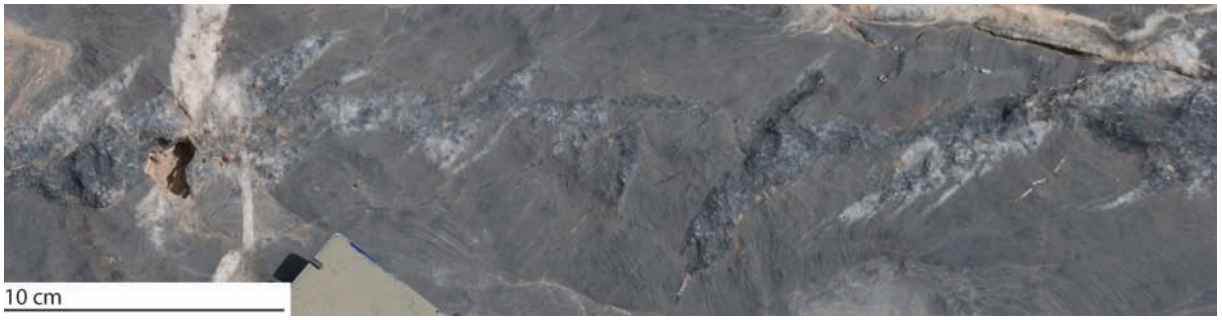


Figure 2.4: Outcrop photograph at Al Raheba showing a sinistral en échelon array of black impregnated veins with a straight black impregnated vein in the centre. View is down to the surface. Top of photograph is to the north east.

Straight veins in Natih A

Straight black impregnated veins within the Natih A member have been found at Al Raheba and Wadi Ghul. Figure 2.6 shows outcrop photographs of straight black impregnated veins at Wadi Ghul. Some consist of a mixture between black and white calcite with a good separation of the components, others have a homogeneous black impregnation. Black impregnated veins run subparallel to each other and are oriented $\pm$ normal to bedding. Many of these veins are reactivated by white calcite, mostly in the centre. Moreover, they have apertures $<$ 1 cm to 10 cm and can be longer than 10 metres. Some straight black impregnated veins have a strike slip component (fig. 2.5).



Figure 2.5: Outcrop photograph showing a straight black impregnated vein (orientation 024/74) displacing two chert nodules horizontally by 2 cm. Aperture is approximately 1-1.5 cm. Sense of shear is sinistral. View is down to the surface. Top of image is to the north. Sample location of OM12 B29.

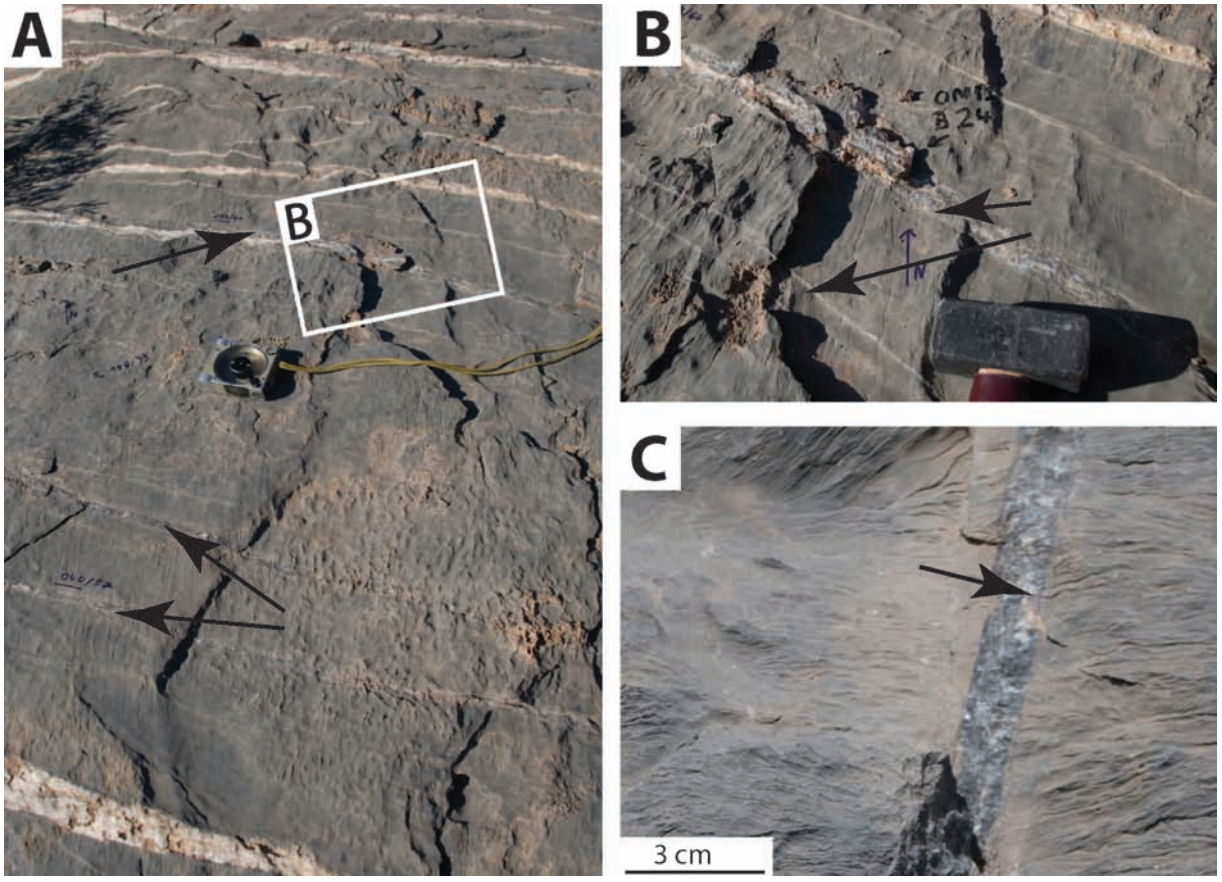


Figure 2.6: ***A*:** Outcrop photograph showing at least four straight black impregnated veins (black arrows) which run parallel. Nearby, there are at least four more. These veins are longer than 2 m and consist of black impregnated calcite or mixed white and black impregnated calcite with a clear separation of the components. Location is Wadi Ghul with view to the north. Compass is for scale. Sample location of OM12 B24. ***B*:** Close-up view (white box in A) of a reactivated vein (orientation 033/65) and a small vein (aperture <0.5 cm). View is to the north, hammer for scale. ***C*:** Detail view of straight black impregnated vein (orientation 028/50) in Wadi Ghul with no reactivation. Aperture is approximately 1.5 cm. View is down to the surface. Top of photograph is to the west. Sample location of OM12 B31.

Veins in Natih B

Black impregnated veins in Natih B have been found between the small village Ghul and Ghul ramps. They usually have an aperture of 1 cm, run subparallel to each other and are up to more than 7 m long. Moreover, some of them cut through multiple layers and have drusy rims with a brown weathering mineral in the interior of the vein (fig. 2.7 A, B). The rims may run further with host rock material filling the center. At the surface of a small Wadi (sample location of OM12 B15), a zone with a sharp material contrast compared to the surrounding rocks has been found (fig. 2.7 C, D). The zone (orientation 346/56) contains vein-like structures forming a network which runs parallel to the zone. The vein-like structure, split have a high sinuosity and change their aperture. They are filled with black impregnated calcite which appears drusy. It is unclear, if the zone is of tectonic, diagenetic or sedimentary origin.

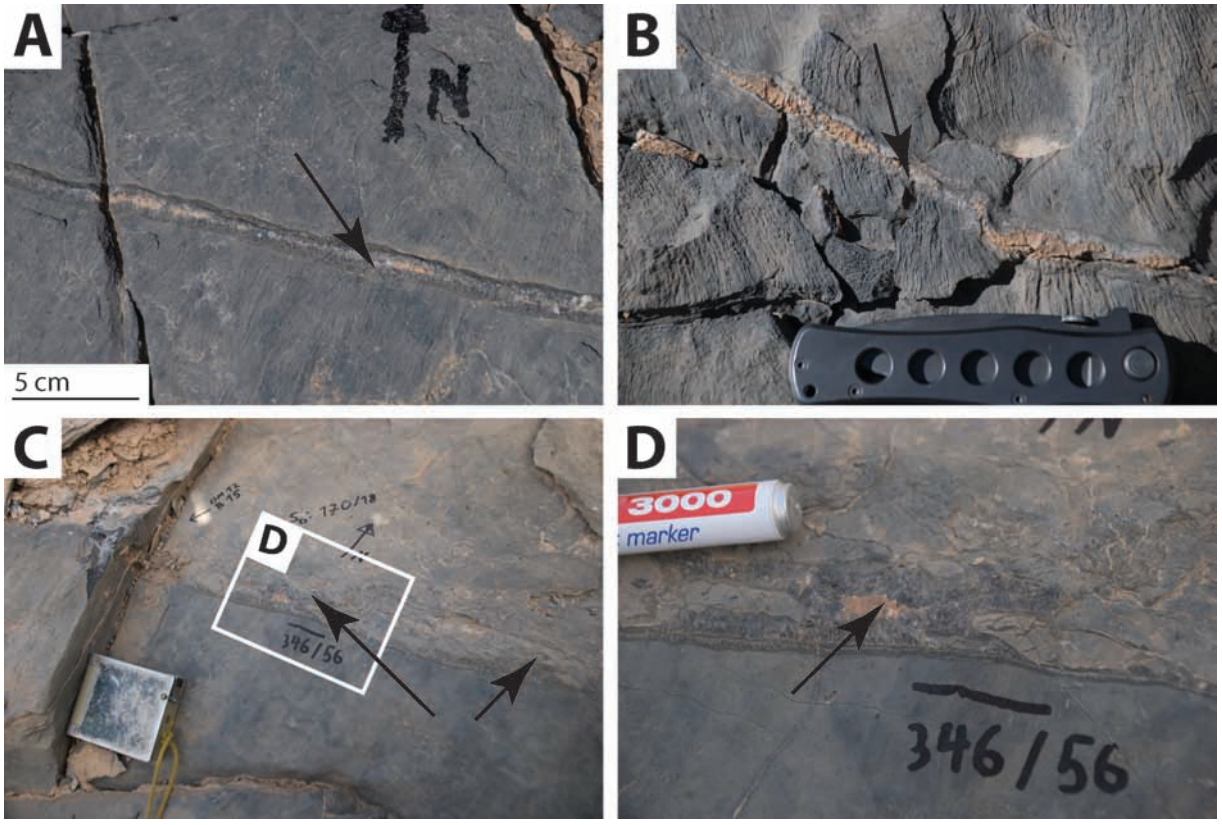


Figure 2.7: Outcrop photographs showing black impregnated veins at Ghul ramps: ***A*:** Straight black impregnated vein (black arrow) with a width of 1 cm (orientation 009/86). The center of the vein has a brown weathering colour whereas the rims consist of black impregnated calcite. Note that the black impregnated rims run further with host rock material filling the center. Looking down on the surface. Sample location of OM12 B17-19. ***B*:** Straight black impregnated vein with rims which split up and reunite several times. At places where the rims split, the vein is filled with a brown weathering mineral. Note that this vein cuts at least five sedimentary layers within the Natih B member (compare fig. 1.4) normal to bedding. View is to the north, knife for scale. Looking down on surface. ***C*:** Zone with material contrast which contains vein-like structures forming a network running parallel to the zone. The vein-like structures (black arrow) split, have a high sinuosity and change their aperture. They are filled with black impregnated calcite which appears drusy. The formation process (e.g. tectonic, diagenetic) of this zone is unclear. Compass for scale. Sample location of OM12 B15. ***D*:** Drusy structure with black impregnated calcite crystals within the zone of image C (white box). Pen is for scale.

Structural field data

The orientation of black impregnated structures and the bedding have been measured where possible. The results are shown in figure 2.8 and 2.9. The bedding is dipping 10-35 ° to the south at Wadi Ghul, the entrance of Wadi Nakhr and Ghul ramps at the southern flank of the anticline. This changes to a westward dipping of the bedding at Al Raheba at the western flank of Jebel Shams.

All data of black impregnated structures is plotted unrotated and backrotated by one rotation in the way that bedding becomes horizontal. This was done for each data point with its corresponding bedding. The results are shown next to each other for each structure type (fig. 2.8 and 2.9).

Sinistral en échelon arrays of black impregnated veins strike 135 °. Dextral en échelon arrays strike 110 °. The corresponding veins strike 100 ° for sinistral shear and 120 ° for dextral shear with a larger scatter of data. Three data points from sinistral veins have different orientations and strike approximately 170 °.

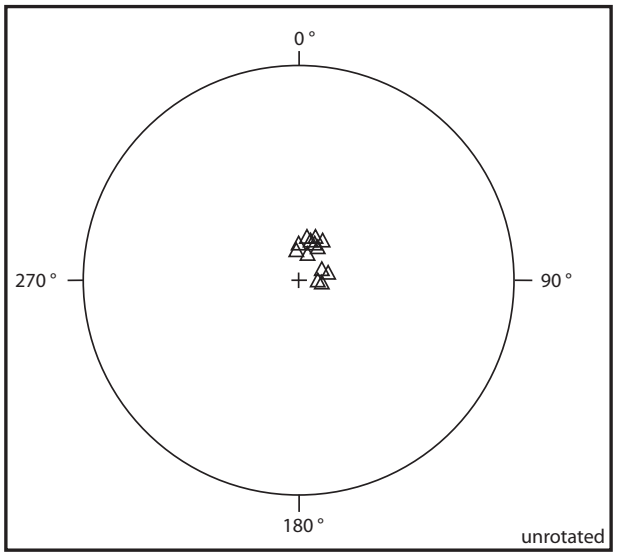
Straight veins in Natih A strike 115 ° with a dipping close to 90 °.

Straight veins in Natih B are lacking data. It was only possible to measure three straight veins which strike roughly 90 ° with a high scatter.

Faults interpreted as normal faults (Holland et al., 2009b) strike 120° with a backrotated dipping close to 90°. All structures have similar orientations with a WNW strike and a dipping close to 90°.

Figure 2.8 ***(facing page)*****:** Structural data (lower hemisphere stereoplots, equal area projection) of bedding poles, en échelon array poles, veins of en échelon array poles and veins from Natih A poles. The stereoplots on the left hand side are backrotated by one rotation in the way that bedding is horizontal, because these structures are thought to have formed when bedding was horizontal.

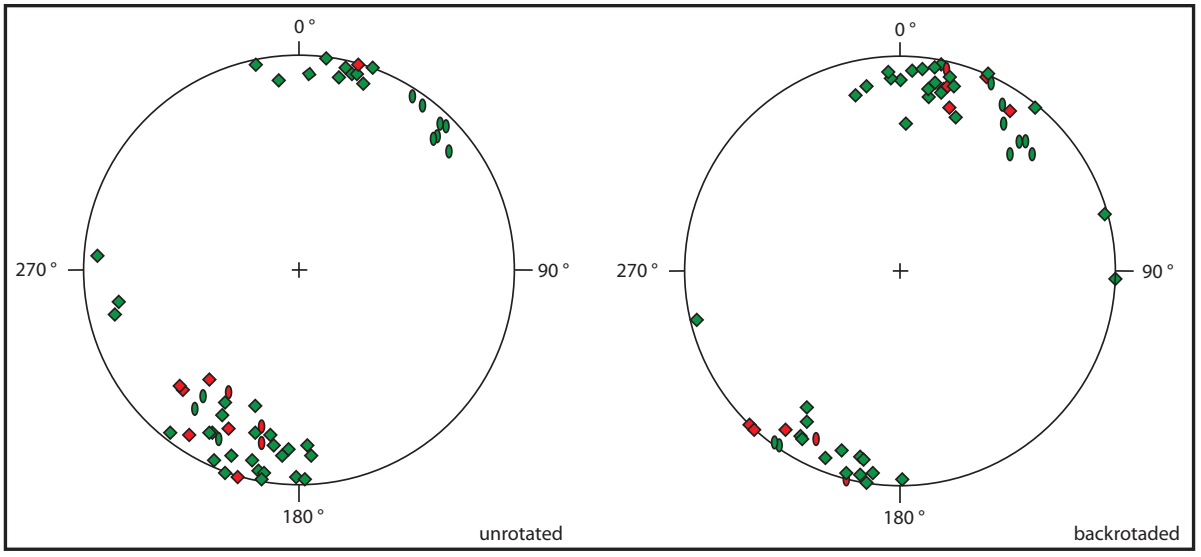
Bedding at Al Raheba, Wadi Nakhr, Wadi Ghul and Ghul ramps



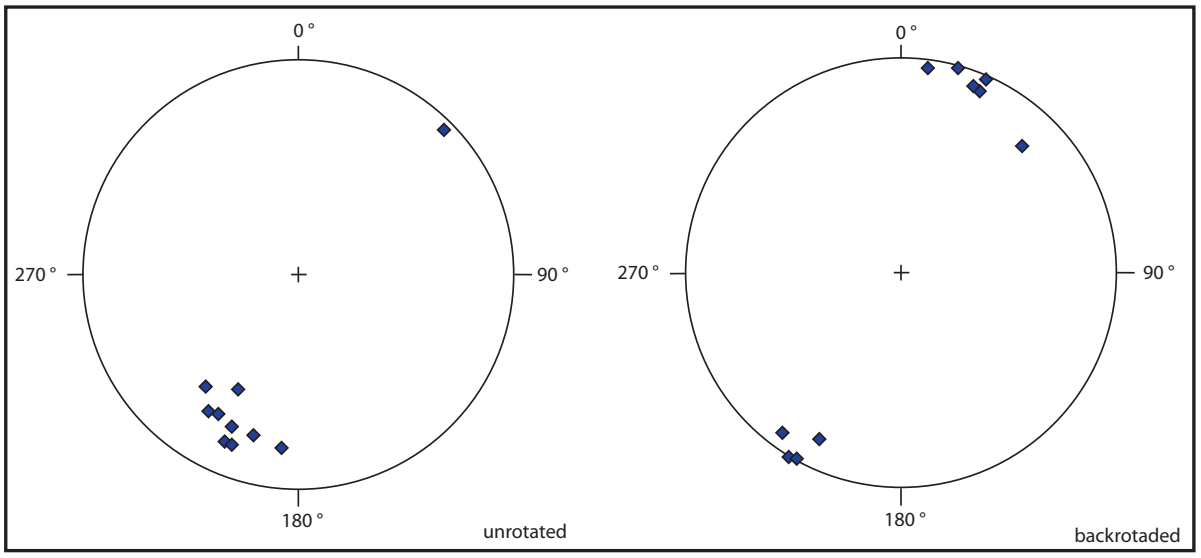
Legend:

- vein of array (sinistral)
- en echelon array (sinistral)
- vein of array (dextral)
- en echelon array (dextral)
- straight vein
- fault
- bedding

En echelon array of black veins at Wadi Ghul and Al Raheba



Straight veins Natih A at Wadi Ghul and Al Raheba



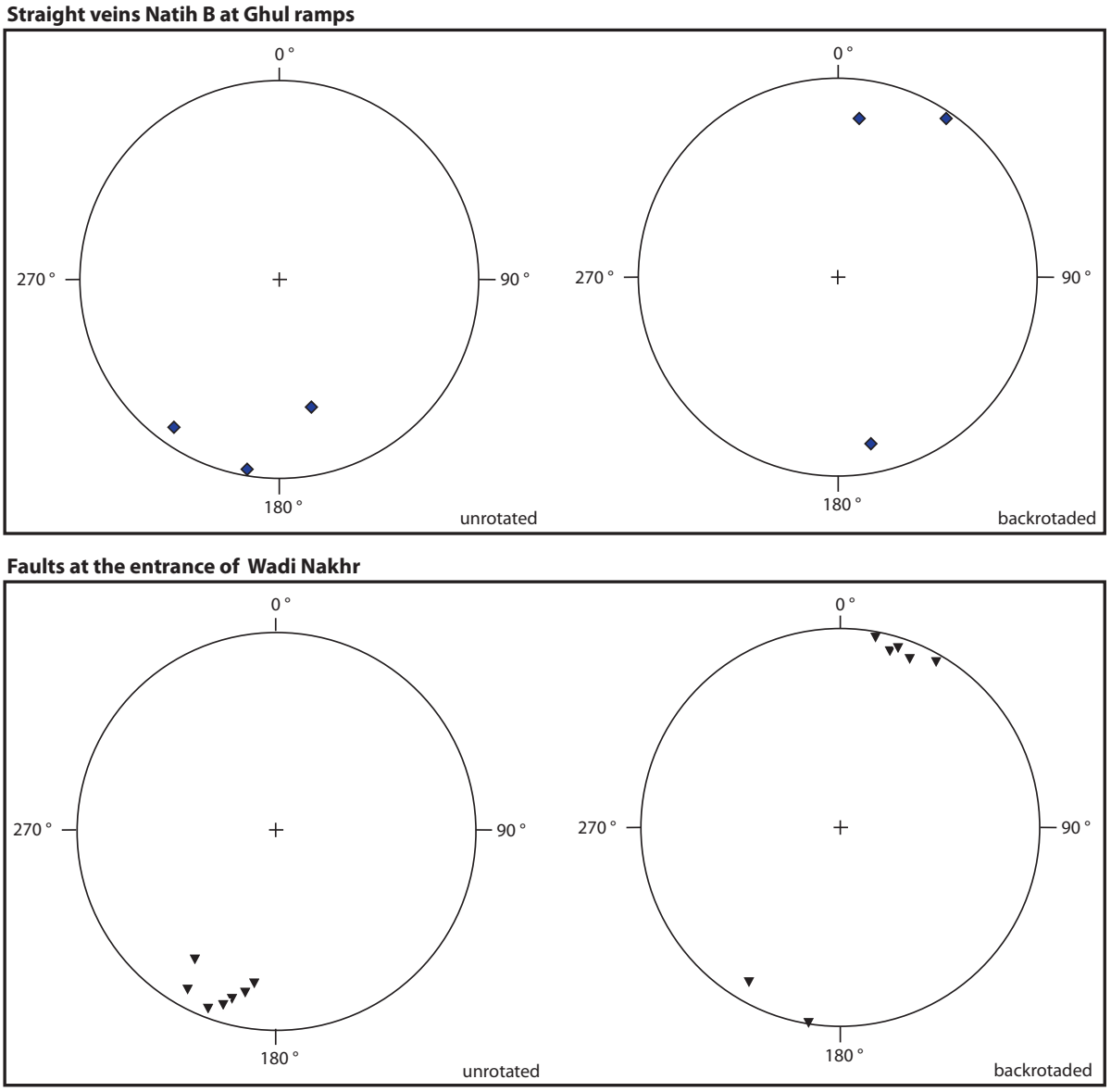


Figure 2.9: Structural data (lower hemisphere stereoplots, equal area projection) of Natih B vein poles and fault poles. The orientation (045/15) of the thrust fault at Ghul ramps is not plotted, because it is a stand-alone structural element and does not belong to the set of normal faults at the entrance of Wadi Nakhr. The stereoplots on the left hand side are backrotated by one rotation in the way that bedding is horizontal. Legend is shown in figure 2.8.

Reactivation and age relationships

Many black impregnated veins from Natih A are reactivated and cross-cut by white veins. Reactivation of black impregnated veins means a reopening and resealing parallel to the pre-existing vein. Fortunately, these are easy to see in the field due to the colour contrast compared to white veins reactivating or cross-cutting white veins. This is used for age relationships, because veins which are cross -cut by other veins have to be older than the cross-cutting veins. These age relationships were marked in the field and on photographs using a simple dot system starting with the youngest vein as indicated in fig. 2.10 A. There is not a single black impregnated vein found to cross-cut a white vein.

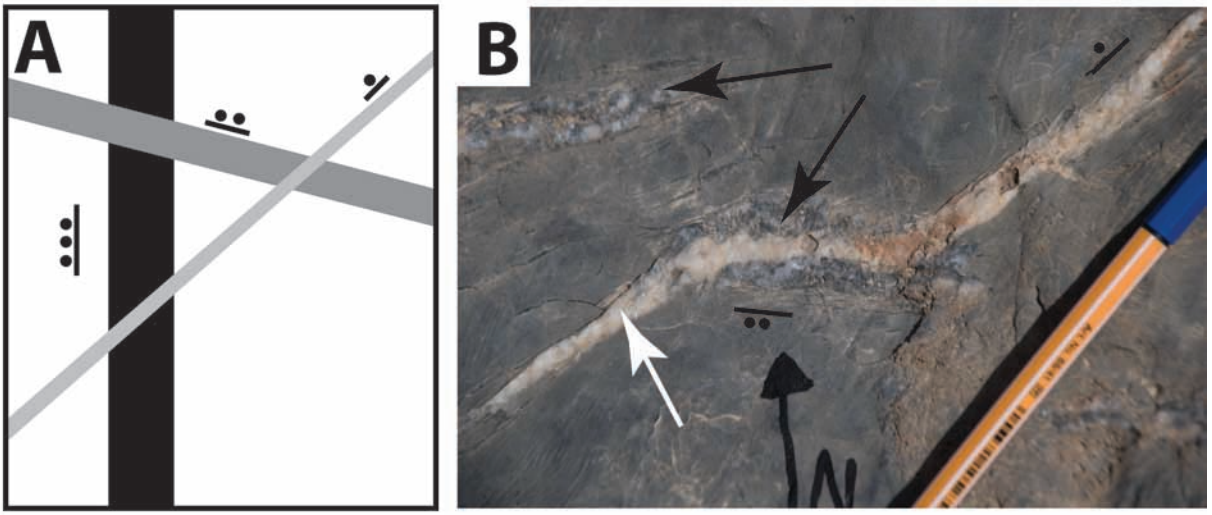


Figure 2.10: ***A*:** Shematic illustration of cross-cut relationships (e.g. Holland et al., 2009b). Relative ages of veins can be estimated using cross-cut relationships. Starting with the youngest vein, every vein is marked with an increasing number of dots with increasing relative age. ***B*:** Reactivated black impregnated vein (black arrow) from a sinistral en échelon array at Wadi Ghul. The white vein (white arrow) strikes the black vein in a 30 ° angle, gets deflected, and runs parallel to the black vein reactivating it in the center. At the tip of the black impregnated vein it changes the direction and leaves it parallel in the same direction as it was before. View is down to the surface with the top of the image to the north. Pen for scale.

In contrast to this, white veins often cross-cut and reactivate black impregnated en échelon arrays of veins and straight veins in Natih A. White veins can get deflected by black impregnated veins if they strike the black vein in a low angle (<30 °) (fig. 2.10 B). These veins can reactivate black impregnated veins over metres, mostly in the center. Deflection of reactivating veins running parallel in reactivated veins show that pre-existing veins can change the local stress regime. Moreover, black impregnated veins are found to be the oldest veins in Natih A. Cross-cut relationships for Natih B veins and faults have not been found.

Simplified block model at the field scale

Figure 2.11 shows a simplified block model at the field scale which summarizes the main black impregnated structures and their relationship to other structures.

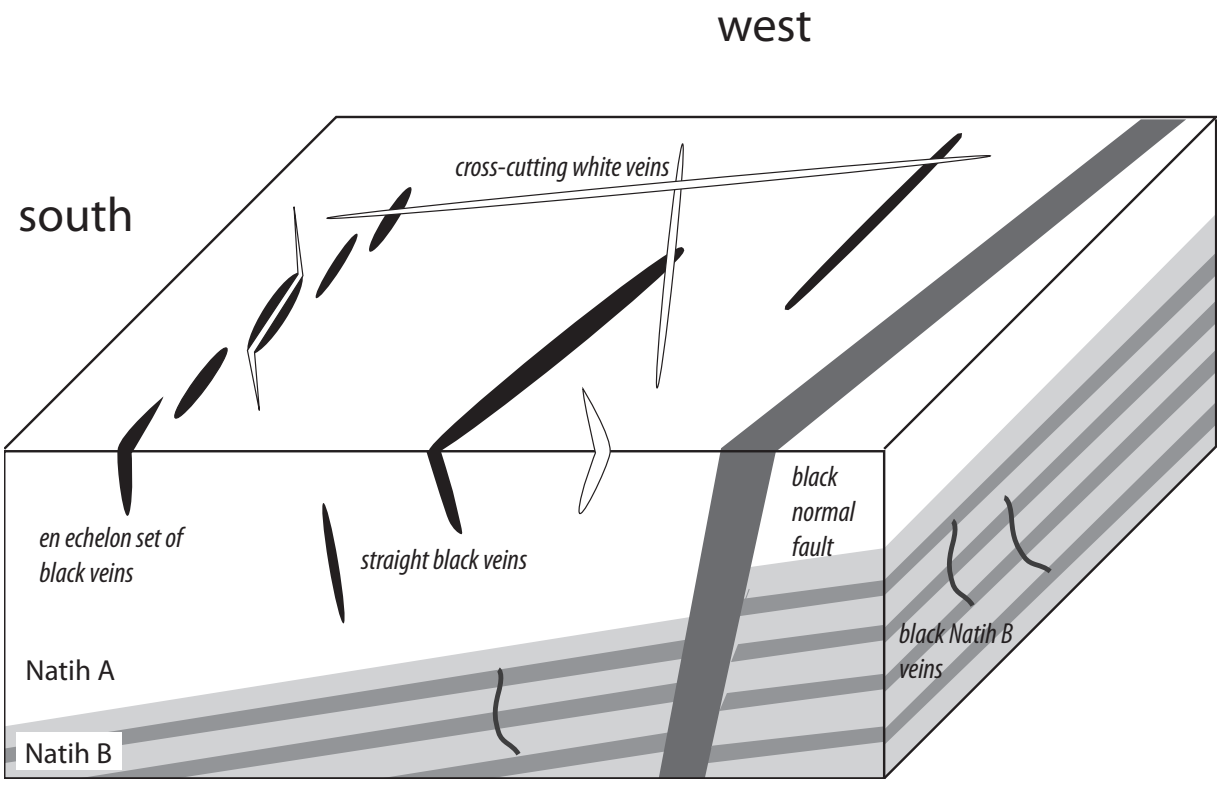


Figure 2.11: Block model illustrating main structures and their relationship in the field scale. There are four types of black impregnated structures: Faults, en échelon arrays of veins in Natih A, straight veins in Natih A and veins in Natih B. White Natih A veins cross-cut black impregnated Natih A veins.

2.3 Sampling

During the fieldwork, 46 samples (see appendix table .0.1) were taken from outcrops at the entrance of Wadi Nakhr, Ghul ramps, Wadi Ghul, Al Raheba, center of Wadi Nakhr and Hayl Al Shaz (see figure 2.1). The focus of the sampling was on black impregnated structures. We sampled faults, veins from en échelon arrays in Natih A, straight veins in Natih A and veins in Natih B. Moreover we took host rock samples from the known and described Natih B source rock interval (Homewood et al., 2008). All samples are from the Natih A or B member, except OM12 B39 which is a fault sample from the Sahtan formation, approximately 1000 m below the Natih formation in the center of Wadi Nakhr and a fault sample from Hayl Al Shaz which is from the Kahtan formation.
Samples were taken using hammer and chisel which is easier and faster than using a drilling machine.

Before sampling, the orientation of most samples have been measured with a geological compass. The orientation was marked on the sample with a north arrow, a horizon line, dipping of the vein and a top mark if possible. Others are bulk samples with no orientation. Sample SV2010-002 was taken by Simon Virgo in 2010 at Wadi Ghul and was used during this study.

Chapter 3

Methodology

3.1 Sample Preparation for Microscopic Study

3.1.1 Highly Polished Thin Sections

Highly polished thin sections were prepared by polishing of standard thin sections used at the institute of Structural Geology, Tectonics and Geomechanics (GED). Polishing was done stepwise with different polishes using a polishing machine. The procedure is briefly described below.
Preparation of standard thin sections:

- Saw the block of interest out of the rock sample with a diamond saw (formatting).
- Grind the side of interest of the block ground flat on a thick glass plate by hand. For this purpose, silicon carbide powder and DP-Lubricant Green from the company Struers must be added. This is done stepwise from grid 120 to 1200. If the sample is fragile, it has to be hardened in the forehand with instant adhesive.
- Clean the block in an ultrasonic bath and then dry it at 60 °C.
- Mount the piece on a standard object slide for microscopy (so called Gießener format, 28x48 mm and 1,55 mm thick, one matt and one shiny side) using Korapox 439 two component resin-hardener mixture in the mass ratio 1:1. It is important to heat both the glass plate and the sample to 60 °C before glueing. This facilitates extrusion of any bubbles between the object slide and the sample easier.
- Label the object slide with number and orientation of the sample using a glass diamond writer.
- Cut the block off the object slide at a distance of approximately 0.7 mm using a vacuum chuck for microscopy object slides on a suitable diamond saw.

- Grind the sample to a thickness of approximately 50 µm using a diamond cup-wheel with the object slide mounted on the vacuum chuck.

- Grind the sample to a thickness of approximately 30 µm by hand with silicon carbide powder and a DP-Lubricant Green from Struers on a thick glass plate. This is done stepwise from grit 600 to 1200 with cleaning it after each step in an ultrasonic bath.

These standard thin sections were then polished in five steps on a CP40 polishing machine from Logitech with the parameters listed in table 3.1.1. During each step of polishing, DP-Lubricant Green was added at least three times to both, the diamond particles and the silica suspension (all produced by Struers). After each step the thin sections were put into an ultra sonic bath for cleaning.

Table 3.1.1: Polishing procedure of highly polished thin sections. During all steps some millilitres of DP-Lubricant Green from Struers has been added several times. All Discs are produced by Struers.

Step	Disc	Time [min]	Force [N]	Speed [rpm]	Addition
1)	MD-Rondo	8	4	100	DP-Spray 6 µm diamond particles
2)	MD-Rondo	8	4	100	DP-Spray 3 µm diamond particles
3)	MD-Rondo	8	4	100	DP-Spray 1 µm diamond particles
4)	MD-Rondo	8	4	100	DP-Spray 0.25 µm diamond particles
5)	MD-Plus	8	4	100	OP-U colloidal silica suspension

3.1.2 Polished Blocks

Polished blocks were made by the standard procedure for coal and shale samples at the Institute of Geology and Geochemistry of Petroleum and Coal (LEK) which is proven scientific practice. Firstly, the piece of interest was sawed out of the rock sample (formatting) and then put into a container with the area of interest being on the bottom. This container was then filled with Araldit epoxy-hardener mixture in the mass ratio 10:3. After hardening for 24 h, the block was grinded and polished on a Struers Tegra Pol polishing machine as described in table 3.1.2.

Table 3.1.2: Grinding and polishing procedure of polished blocks on a Struers Tegra Pol polishing machine at the LEK.

Step	Disc	Time [min]	Force [N]	Speed [rpm]	Addition
1)	MD-Piano 220	1	20	300	water
2)	MD-Piano 1200	0.5	10	300	water
3)	MD-Plan	4.4	20	150	Dia Pro 9 µm diomond suspension
4)	MD-DAC	2.3	20	150	Dia Pro 1 µm diomond suspension
5)	MD-Plus	1	15	150	OP-U colloidal silica suspension

3.2 Microscopic Study

3.2.1 Solid Bitumen Reflectance (BR_r) Measurements

Solid bitumen reflectance measurements have been carried out at the LEK on highly polished thin sections and on polished blocks under reflected light in oil immersion with $n_e = 1.518$. The used Zeiss microphotometric system was calibrated by an Yttrium-Aluminium-Garnet standard (YAG) with a reflectance of 0.889 % or a Cubic-Zirconia standard with a reflectance of 3.124 % before measuring the reflectance at a wavelength of 546 nm on an area of approximately 20 μm^2.

The validity of the BR_r measurements on polished thin sections has been tested by comparative measurements on polished blocks (see chapter 4). Reflectance measurements on polished blocks are the standard procedure which is proven scientific practice.

3.2.2 Microstructural Analysis

Highly polished thin sections were analysed by combining reflected light microscopy under immersion oil and transmitted light microscopy. Therefore, a ZEISS 20x/0.85 and a ZEISS 50x/0.85 oil objective were installed into a ZEISS microscope with light sources for reflected and transmitted light microscopy. With this set up it is possible to switch continuously between reflected and transmitted light under immersion oil as shown in figure 3.1 which allows for the identification of organic material and simultaneous analysis of the microstructure. Reflected light overview images of blocks were made by scanning them with a photo scanner. Transmitted light overview images without polarisers were made by scanning the whole thin section with a photo scanner.

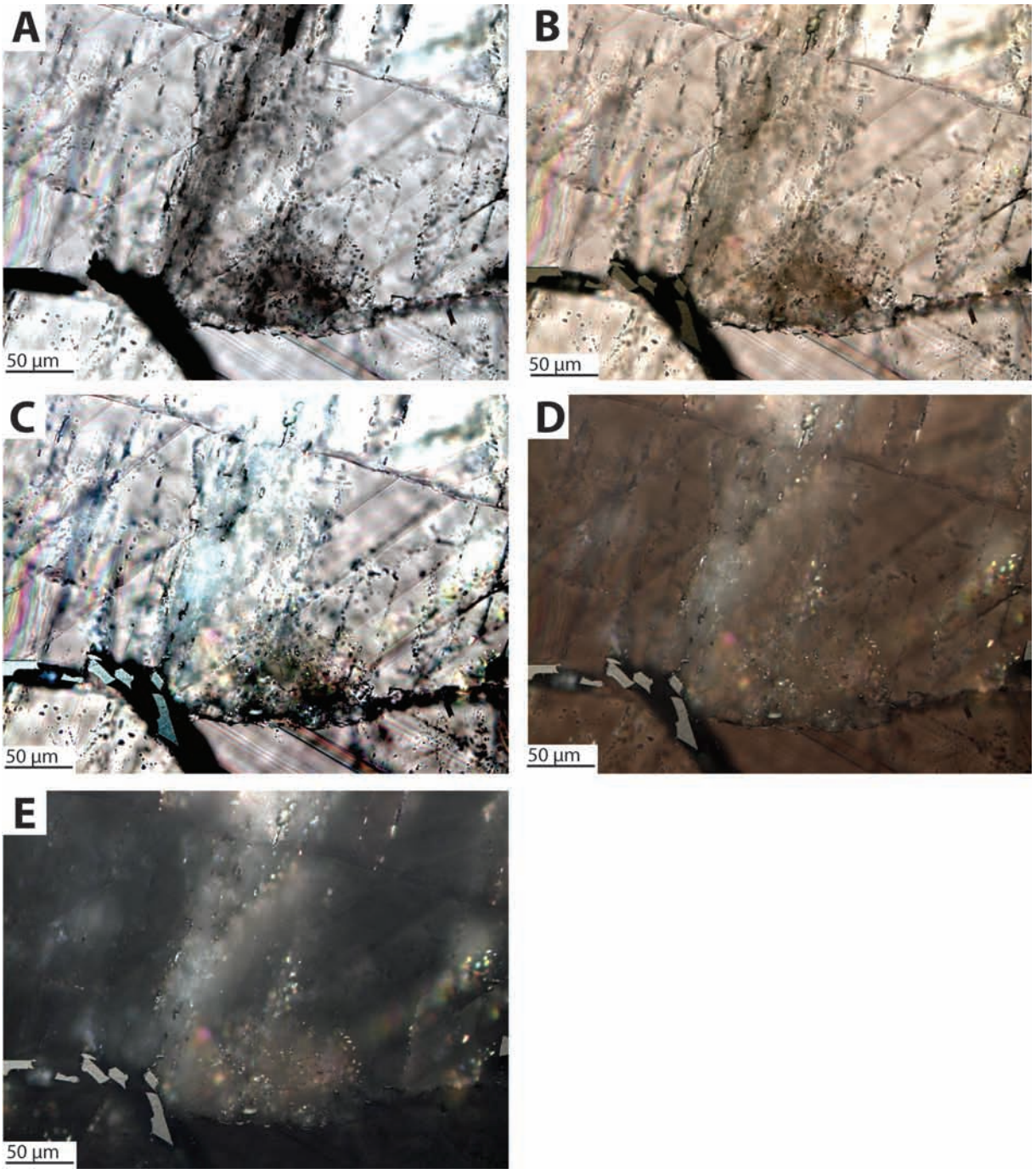


Figure 3.1: Series of microphotographs from transmitted light (***A***) to reflected light (***E***). The microphotographs were made by switching down the light source of the transmitted light and simultaneously increasing the reflected light source. Therefore, B, C and D are both, transmitted and reflected light microphotographs. Microphotograph A shows many linear aligned inclusions and two big opaque areas in the bottom left corner. From microphotograph B to E, most small inclusions disappear and inclusions situated at the surface are becoming shiny dots in reflected light. Within the big opaque areas, grey, homogeneous reflecting surfaces appear which can be identified as solid bitumen. Plane-polarised light under immersion oil. Thin section SV2010-002b.

3.2.3 Cathodoluminescence Microscopy

For cathodoluminescence microscopy, highly polished thin sections were coated with carbon and analysed with a hot cathode HC1-LM Lumic Special microscope. Operating conditions were 0.6-0.7 mA for the beam current, 14 kV for the beam voltage and 1.5 - 2.5 A for the filament current. The vacuum was < 0.01 mbar.

3.3 Geochemical Study

3.3.1 Total Organic Carbon (TOC) Measurements

TOC measurements were performed using a Liqui TOC II with an additional solids-module instead of the standard liquids module from the company Elementar Analysesysteme GmbH. Approximately 100 mg of powdered rock were measured in a single run in a non-isothermal mode by detecting the released CO_2 from catalytic oxidation with a NDIR (non dispersive infrared) sensor. The used temperature program is 550 °C for 600 s, then cooling to 400 ° for a better seperation of the TOC and the following TIC (total inorganic carbon) peak which is detected at 1000 ° for 400s.

3.3.2 Rock-Eval Pyrolysis

Rock-Eval pyrolysis was performed with a Rock-Eval II from DELSI INC. Approximately 100 mg of powdered rock is pyrolysed in an inert helium atmosphere. At the beginning, the sample is rapidly heated to 300 °C and remains at this temperature for 3-4 min. Then, the sample is heated at a rate of 25 °C to 550 °C. Released hydrocarbons are detected by a flame-ionisation detector (FID). Volatiles which are released by thermal desorption, form the S_1 peak, whereas volatiles released from thermal cracking of the kerogen at higher temperatures form the S_2 peak. Simultaneously released carbon dioxide forms the S_3 peak which is detected by a thermal conductivity scanner (TCD). The signals of each detector are integrated and quantified by comparison to the integrated signals of a measured standard. Rock-Eval also records T_{max} which is the temperature with highest intensity of hydrocarbon release due to thermal cracking (S_2 peak) of kerogen. This provides information on the thermal stability and maturity of the organic matter.

3.4 Residual Analysis of Fault Samples with Scanning Electron Microscope (SEM)

Residues of fault samples were prepared by dissolving 5 - 10 g unweathered, black impregnated calcite crystals in 200 ml HCl (10 %). After the reaction had eased, 100 ml of 10 % HCl was added to guarantee that the calcite has dissolved completely.

The solution with the residue was filtered using a DURAN filter crucible with the porosity 4 or 5 which was put on a filter flask connected to a trap and a vacuum pump. Then, some ml of high concentrated HCl (37 %) were dropped on the black residue on the filter and filtered to dissolve slightly soluble carbonates. The residue was then washed by filtering it with de-ionised water. For safety reasons, the hole procedure of dissolving and filtering was done using a fume cupboard.

After drying at 50 °C, the filter was separated from the surrounding crucible by destroying it carefully. Before analysing it with a SEM ZEISS-Supra 55, the filter was coated with Au. For the identification of the residue, secondary electron (SE) and back-scattered electron (BSE) images were combined with energy dispersive X-ray (EDX) maps. Then particles of interest were identified by their morphology and EDX spectra.

Chapter 4

Results

4.1 Microscopic Analysis

4.1.1 Solid Bitumen Types under Immersion Oil

Four different types of solid bitumen could be distinguished from each other by their optical appearance under reflected light microscopy with immersion oil: low reflective granular solid bitumen (fig. 4.1 A), low reflective homogeneous solid bitumen (fig. 4.1 B), high reflective mosaic solid bitumen (fig. 4.2 A) and high reflective homogeneous solid bitumen (fig. 4.2 B).

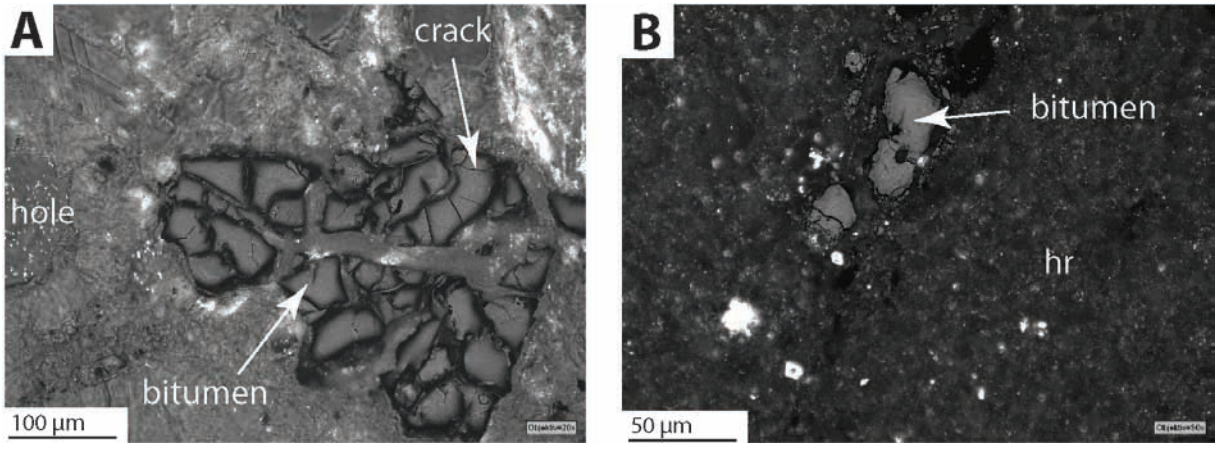


Figure 4.1: Microphotographs showing low reflective solid bitumen types under reflected light with immersion oil. ***A*:** Granular solid bitumen in a calcite vein. Granular solid bitumen has an inhomogeneous surface with a grainy texture of very small dark and bright spots. It is found as round aggregates with a size of several 100 µm in diameter. The grains within the aggregate are often angular and broken. Sample OM12 B14. ***B*:** Homogeneous solid bitumen in Natih B host rock (hr). Homogeneous solid bitumen has a very homogeneous surface with almost no colour change. The bitumen particles are often broken and have an angular shape. They usually do not built aggregates. Sample OM12 B41B.

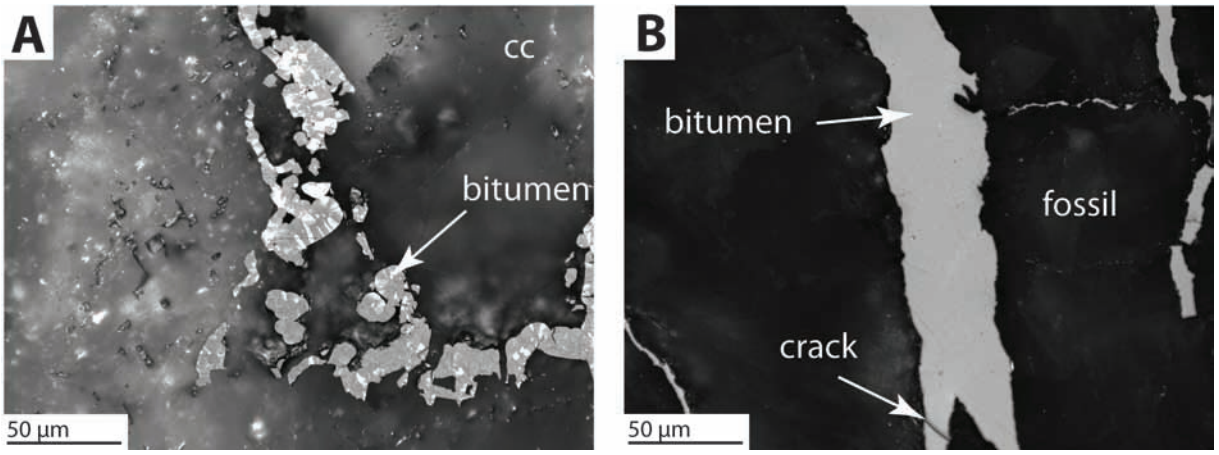


Figure 4.2: Microphotographs showing high reflective solid bitumen types under reflected light with immersion oil. ***A*:** Mosaic type solid bitumen in calcite (cc) vein. Mosaic type solid bitumen shows a strong anisotropy in reflectance between different parts in one grain. The parts have clear boundaries and form a mosaic structure. However, each mosaic part itself has a homogeneous surface. Grains often have a negative crystal shape or they occur in aggregates with an elongated shape. Sample SV2010 002. ***B*:** Homogeneous, high reflective solid bitumen vein in a fossil. Homogeneous high reflective solid bitumen often has cracks and does not form aggregates. Sample OM12 B13.

4.1.2 Microstructural Description

For the microscopic study 25 highly polished thin sections from 21 samples have been analysed. A list of thin sections is shown in the appendix table .0.2. In the following, eight samples with different properties will be described exemplary for the rest.

Sample SV 2010 002

The sample is part of a black impregnated straight vein from Wadi Ghul with the orientation 031/83. The thin section has been cut perpendicular to bedding and perpendicular to the vein. Figure 4.3 shows a suite of overview images which highlight the advantages and disadvantages of the used overview imaging techniques. Under transmitted light without polarisers (A), host rock, host rock inclusions and fine black veinlets can be seen in the vein. (B) shows the cut side of the rock sample that was used for thin section preparation. It can bee seen that the vein is reactivated in the center by white calcite and that the veinlets colour the vein calcite black. Under crossed-polarised light (C), crystal shape and texture of the vein can be studied. It is difficult, however, to identify the veinlets as well as the white calcite overprinting. In combination, this shows that the sample can be macroscopically divided into three parts: the host rock, the black impregnated part of the vein and the white part of the vein.

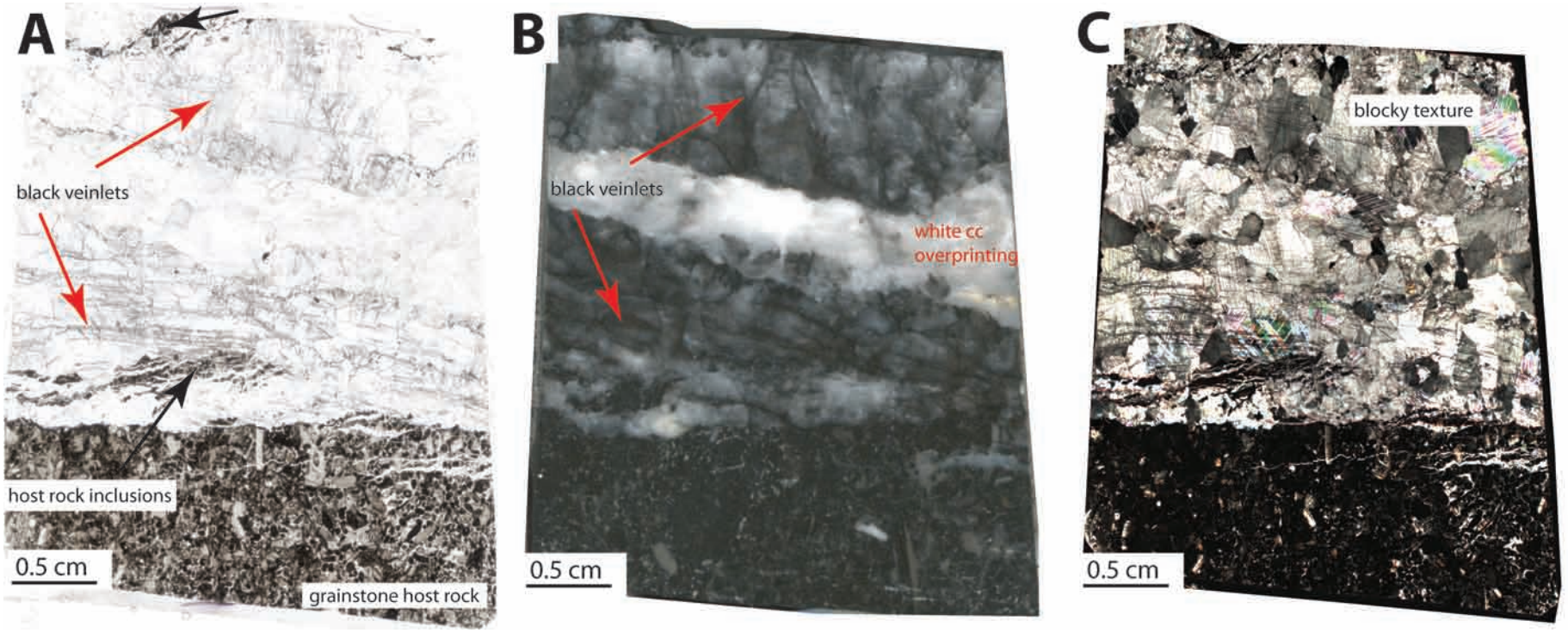


Figure 4.3: Overview images of thin section SV 2010 002b. ***A*:** Photograph of the thin section under transmitted light without polarisers. The grainstone host rock, host rock inclusions and fine black veinlets running through the vein can be identified. ***B*:** Photograph of the block from which the thin section was made. The sample is overprinted in the center by white calcite and the veinlets impregnate the sample black. ***C*:** Stitched microphotograph of the thin section with transmitted, crossed-polarised light. Crystal shape and mineralogy can be identified, but the white calcite overprinting and the black veinlets are difficult to recognise. Sample is oriented vertical to bedding.

Figure 4.4 shows an overview image of the three main zones with areas of interest being highlighted. The host rock consists of a peloidal, well cemented grainstone from the Natih A member. Most of

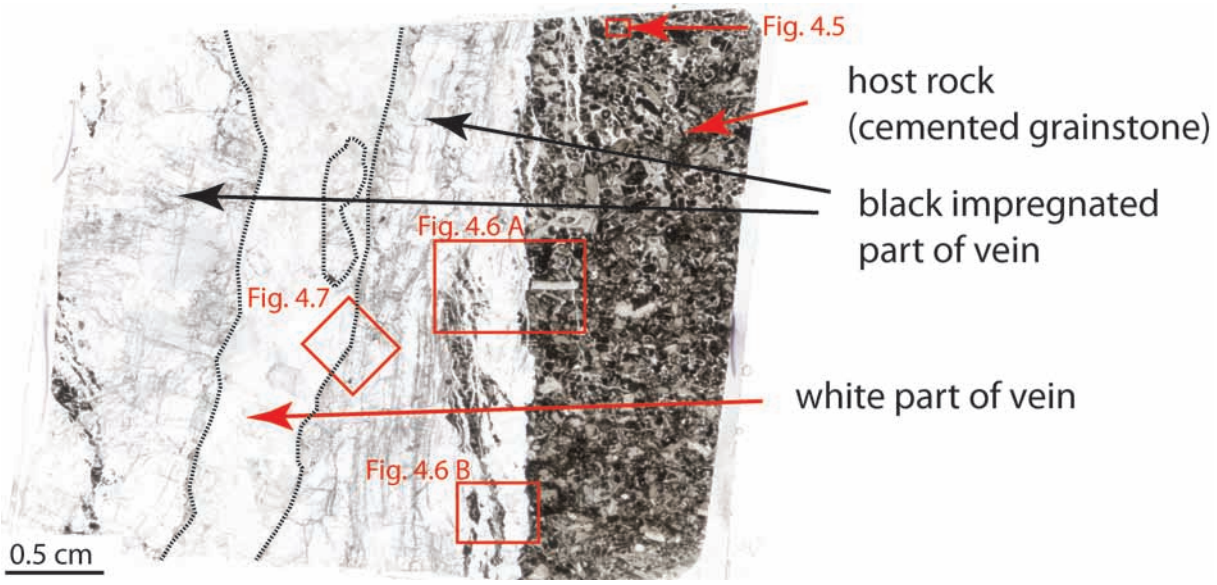
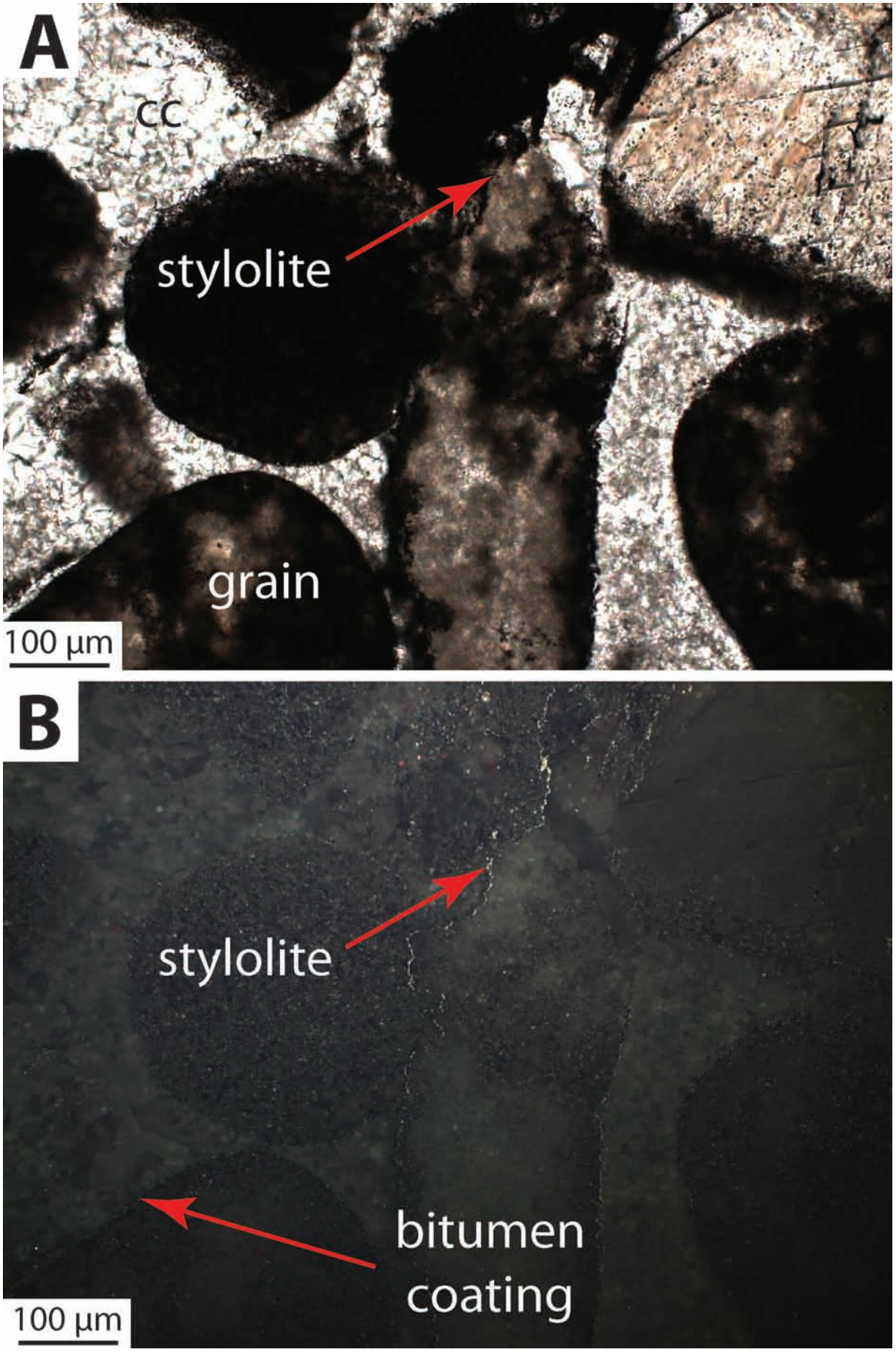


Figure 4.4: Overview image of thin section SV2010 002b. The sample consists of three zones: the cemented grainstone host rock, the black impregnated part of the vein and the white part of the vein (dashed line). Red boxes show location of micrographs presented in figure 4.5, 4.6 and 4.7. Transmitted, non-polarised light. Image is rotated 90° compared to fig. 4.3.

the grains contain very fine solid bitumen particles and a solid bitumen grain coating. Moreover, these small particles are enriched along tectonic stylolites which are oriented parallel to the vein and perpendicular to bedding. These stylolites are identified very well by reflected light under immersion oil whereas they are easily overlooked under transmitted light (fig. 4.5). This is the only Natih A sample with fine dispersed solid bitumen in the host rock. Nevertheless, it is a common feature of Natih B source rocks.

The host rock is cross-cut by several microveins which are oriented parallel to the main vein. These microveins often cut straight through grains and sometimes they run around grains. Figure 4.6 shows host rock inclusions at the vein margin. Most inclusions are separated by numerous microveins which indicate multiple cracking and resealing of the vein at the vein margin. A large, multiple cross-cut

Figure 4.5 ***(facing page)*****:** Micrographs of a stylolite showing the same section of thin section SV 2010 002b in transmitted, plane-polarised light (A) and reflected light under immersion oil (B). ***A*****:** Host rock consists of calcite (cc) cemented grains. The stylolite is hardly visible. ***B*****:** Stylolites can be identified by an enrichment of fine solid bitumen (bright shiny dots). Fine solid bitumen particles can also be found on grains as coating and dispersed in grains. They do not occur in the calcite cement.

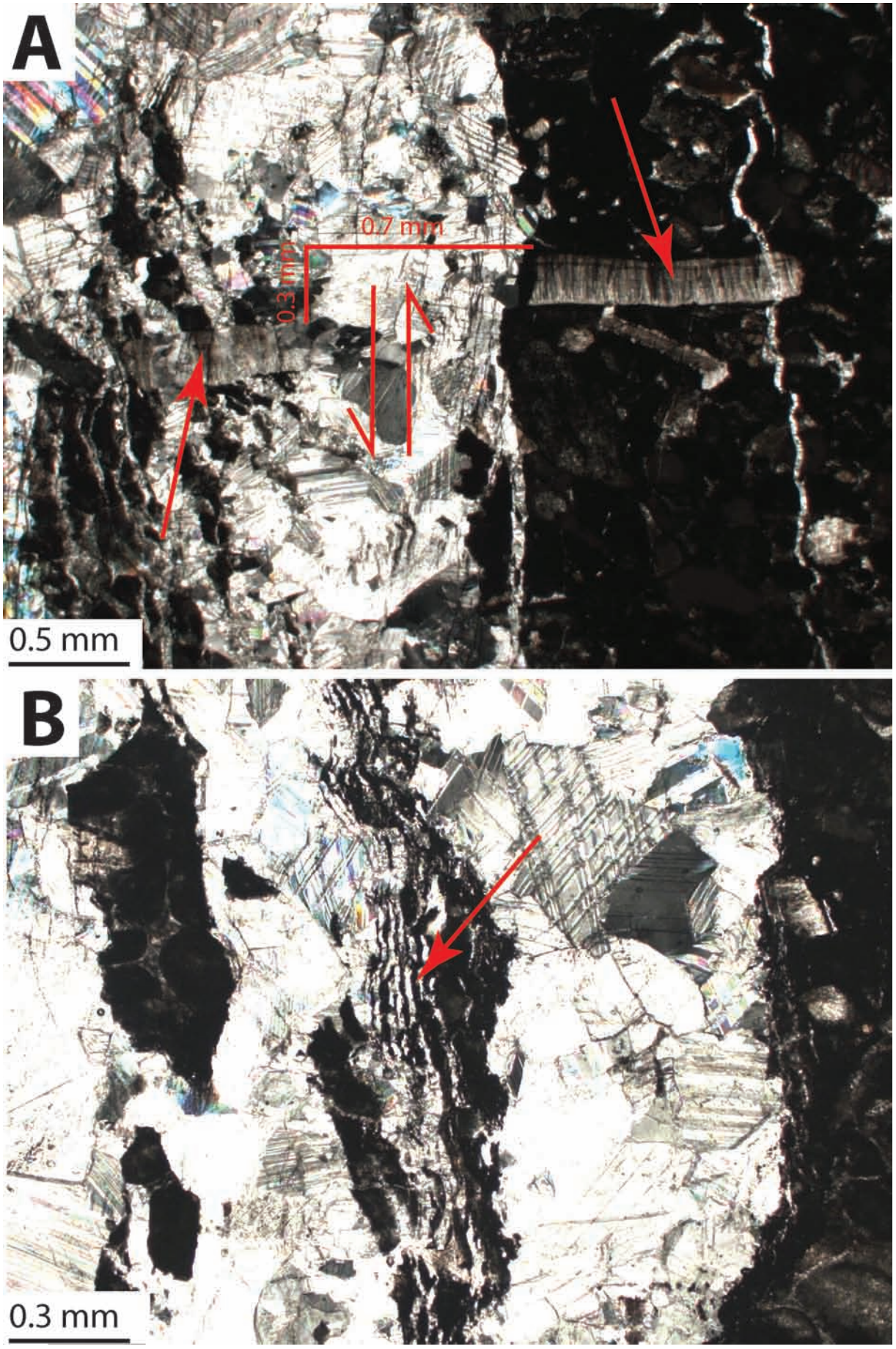

A
CC
stylolite
grain
100 µm
B
stylolite
bitumen
coating
100 µm

fossil, shown in figure 4.6 A, can be used for correlation between the host rock inclusion and the host rock. It shows that there is a separation of approximately 0.7 mm perpendicular to the vein and an offset of approximately 0.3 mm along the veins plane with a sinistral sense of shear. Black lines within the fossil consist of small solid bitumen inclusions. They can be found in the fossil within both, the host rock inclusion and in the host rock. There is no clear age indicator which indicates whether the fossil was cut by the vein before or after solid bitumen incorporation, because some bitumen arrays cross-cut the fossil's wall and run into the vein while others end at the fossil's border.

The black coloured parts of the vein are separated by white calcite. This will be called a white calcite reactivation in the following. The white calcite reactivation lacks small bitumen inclusions which occur in the black impregnated part arranged as intracrystal solid bitumen trails (compare appendix figure 1). They are often oriented parallel to twinning of calcite crystals. If the trails are not formed parallel to twins, single inclusions are sometimes situated at the crossing point between inclusion trail and twin. Single inclusions usually have a negative crystal shape with solid bitumen forming a coating of the inclusion. This can be seen under reflected light where the solid bitumen is observed as a fine line forming a trapezium. Under transmitted light, these inclusions are brown in the center. Within existing micro-cracks, small solid bitumen inclusions have a worm-like shape (compare to appendix fig. 2). Moreover, solid bitumen forms elongated intracrystal or intercrystal particles. Intracrystal elongated solid bitumen usually runs in a rectangular pattern through calcite crystals. Intercrystal, elongated solid bitumen often builds aggregates on grain boundaries. In three dimensions, elongated bitumen is forming planes. They appear wider in transmitted light compared to reflected light, if they are inclined to the height of the thin section.

Quartz is found at the interface of the white reactivation and the black impregnated area. Crystals from the white reactivation are sometimes oriented after the black impregnated crystals and sometimes show new orientations. The zone between black impregnated area and white reactivation consists at some places of smaller crystals and is assumed to be a very solid bitumen rich area. Moreover, there are microveins with big mosaic type solid bitumen particles which cross-cut solid bitumen inclusion rich crystals. These microveins can only be observed, because they do not contain small solid bitumen particles. In cathodoluminescence microscopy (fig. 4.7), these microveins have a small difference

Figure 4.6 ***(facing page)*****:** Microphotographs of host rock inclusions in thin section SV 2010 002b. ***A*****:** Fossil (red arrows) is cross-cut and separated by the vein. The separation is 0.7 mm perpendicular to the vein with an offset of 0.3 mm. Sense of shear is sinistral. Transmitted, crossed-polarised light. ***B*****:** In the center, the host rock fragment is cross-cut by several microveins separating the fragment in multiple subparallel host rock inclusion bands (red arrow). Transmitted, crossed-polarised light.


A
0.7 mm
0.3 mm
0.5 mm
B
0.3 mm

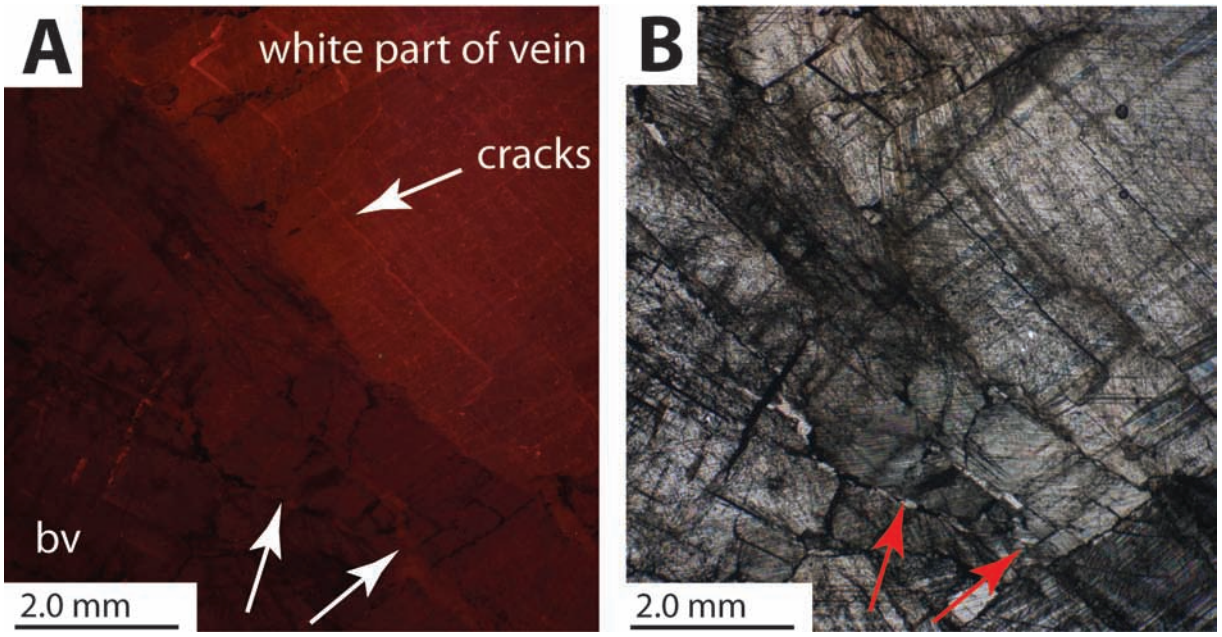


Figure 4.7: Micrographs of thin section SV 2010 002b showing the same section with cathodoluminescence (A) and transmitted, plane-polarised light (B). ***A*:** Luminescence colours show a clear difference between white part of vein (weak luminescence) and black impregnated vein (bv) (almost non luminescence). Cracks show bright luminescence. Microveins with mosaic type bitumen (white arrow) show very weak luminescence. ***B*:** Red arrows show microveins which can be seen due to a different orientation of their crystal lattice and because of the lack of solid bitumen trails.

in luminescence colour compared to the almost non-luminescent black impregnated part. The white reactivated part shows a clear difference in luminescence compared to the black impregnated part. However, it is difficult to link the small reactivations to one or the other. Both parts do not show any interior change in luminescence which could be linked to crystal growth. Cracks on cleavage planes show bright luminescence.

The prior mentioned black veinlets consist of solid bitumen. They run subparallel to the vein between host rock and reactivation and perpendicular at the other side of the reactivation (compare fig. 4.3 A). Around these fibres, there is a higher density of small solid inclusion trails which are often oriented perpendicular to them.

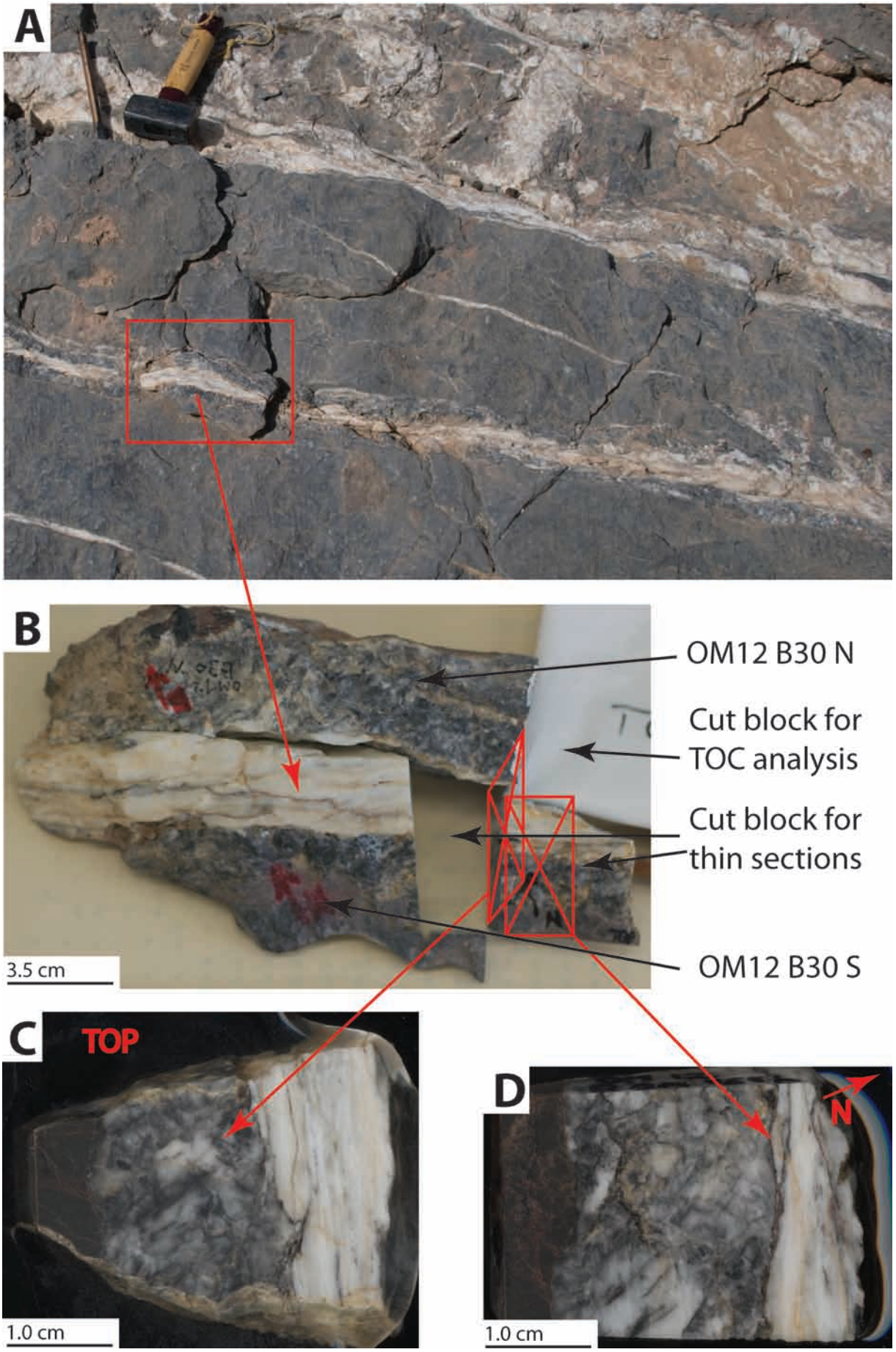
OM12 B30

Sample OM12 B30 is a straight black impregnated vein from the Natih A member which was taken in Wadi Ghul. The vein is reactivated several times and has an orientation of 024/60. Figure 4.8 shows an outcrop photograph (A) from the sample location as well as the sample itself (B) with locations of the prepared thin sections OM12 B30 S and OM12 B30 S b and photographs of the blocks the thin sections were made of (C, D).

The sample can be subdivided into three parts as shown in figure 4.9: the packstone host rock, the black impregnated blocky calcite vein and a white reactivation consisting of elongated calcite crystals. The sample shows pressure solution indicated by stylolites with different orientations. Stylolites may be difficult to identify within a vein, because there usually was not enough unsoluble material, such as clay or organic particles, which could be enriched. Yet, using reflected light, solution features indicated by open voids, secondary minerals or serrated grain-grain contacts, can be identified on grain boundaries. Four types of stylolites can be distinguished in figure 4.9. (1) Stylolites running at the host rock vein interface associated with a fibrous calcite band (compare microphotograph of thin section OM12 B30 S b. Appendix fig. 5 A). (2) Bedding parallel stylolites within the host rock. (3) Stylolites along grain boundaries within the black impregnated area with different orientations. These stylolites are often difficult to identify, however, they occur frequently. Moreover, they contain low reflective solid bitumen particles (compare appendix fig. 3). (4) Big stylolite at the black impregnated vein and white reactivation interface running parallel to the vein. The stylolite contains abundant low reflective solid bitumen particles and cross-cuts the white calcite reactivated area.

Solid bitumen is found as trails within the black impregnated area, as mosaic type solid bitumen particles within reactivations (fig. 4.23) and inclusion poor calcite crystals, and as low reflective homogeneous type which is abundant along stylolites or associated with solution structures. Bitumen inclusion trails very often end at grain boundaries and are curved. They do not have a preferred orientation. Mosaic type bitumen is also found within the reactivated white calcite zone as aggregates between elongated crystals.

Figure 4.8 ***(facing page)*****:** Photgraphs of sample OM12 B30. ***A*****:** Outcrop photograph of sample location. Red box indicates the position of the sample. View is down to the surface. View is to the north and hammer is for scale. ***B*****:** : Sample OM12 B30 which broke into two parts. Sample consists of host rock with a black impregnated vein which is separated in the center by a white reactivation. Red crossed boxes indicate locations of thin sections OM12 B30 S and OM12 B30 S b. ***C*****:** Overview image of the block thin section OM12 B30 S was cut from. Reflected, non-polarised light. ***D*****:** Overview image of the block thin section OM12 B30 S b was cut from. Reflected, non-polarised light.


A
B
OM12 B30 N
Cut block for
TOC analysis
Cut block for
thin sections
OM12 B30 S
3.5 cm
C
TOP
1.0 cm
D
N
1.0 cm

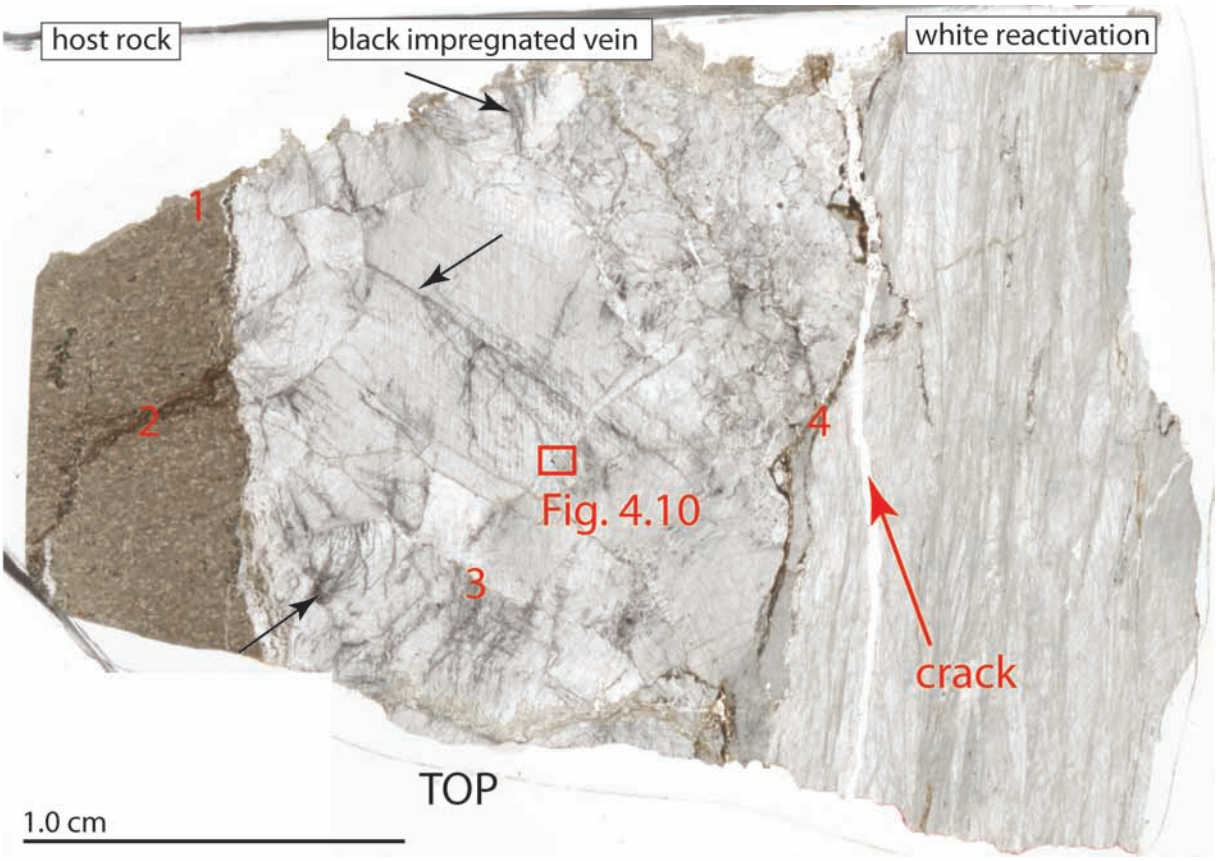
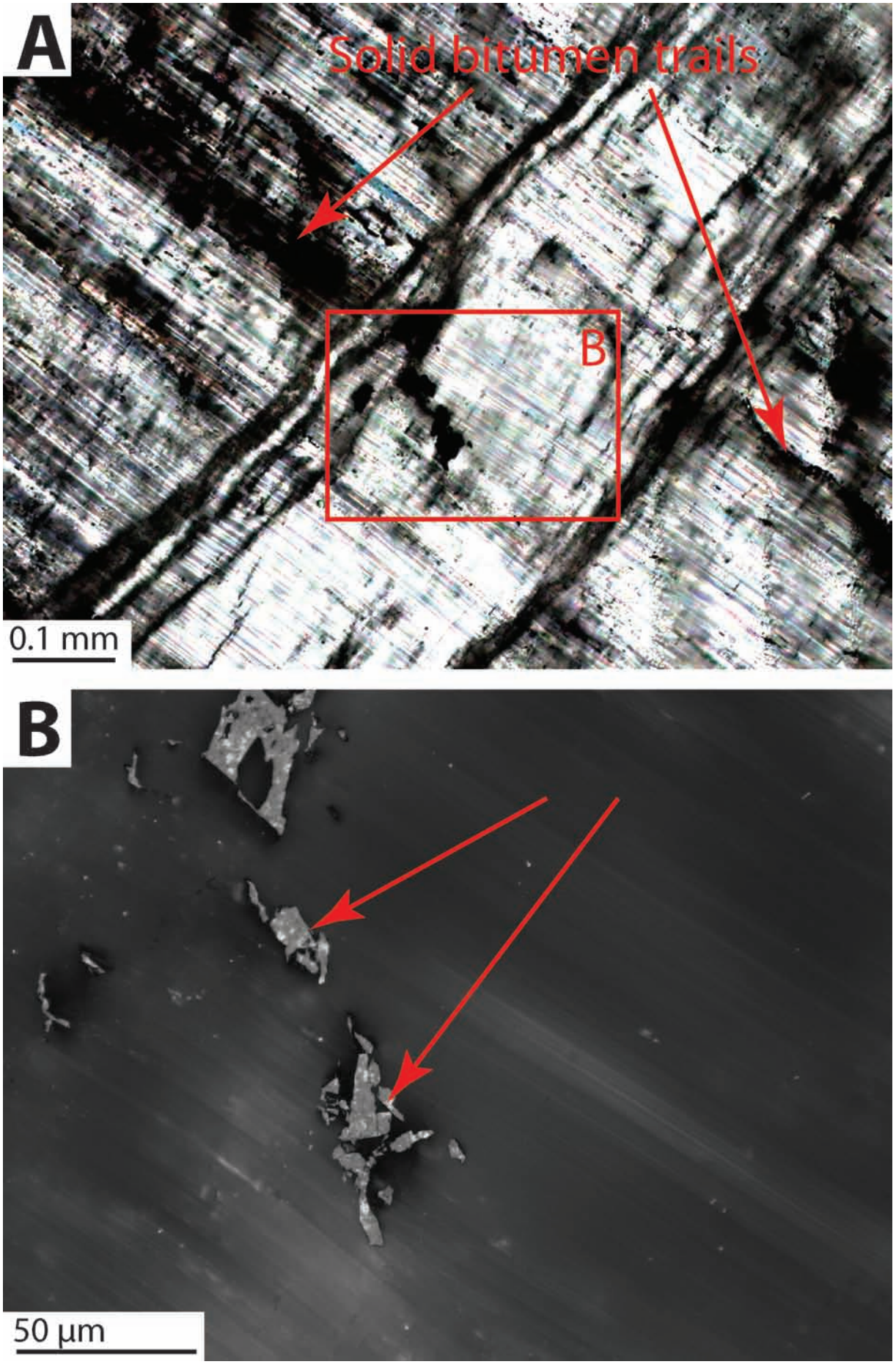


Figure 4.9: Overview image of thin section OM12 B30 S: The sample can be subdivided into three parts: the host rock, the black impregnated blocky calcite vein and the white reactivation consisting of elongated calcite crystals. Numbers show locations of stylolites which are discussed in the text. Black arrows highlight large intracrystal solid bitumen trails. Red box indicates location of microphotographs in fig. 4.10. The sample was glued before thin section preparation at the marked crack. Transmitted, non-polarised light.

Small reactivations (compare microphotograph of thin section OM12 B30 S b. Appendix fig. 5 B) can be found in many parts of the black impregnated area. They cut through big calcite crystals and separate solid bitumen trails. Moreover, they often have the same crystal orientation as surrounding crystals. Calcite within small reactivations is often less twinned in comparison to calcite within the surrounding vein.

Figure 4.10 ***(facing page)*****:** Microphotographs of thin section OM12 B30 S. ***A*****:** Reactivated calcite crystal within black impregnated part of the vein. The reactivation does not contain any small solid bitumen inclusions and has the same orientation of twinning as the surrounding calcite which contains solid bitumen inclusions along trails, parallel to twinning. Red box indicates location of microphotograph B. Transmitted, plane-polarised light. ***B*****:** Mosaic type solid bitumen particles (red arrows) within reactivated area. Reflected light under immersion oil.


A
Solid bitumen trails
B
0.1 mm
B
50 µm

OM12 B32

Sample OM12 B32 is a vein (orientation 001/86) from a sinistral en échelon set (orientation of array 026/75) in Wadi Ghul. Macroscopically, the vein is grey/white at the borders and is becoming black towards the center. However, the darkest part is found around a white vein reactivation running subparallel through the vein (fig. 4.11). Thin section OM12 B32 is oriented perpendicular to bedding

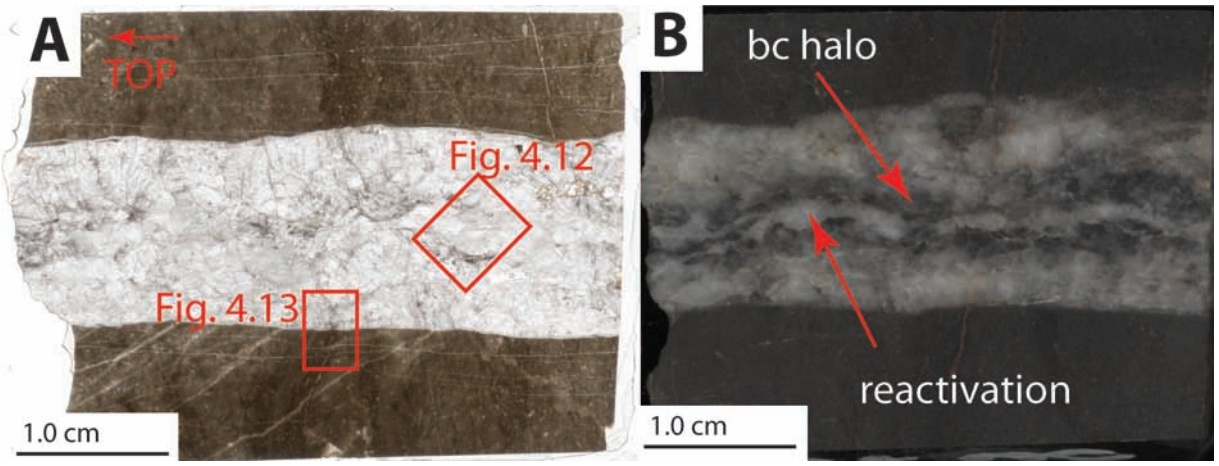


Figure 4.11: Overview images of sample OM12 B32. ***A*:** Overview of thin section under transmitted, non-polarised light. Red boxes indicate location of microphotographs in fig. 4.12 and 4.13. ***B*:** Overview of the block the thin section was made of with reflected light. The vein is reactivated in the center. Around the reactivation, the vein is impregnated with solid bitumen which results in a black calcite (bc) halo.

and shows a section through the whole vein. The vein has a sharp border and consists of blocky calcite. Moreover, an open crack is running subparallel to the vein. Microveins also run subparallel to the vein through the grainstone host rock. Besides, there are microveins which are oriented perpendicular to the vein. Some of them continue across the host rock-vein interface into the wackestone host rock. Bedding parallel stylolites run through the host rock and continue into the vein (fig. 4.13). This has been found in many black impregnated veins with stylolites often being red in the host rock. Solid bitumen occurs as inclusion trails which run parallel or perpendicular to the vein, as mosaic type solid bitumen in clear, less deformed calcite crystals, and as low reflective homogeneous type solid bitumen along stylolites or associated with solution structures. At the border of the vein, an approximately 0.2 mm wide zone with open voids, small calcite crystals and aggregates of low reflective solid bitumen is found. Moreover, solid bitumen was found as inclusions in quartz crystals (compare appendix fig. 8) situated along the central reactivation. Cathodoluminescence can help to identify structures and solid bitumen trails as shown in figure 4.14. The area at the border of the vein is separated separated from the vein interior by a vein parallel stylolite.

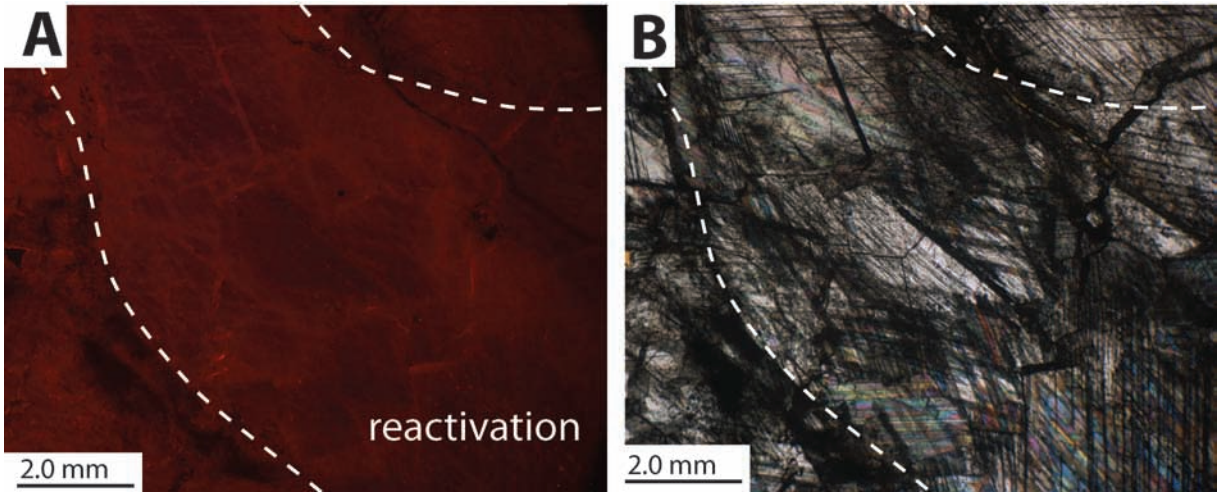
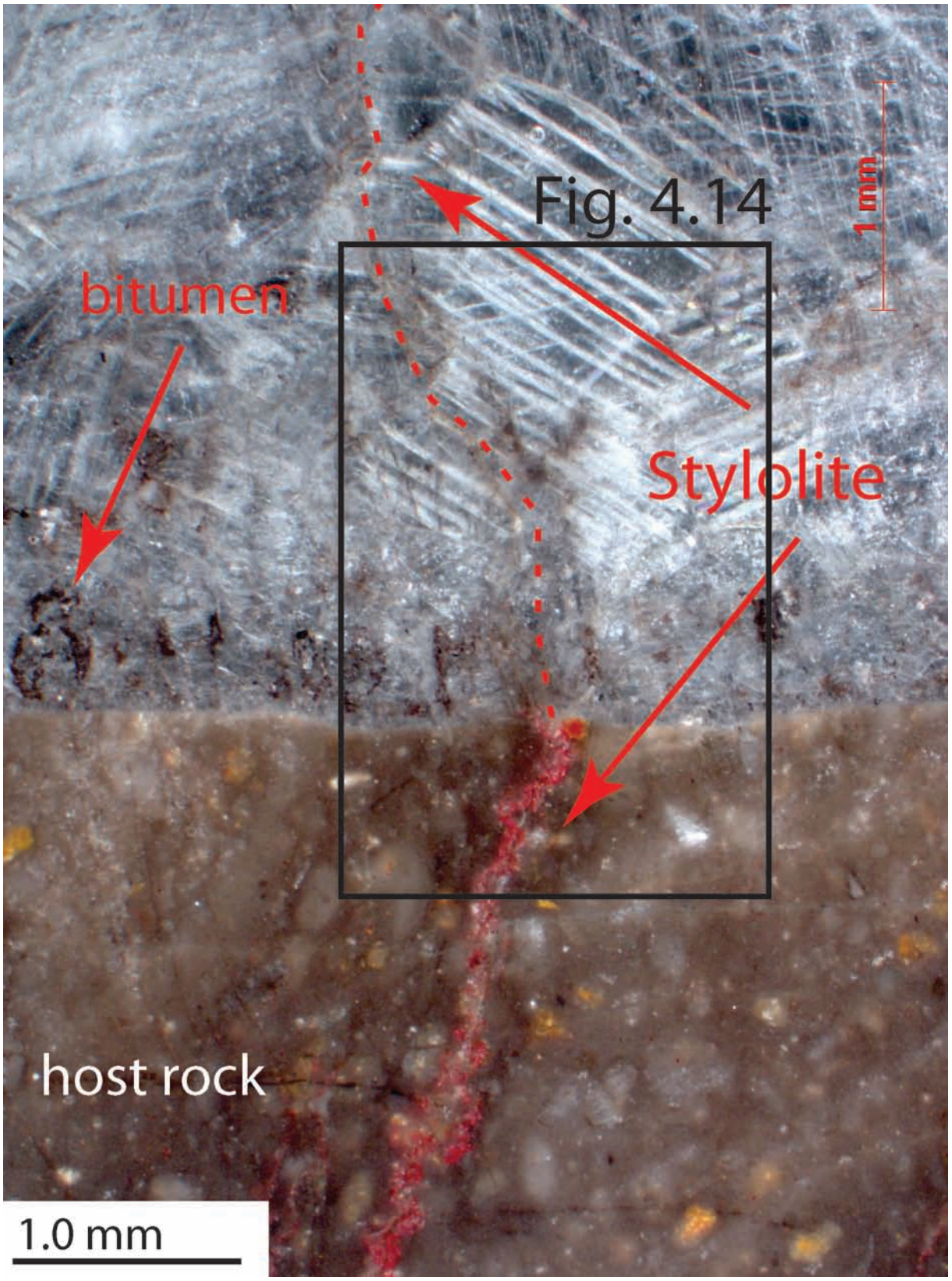


Figure 4.12: Microphotographs showing the same section of thin section OM12 B32 with cathodoluminescence (***A***) and transmitted, plane-polarised light (***B***). The white calcite reactivation has the same dark red luminescence colour as the black impregnated area. Single crystals do not show growth zonations.

The reactivation in the center is hardly recognisable under transmitted light. Cathodoluminescense does not show differences in luminescence between the reactivation and the black impregnated area (fig. 4.12). Moreover, luminescence is weak with a dark red colour. No growth zonations within calcite crystals are visible. Some cracks have a bright luminescence colour.

Figure 4.13 ***(facing page)*****:** Microphotograph of thin section OM12 B32. The bedding parallel stylolite is red coloured in the host rock and almost transparent in the vein. Therefore, the stylolite is marked by a red dashed line. Low reflective homogeneous type solid bitumen occurs along solution structures at the vein margin. Red box shows location of microphotographs in fig. 4.14. Reflected, plane-polarised light.


Fig. 4.14
bitumen
Stylolite
1 mm
host rock
1.0 mm

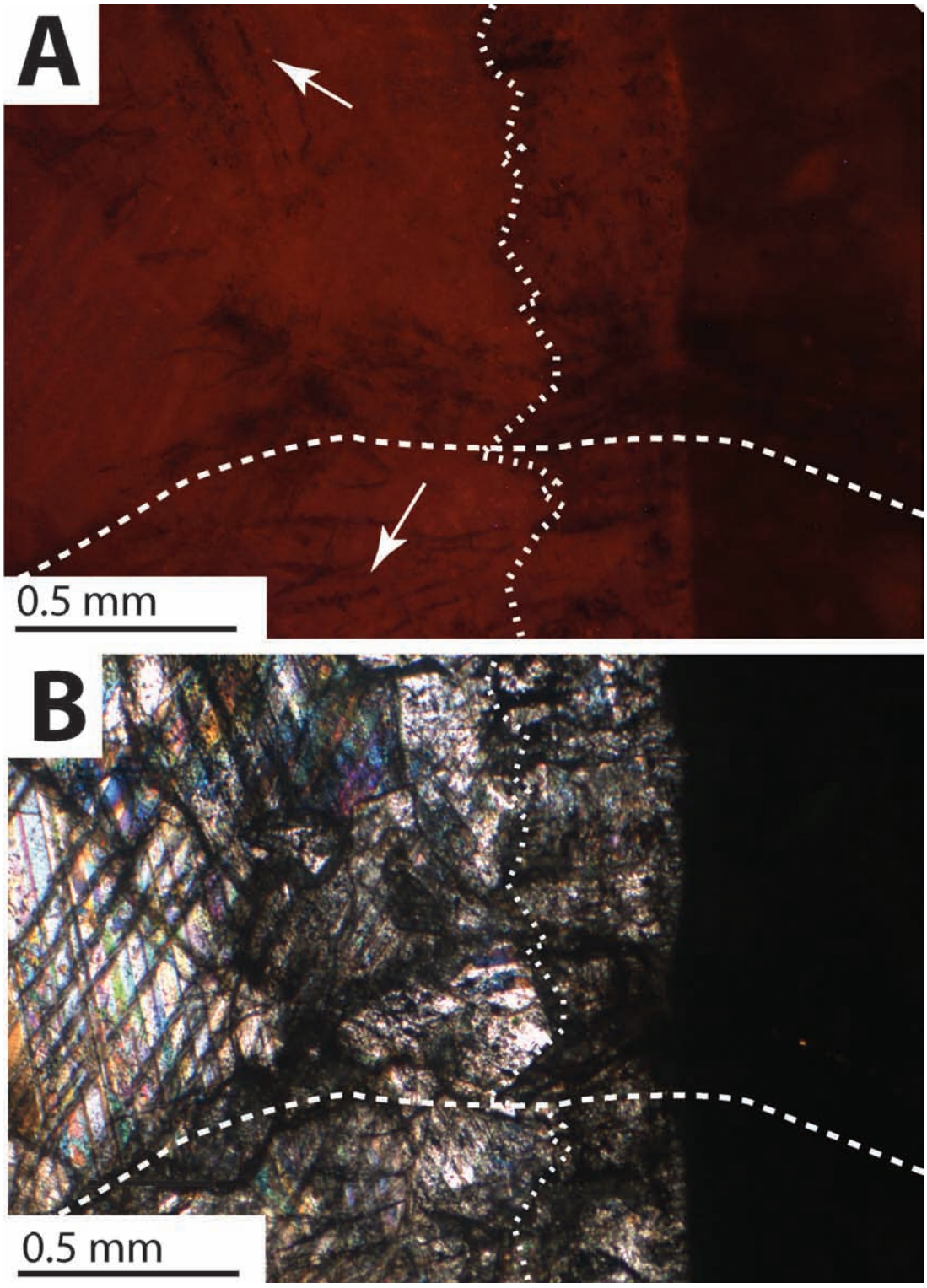


Figure 4.14: Microphotographs of the same section of thin section OM12 B32 with cathodoluminescence ***A*** and transmitted, plane-polarised light ***B***. Micrographs are rotated 90° compared to fig. 4.13. Stylolites are indicated by white dashed lines. One runs parallel to the vein wall and the other one parallel to bedding. White arrows show solid bitumen trails which are hardly recognizable under plane-polarised light.

OM12 B35 S

OM12 B35 S is an en échelon set of sigmoidal shaped black impregnated veins from Wadi Ghul. The set is strikes 133 °. It is situated next to a straight black impregnated vein (sample OM12 B35 N) which is oriented 006/70 (fig. 4.15). The tips of each sigmoid run subparallel to the straight vein.
Thin section OM12 B35 S b is oriented parallel to bedding. It consists of a black impregnated sigmoidal shaped vein with a reactivated white center and a wackestone host rock which is cut by many microveins (fig. 4.16 A). The strike of microveins changes from E to NE and back to E (from E-W). Note that the strike of the microveins next to the deflected area is similar to the black impregnated vein from OM12 B35 N some cm to the north.
Each black impregnated microvein within the deflected area is straight and not bend. The change of the strike direction is caused by stylolites oriented perpendicular to bedding. Their strike changes track from N to NE and back to N (from E-W) as indicated in figure 4.16 B. Moreover, the density of microveins increases towards the deflected area.
The black impregnated microveins are cross-cut by a set of white microveins. Figure 4.16 C shows a white microvein which cross-cuts a black impregnated microvein. Moreover, the white microvein gets approximately 20° deflected by the black microvein similar to field observations (compare to fig. 2.10).
Within microveins, solid bitumen occurs around crystals (fig. 4.17). In contrast, within the macroscopically visible black impregnated area, it occurs as small inclusions, which are often arranged as trials. Moreover, the sample contains mosaic type intracrystal solid bitumen particles with some of these having a wing shape (compare appendix fig. 7). Low reflective homogeneous type solid bitumen occurs associated with solution structures (fig. 4.18) or along stylolites.
The reactivated white part consist of large blocky euhedral calcite, whereas the calcite in the black impregnated part is also blocky and smaller.

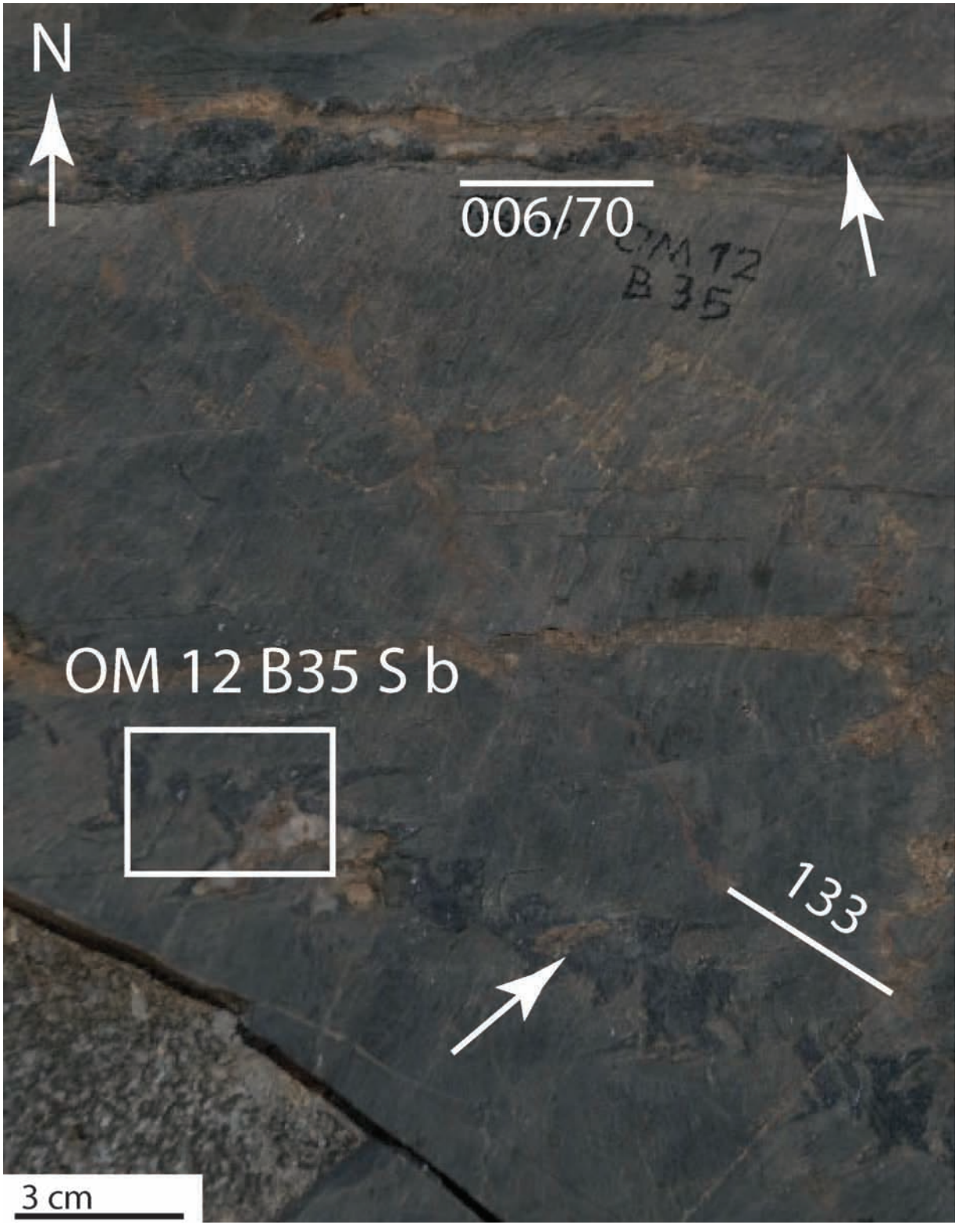


Figure 4.15: Outcrop photograph of sample OM12 B35: The northern part of the sample contains a straight black vein (sample OM12 B35 N) which is oriented 006/70. Within the southern part, there is an array of en échelon arranged sigmoidal shaped (sig) veins (sample OM12 B35 S), which strike 133°. The tip of each vein is subparallel to the straight vein of OM 12 B35 N. The white box indicates the position of thin section OM12 B35 S b. White arrows show black impregnated structures.

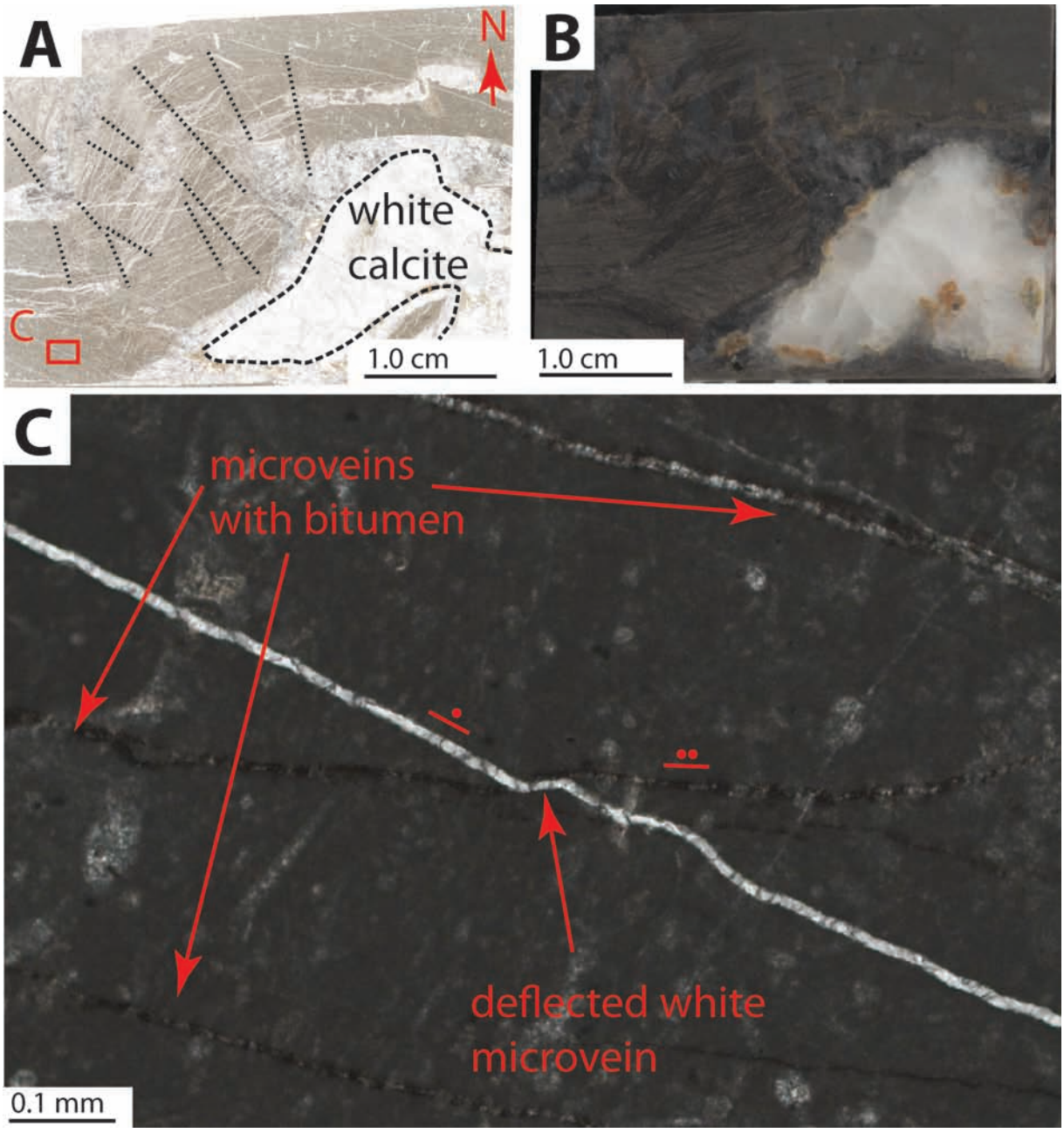


Figure 4.16: Microphotographs of sample OM12 B35 S b. ***A*:** Overview image under transmitted, non-polarised light. Small dashed lines indicate stylolites which change track from N to NW and back to N (from E-W). Red box shows position of microphotograph C. ***B*:** Overview image of the block from which the thin section was made. Reflected light. ***C*:** White microvein which cross-cuts a black impregnated microvein containing solid bitumen. Note that the white microvein gets deflected and changes track. Age relationships are indicated by dots. Transmitted, plane-polarised light.

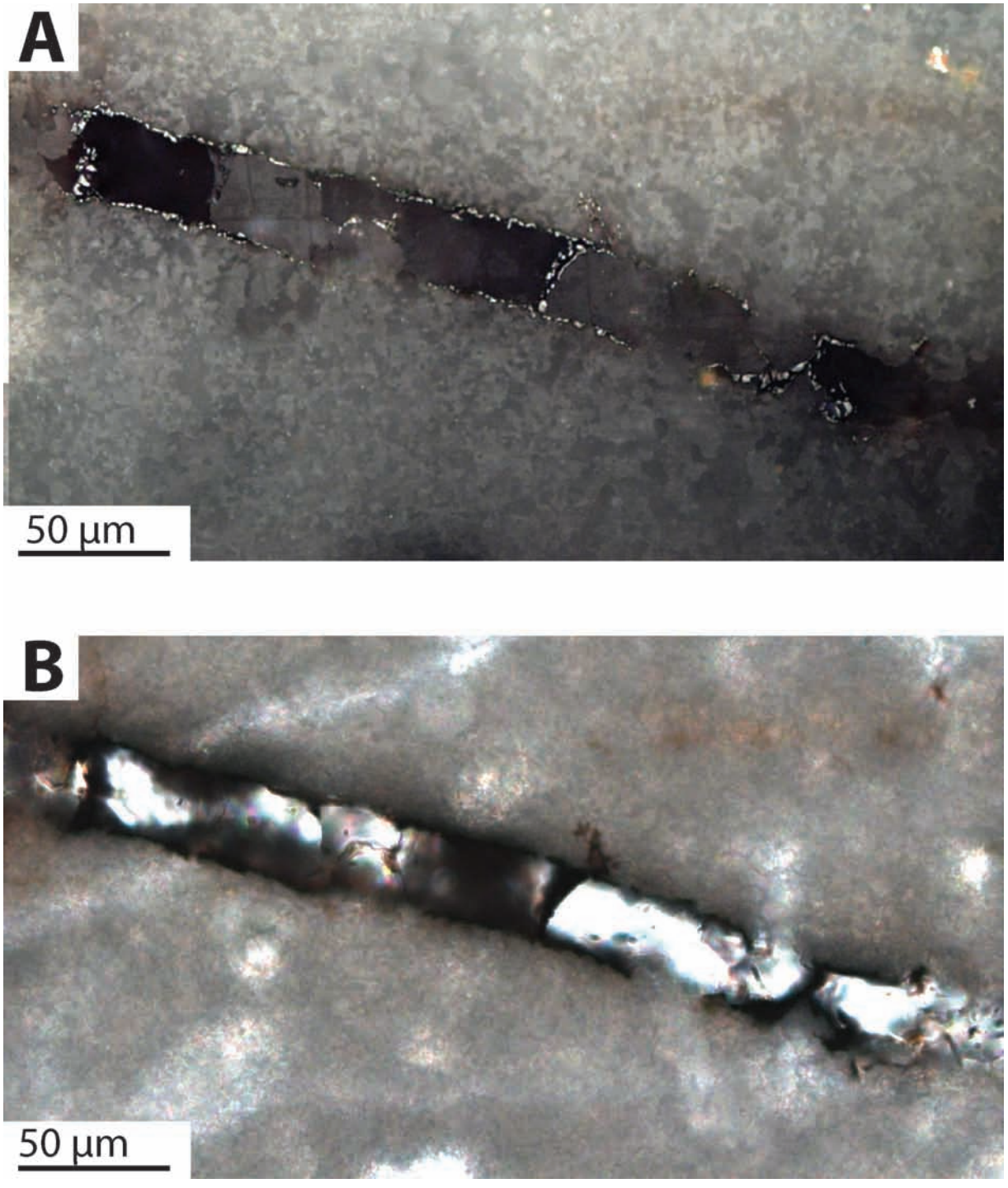


Figure 4.17: Microphotographs of thin section OM12 B35 S b showing the same section with reflected light under immersion oil (***A***) and transmitted, plane-polarised light under immersion oil (***B***): Microvein with solid bitumen around calcite crystals.

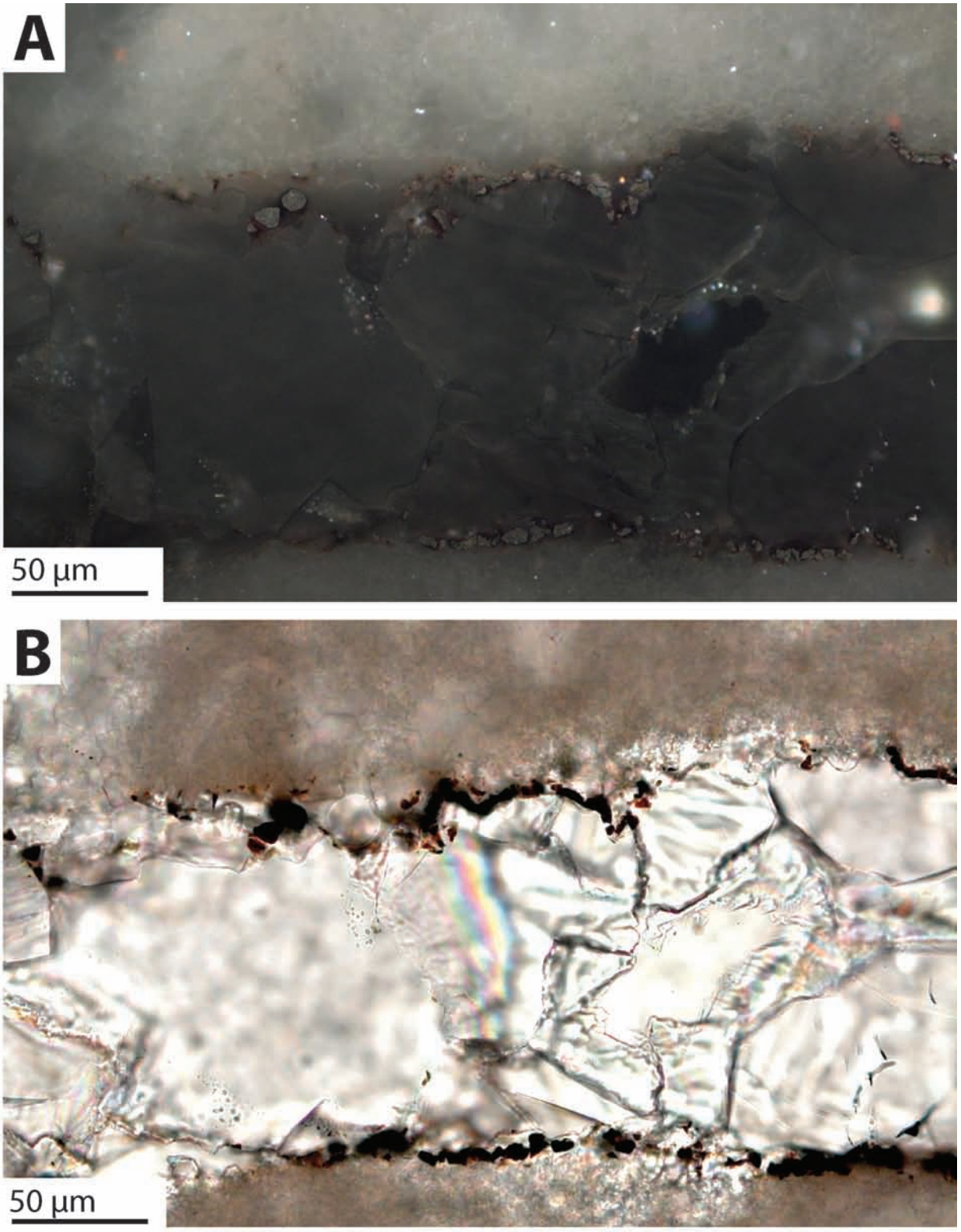


Figure 4.18: Microphotographs of thin section OM12 B35 S b showing the same section with reflected light under immersion oil (***A***) and transmitted, plane-polarised light under immersion oil (***B***): Homogenous low reflective solid bitumen in solution structures at a vein margin. Open voids at the margins indicate solution. Calcite crystals have curved or serrate boundaries where solution occurs.

OM12 B21

Sample OM12 B21 was taken from the Natih B member at Ghul ramps (see fig. 2.1). The vein is oriented 351/80 and cross-cuts at least five, 30 cm thick, sedimentary layers within the Natih B member. The thin section is oriented normal to bedding and perpendicular to the vein. Figure 4.20 shows a number of overview images of the block from which the thin section was cut and from the thin section. The sample can be subdivided into four parts which are typical for all Natih B veins. (1) A wakestone or packstone host rock with abundant fossils. (2) Calcite cemented vein which often has a syntaxial competition of growth texture. (3) Vein interior of white dolomite showing brownish polarisation colours. (4) Vein infill at the bottom which consists of host rock clasts and fine sediment. Dolomite was identified by point XRD measurements directly on the rock sample using a 2D-XRD system Bruker D8 ADVANCE GADDS (Reuning, 2012).

Figure 4.22 shows the competition of growth texture in the calcite cemented part of the vein. Crystals started growing on clasts, the vein margin and on the interface between calcite cemented vein and sediment infill at the bottom of the vein. The distance between the clast and the dolomite in the center is constant, forming a rounded boundary between the dolomite and the calcite cemented vein (fig. 4.20). Moreover, crystals grow around the whole clasts, which are not cracked and the bottom of the vein had been filled by loose sediment which was cemented afterwards. This indicates that the vein opened in one single increment.

All Natih B vein samples contain veins which are not straight. These veins have a high sinuosity and may end with a high aperture close to the tips. Their growth is in some places influenced by fossils. In other places they cross-cut fossils. They often have the same sediment infill at the bottom as the main vein.

Solid bitumen is found within the host rock as homogeneous type or as solid bitumen trails in both, fossil shells and vein filling calcite crystals. Some solid bitumen trails in the vein are oriented parallel to the vein margin. Nevertheless, most trails run perpendicular to the vein margin and extend into the dolomite in the center. Bitumen trails cross-cut the border between dolomite and calcite vein fill. Within the dolomite, bitumen trails fan out compared to the calcite vein fill. The whole vein is reactivated by small calcite veins which cross-cut the boundary between the interior mineral fill and the calcite cemented area. At least some of these veins have a halo which impregnates the dolomite in the center black. Within the dolomite center, there is an area of low deformed calcite, in which mosaic type bitumen occurs (fig.4.21). Other Natih B veins, such as sample OM12 B19, also contain mosaic type bitumen within reactivations. Bedding parallel stylolites are found within the host rock. In other Natih B veins, e.g. sample OM12 B19, low reflective homogeneous type solid bitumen

occurs along these stylolites, âĂć which cut perpendicular through the vein. Cathodoluminescense (fig. 4.19) shows a luminescence pattern within the calcite vein fill. The pattern consists of a rim around clasts with weak luminescence. Within the calcite part of the vein, cores of crystals have almost no luminescence whereas the rim zones of crystals do often show luminescence. However, these are not growth zonations, because the boundaries between different luminating zones are not straight. Moreover, single crystals next to each other can have different luminescence resulting in a network pattern. Calcite cemented areas at the bottom of veins show similar luminescence compared to the calcite vein fill. Dolomite has a pink-darkred luminescence colour whereas the low deformed calcite

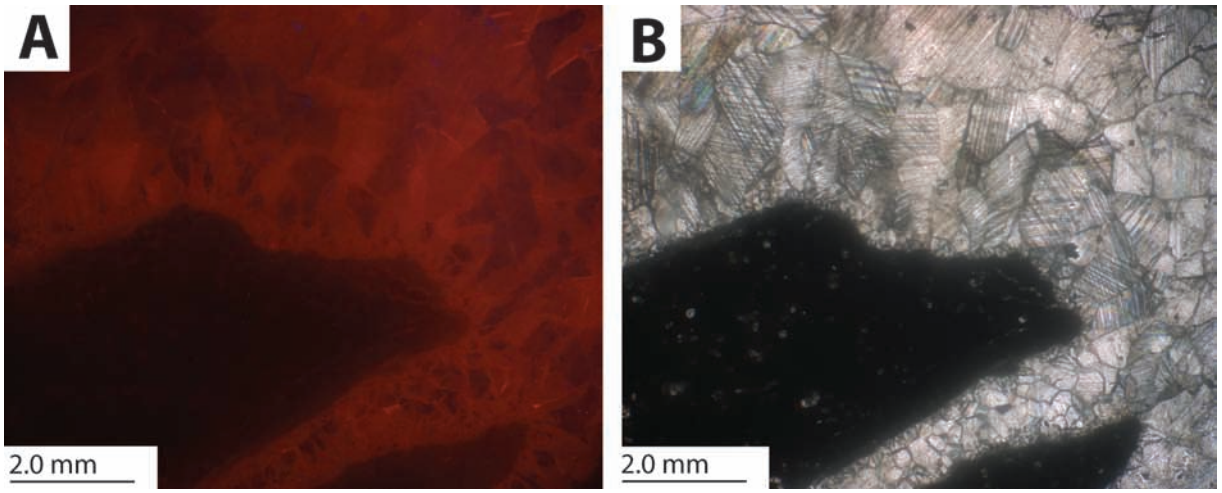


Figure 4.19: Micrographs of a section of thin section OM12 B21b with cathodoluminescences (***A***) and transmitted, plane-polarised light (***B***): Luminescence of calcite around clast. The luminescence shows a network pattern with different darkred colours. There is no growth zonation in calcite crystals visible. Note the low luminescence rim around the clast.

and small reactivations are non-luminescent (compare appendix fig. 4).

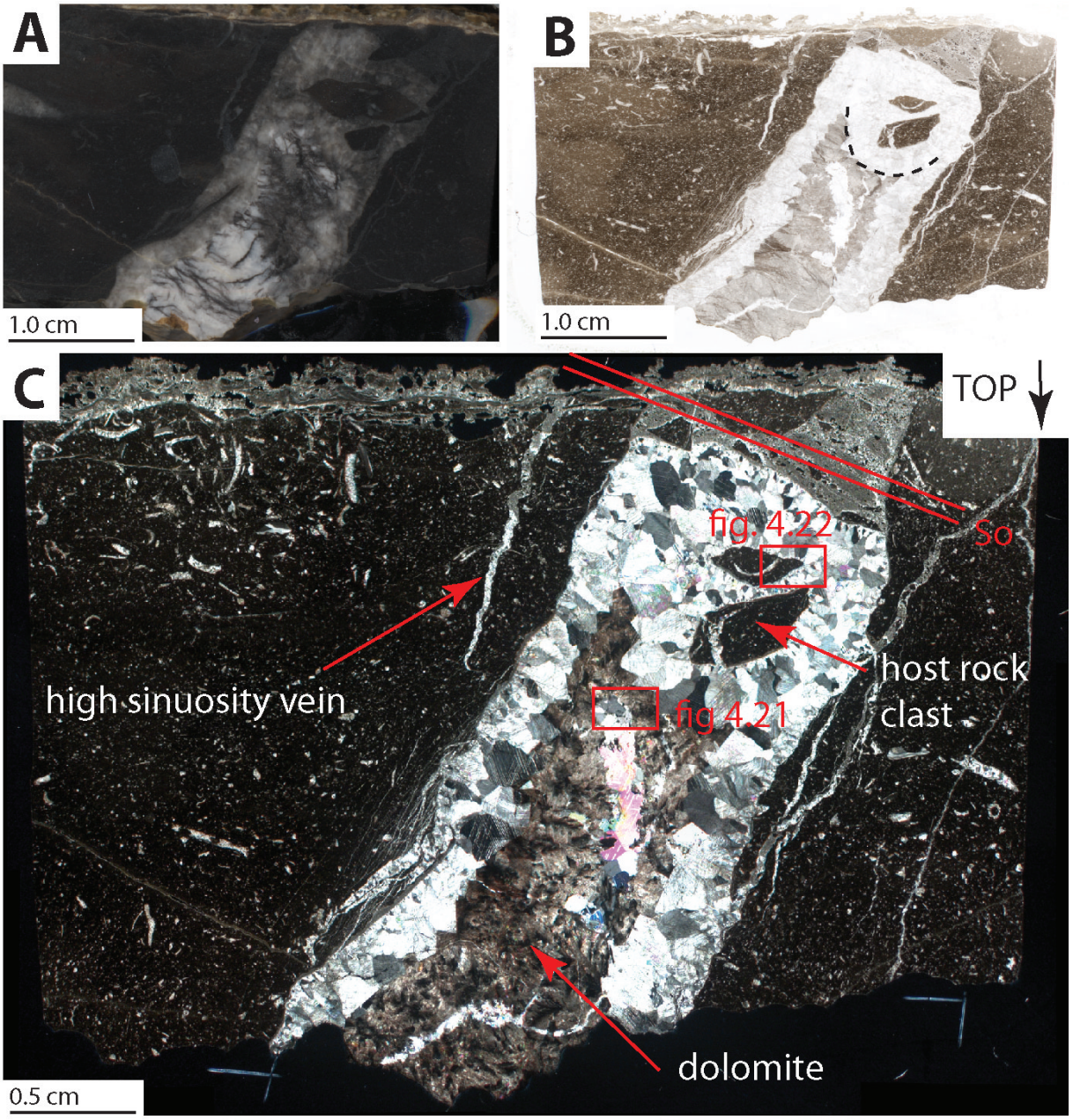


Figure 4.20: Overview images of sample OM12 B21. ***A*:** Overview image of the block from which thin section OM12 B21 b was made. Reflected light. ***B*:** Overview image of thin section OM12 B21 b. Transmitted, non-polarised light. Dashed line indicates curved boundary between dolomite and syntaxial calcite. The boundary formed due to competition of growth around the clast. ***C*:** Stitched microphotographs of thin section OM12 B21 b. The sample can be subdivided into four parts: host rock, calcite cemented vein at the margin, dolomite in the vein center and sediment fill at the bottom indicated by the bedding S0. Red boxes show locations of microphotographs in fig. 4.21 and fig. 4.22. Transmitted, crossed-polarised light.

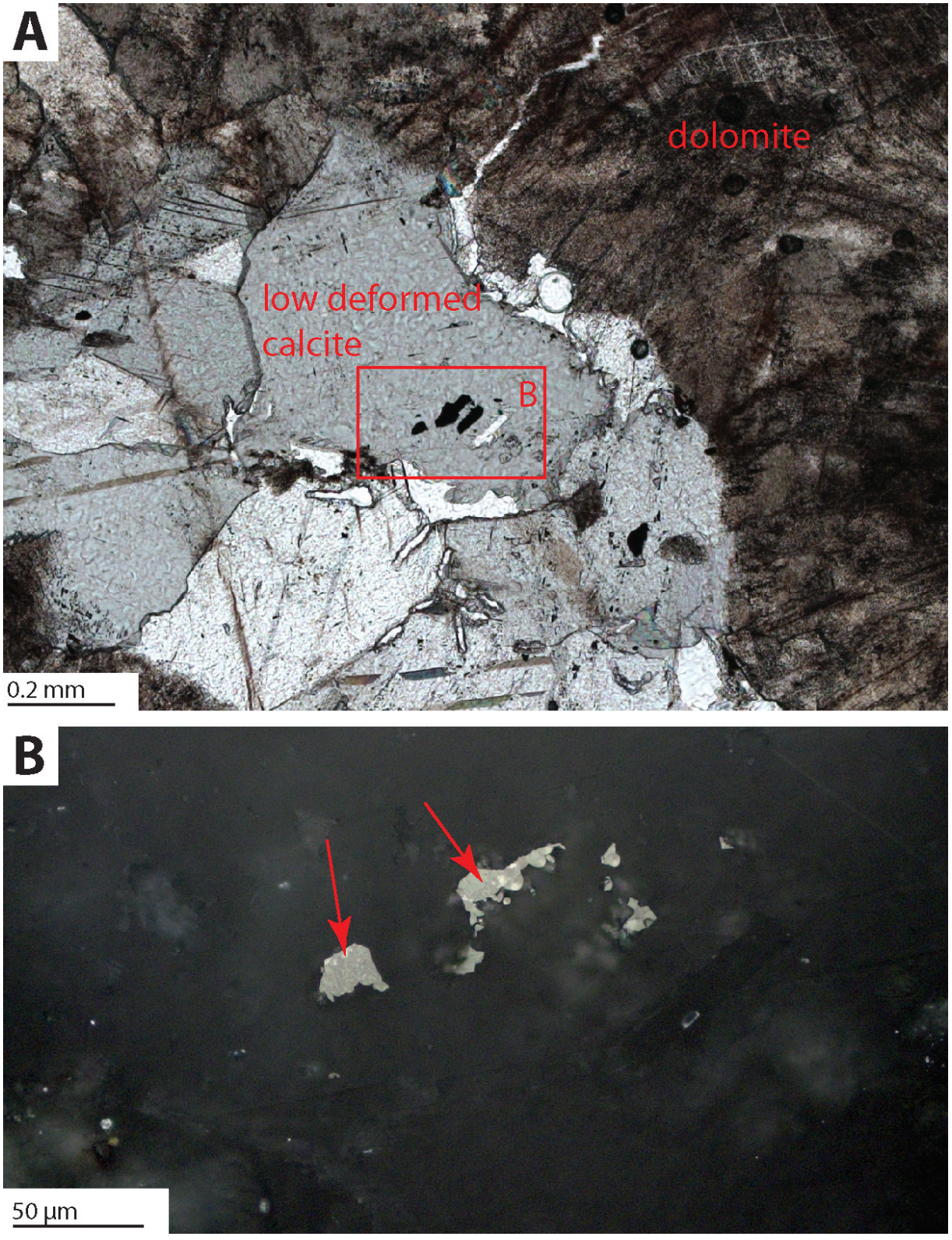


Figure 4.21: Microphotographs of sample OM12 B21b. ***A*:** Low deformed calcite within dolomite. Black particles within low deformed calcite is mosaic type solid bitumen. Red box is indicating location of microphotograph B. Transmitted, crossed-polarised light. ***B*:** Mosaic type solid bitumen (red arrows). Reflected light under immersion oil.

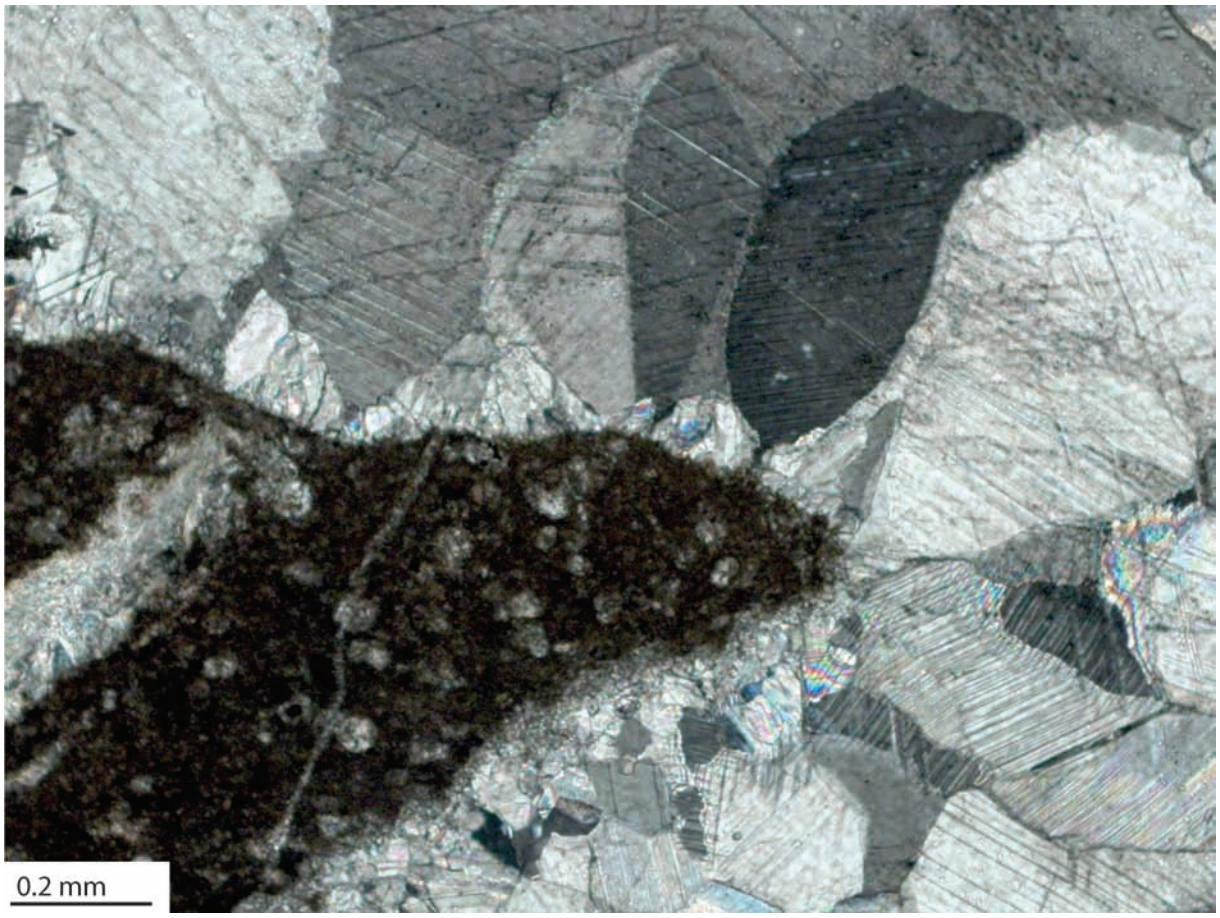


Figure 4.22: Microphotograph of thin section OM12 B21b. Calcite crystals originate at the clast and grow around it. It shows a syntaxial competition of growth texture. This texture forms, if some crystals grow fast into an existing open void and are therefore becoming larger by consuming space of crystals which grow more slowly. Transmitted, crossed-polarised light.

OM12 B09

Sample OM12 B09 was taken from a branch of a fault at the entrance of Wadi Nakhr (compare fig. 1.4 and fig. 2.2 A, C). The branch is oriented 009/65 and situated approximately 0.5 m to the north of the main fault. Figure 4.23 shows an outcrop photograph of the original sample location. The

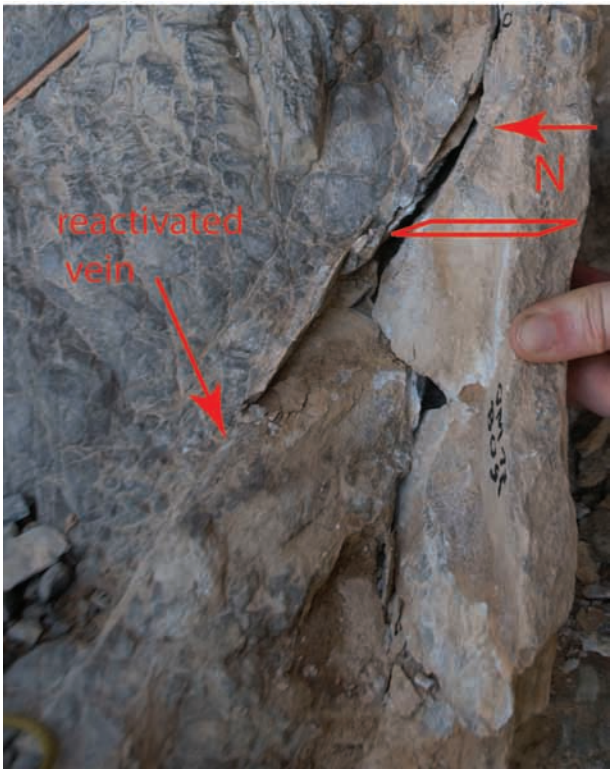


Figure 4.23: Outcrop photograph of sample OM12 B09. Sample OM B09 was taken from a branch, which is oriented 009/65, of a fault (see fig. 1.4 and fig. 2.2 D) at the entrance of Wadi Nakhr. It consists of the black coloured branch, a piece of host rock and a reactivated black impregnated vein. The trapezium shows the location of thin section OM12 B09. Thumb holding sample OM12 B09 is for scale. Looking at a wall. Arrow points to north.

sample consists of the black impregnated side branch to the south, a piece of host rock in the center and a thin, reactivated vein to the north. This is all covered by thin section OM12 B09 which is oriented horizontally.

The overview images (fig. 4.24) reveal that the sample can be segmented into five parts which follow one another from north to south: : (1) Elongated white calcite. (2) Black impregnated blocky calcite rim. (1) and (2) are both part of a reactivated black impregnated vein. (3) Wackestone to packstone host rock with abundant microveins. (4) Black impregnated calcite vein with host rock inclusion bands. (5) Black impregnated calcite vein.

No solid bitumen trails could be unambiguously identified within thin section OM12 B09. However,

there is black impregnated calcite as shown in figure 4.24 A. Close-up microphotographs (fig. 4.25 A, B) of a black impregnated calcite crystal show that most inclusions of unknown type are oriented along one direction of cleavage planes. Moreover, there are inclusion aggregates with straight boundaries along cleavage. This has also been observed in the field within in fault calcite, which often has a very clear colour zonation between black/grey and white with straight boundaries along cleavage planes. Besides, there are almost inclusion free areas with inclusion rich borders (fig. 4.25). Some inclusions appear black under plane-polarised light. As very small gas and brine inclusions may also appear black under the microscope, the black colour is not diagnostic for solid bitumen inclusions. In contrast, gas and brine inclusions are transparent macroscopically. Figure 4.27 A shows host rock inclusions and an inclusion rich area which seems to be solid bitumen under transmitted, plane-polarised light. With reflected light under immersion oil, however, it is not possible to see the small inclusions (4.27 A). Therefore, other methods, such as scanning electron microscopy have to be applied.

The wakestone to packstone host rock is cut by numerous microveins (fig. 4.25 C). Most microveins run E-W to SE-NW. However, there is one microvein which cross-cuts the other microveins in a NE-SW direction. Within this microvein solid bitumen particles could be identified. The fossils within the host rock of sample OM12 B09 are undeformed apart from the previous described microveins.

The host rock, the white calcite and the black impregnated part have a similar dark red luminescence colour. There are no growth zonations within calcite crystals visible. Figure 4.26 shows a cathodoluminescence micrograph of the black impregnated calcite area. Black spots in plane-polarised light stay black with cathodoluminescence as a non-luminescence phase whereas others have a bright luminescence colour and some disappear (they have the same luminescence as surrounding minerals).

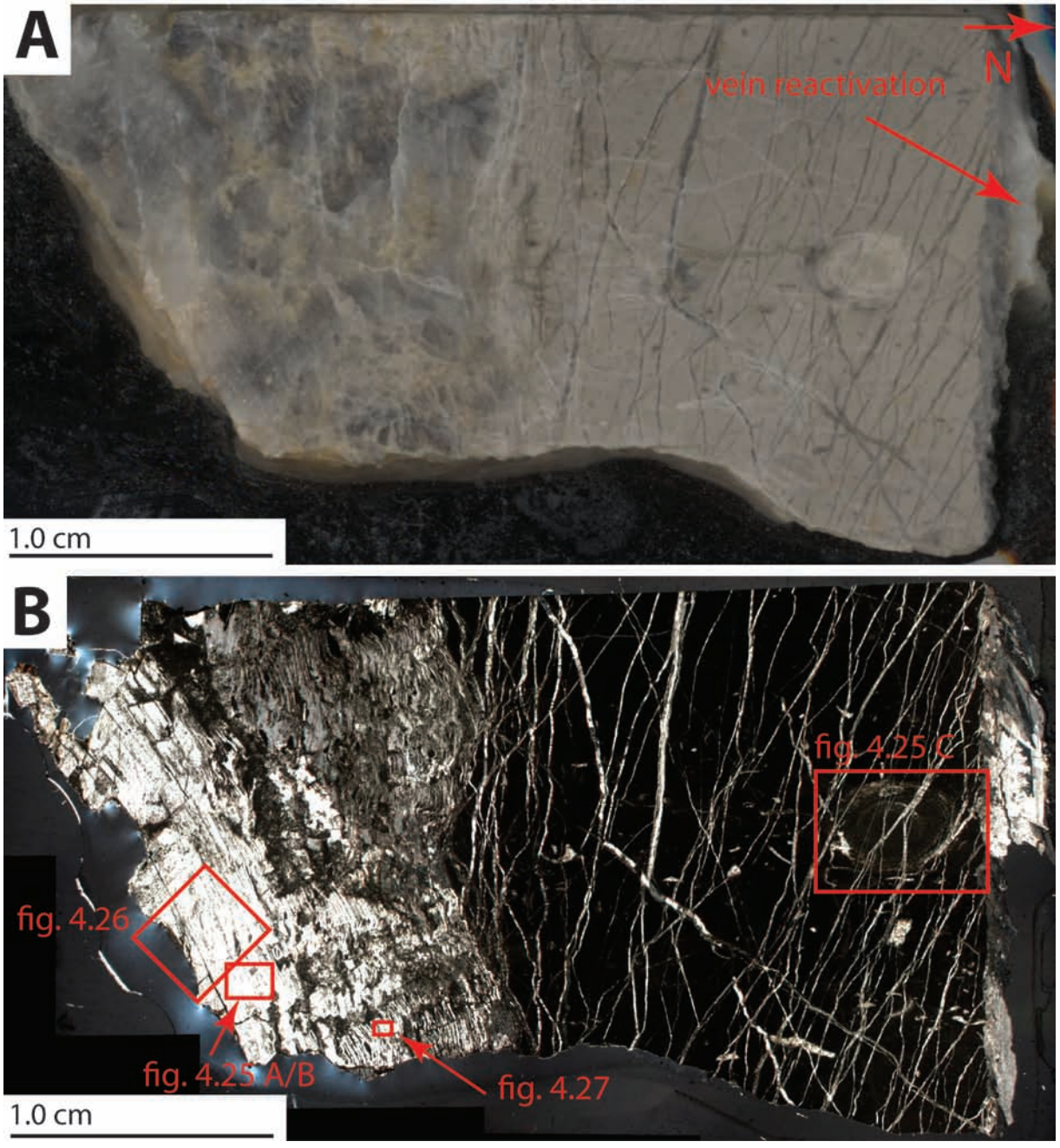


Figure 4.24: Overview images of sample OM12 B09. ***A*:** Overview image of the block the thin section was made of. Reflected light. ***B*:** Stitched microphotograph of thin section OM12 B09. Red boxes indicate location of micrographs in fig 4.25, fig. 4.26 and fig. 4.27. Transmitted, crossed-polarised light.

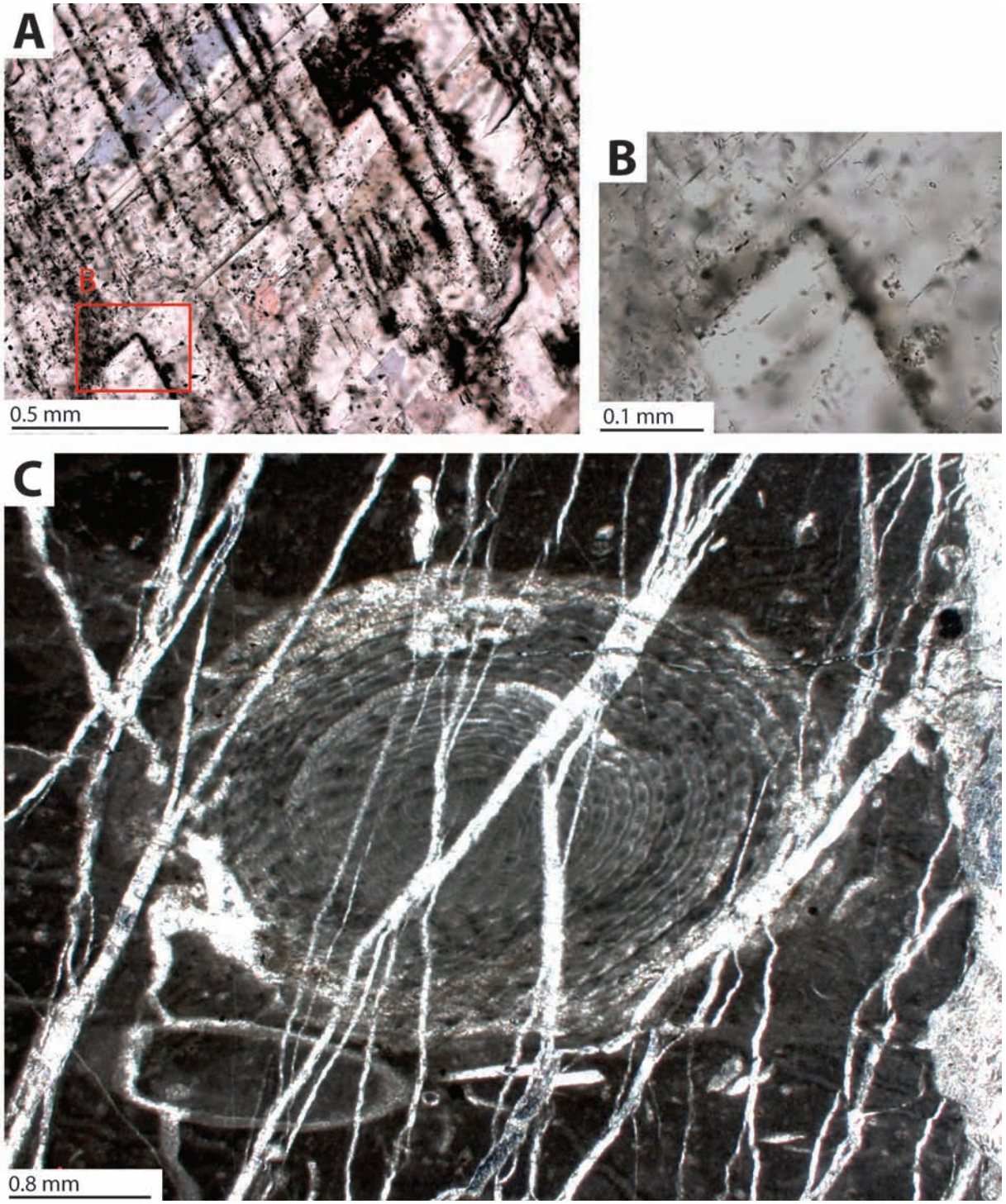


Figure 4.25: Microphotographs of thin section OM12 B09 with transmitted, plane-polarised light. ***A*:** Calcite crystal with unknown inclusions forming trails subparallel to cleavage. The inclusion accumulation at the top has straight boundaries in two directions. The boundaries form a typical calcite cleavage angle. An almost inclusion free area with inclusion rich boundaries, is located at the bottom. ***B*:** Close-up of inclusion rich boundary of inclusion free area. It is not clear if black inclusions contain solid bitumen, because there is no brown background colour. Resolution under reflected light with immersion oil is too low to identify such small solid bitumen inclusions and most inclusions appear transparent. ***C*:** Fossil which is cut by microveins. The fossil is not plastically deformed.

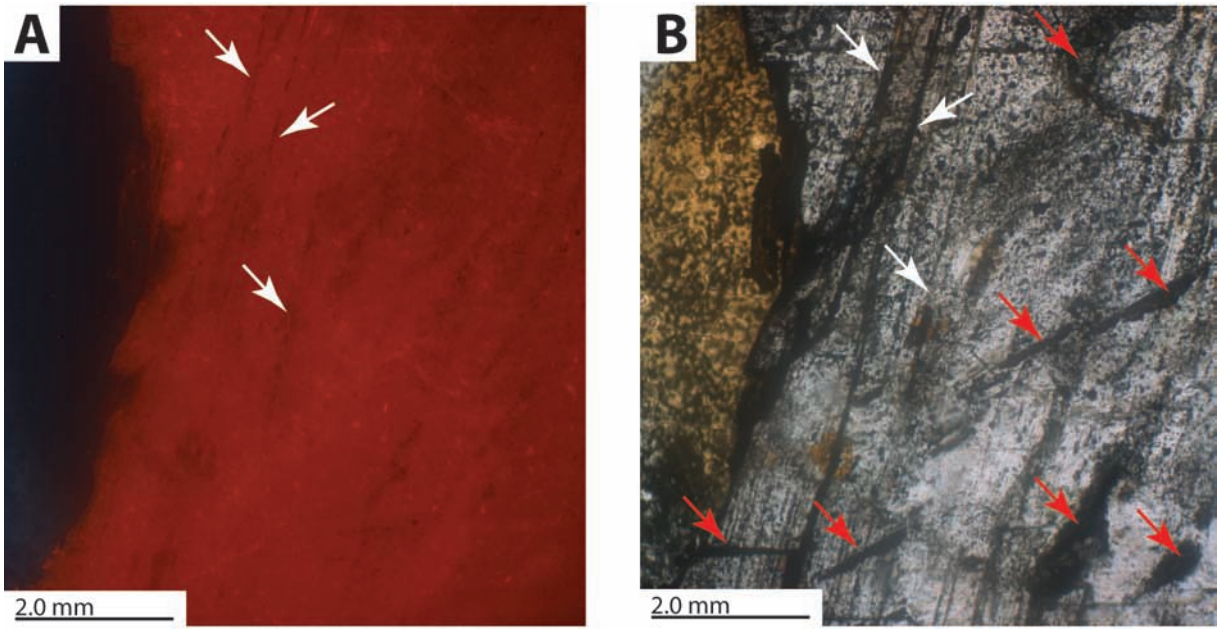


Figure 4.26: Micrographs of a section in thin section OM12 B09 with cathodoluminescences (***A***) and transmitted, plane-polarised light (***B***): The sample has dark red luminescence colours and there are no growth zonations visible. Dark spots in transmitted light disappear under cathodoluminescenses (red arrows), whereas others stay black (white arrows).

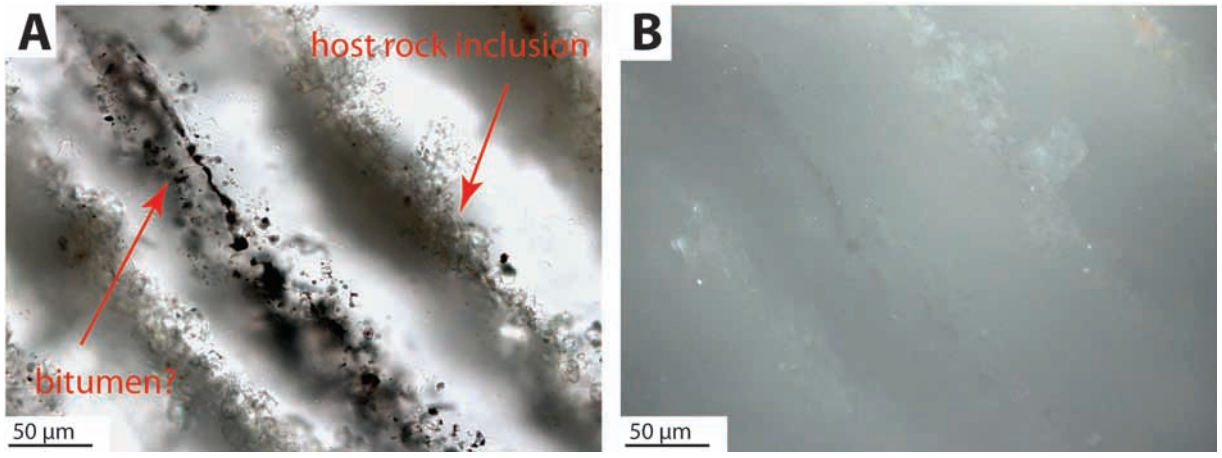


Figure 4.27: Microphotographs of thin section OM12 B35 S b showing the same section with reflected light under immersion oil (***A***) and transmitted, plane-polarised light under immersion oil (***B***). Regularly spaced host rock inclusion bands can be identified with transmitted light. Between host rock inclusion bands a band running subparallel contains black inclusions. These could be very small solid bitumen inclusions. Yet, it is not possible to identify them with reflected light under immersion oil.

OM12 B13

Sample OM12 B13 is an unoriented Natih B source rock sample from a shaly sequence. The thin section was made out of a polished block. The pieces were oriented perpendicular to bedding (see fig. 4.28 A) before block preparation. Most of the pieces contain fragmented oyster shells. The voids are filled with high reflective homogeneous type solid bitumen veins which are oriented approximately perpendicular to bedding. Figure 4.28 C shows a part of an oyster shell (compare to microphotograph B) which is broken into multiple fragments which are separated by solid bitumen veins. Moreover, there is a clear vertical offset indicated by red slip arrows along several solid bitumen veins.

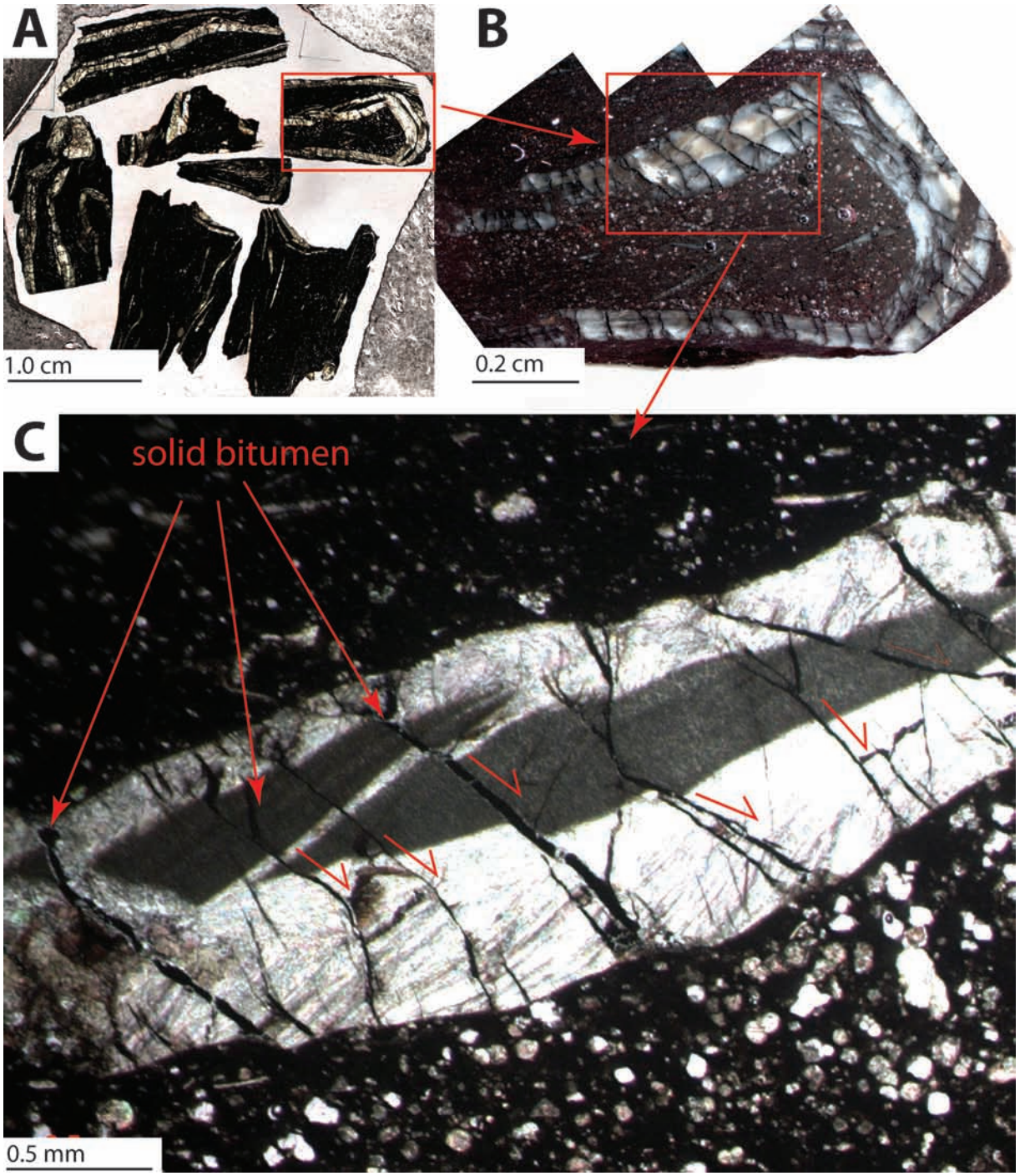


Figure 4.28: Microphotographs of thin section OM12 B13. ***A*:** Stitched overview image with transmitted, plane-polarised light. ***B*:** Oyster shell fragments with solid bitumen veins are oriented perpendicular to bedding. Bedding is assumed to be parallel to the limp of the oyster shell. Reflected, plane-polarised light. ***C*:** Vertical displacement along solid bitumen veins indicated by red slip arrows. Transmitted, plane-polarised light.

OM12 B28

Sample OM12 B28 consists of a branch of a fault at the entrance of Wadi Nakhr. The branch is oriented 022/84.

Thin section OM12 B28 is oriented perpendicular to bedding and shows a section through the whole branch. Low reflective homogeneous type solid bitumen occurs at the margins within solution structures. Only one intracrystal solid bitumen trail which is oriented perpendicular to the branche's plane was identified.

Cathodoluminescence (fig. 4.29) shows growth zonations within calcite crystals. The different luminescence colours range from weak luminescent to bright red luminescent. Some crystals are deformed and sheared along intracrystal slip planes. Moreover, there are non-luminescence microvein reactivations (compare appendix fig. 6).

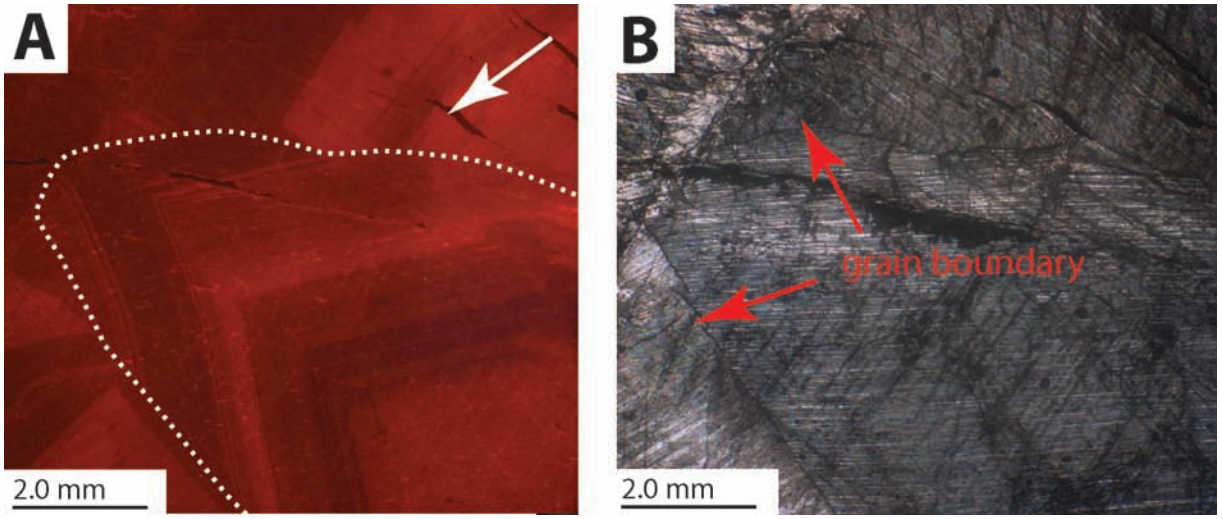


Figure 4.29: Micrographs of a section in thin section OM12 B28 with cathodoluminescences (***A***) and transmitted, plane-polarised light (***B***): Calcite shows interior growth zonation. Luminescense colours are dark red to bright red. Dashed line indicates grain boundary. White arrow indicates hole.

4.1.3 Summary of Microscopic Observations

Microstructure of veins and faults

Microscopy revealed that the microstructure of Natih A veins differ from faults and Natih B veins. Table 4.1.1 shows an overview of analysed thin sections with associated features listed systematically. Natih A straight veins and en échelon veins show similar microtectonic features. They always consist of blocky, black impregnated calcite which can be reactivated by small scale reactivations or by large reactivations which are visible macroscopically. Large reactivations consist of blocky or elongated

Table 4.1.1: The overview of analysed thin sections lists systematically important features which were found during microscopy. Sample OM12 B13 is not shown, because it is a host rock sample which is not comparable to the others. Reactivations were subdivided into small scale and large reactivations. Large reactivations were grouped into elongated or blocky calcite fill. Used abbreviations are recorded in the abbreviation table.

Thin	**Type**	**HRI**	**Stylolites**	**Secondary**	**Reactivation**	**Solid bitumen**		
section				minerals		trails	mosaic	low refl.
OM12 B09	fa	+	-	-	elongated	-	-	-
OM12 B28	fa	-	+	-	blocky	+	-	+
OM12 B15	svB	-	+	dol	-	+	-	-
OM12 B19	svB	-	+	dol	sc	+	+	+
OM12 B21	svB	-	+	dol	sc	+	-	-
OM12 B21 b	svB	+	+	dol	sc	+	+	-
OM12 B23	svA	-	+	qz	elongated	+	-	-
SV 002b	svA	+	+	-	blocky	+	+	-
SV-2010-02	svA	+	+	-	blocky	+	+	-
OM12 B30 S	svA	-	+	qz	elongated	+	+	+
OM12 B30 S b	svA	-	+	-	elongated	+	+	+
OM12 B35 N	svA	-	-	-	-	+	-	-
OM12 B31	svA	+	+	qz	sc	+	+	+
OM12 B29	svA	+	+	-	blocky	+	-	-
OM12 B01	ee(s)	+	+	-	sc	+	-	-
OM12 B03	ee(s)	+	+	-	-	+	-	+
OM12 B04	ee(s)	+	+	-	-	+	-	-
OM12 B37	ee(s)	+	+	-	sc	+	-	-
OM12 B32	ee(s)	-	+	qz	blocky	+	+	+
OM12 B14	ee(s)	+	+	-	-	+	-	+
OM12 B25 N	ee(d)	+	-	qz	blocky	+	-	-
OM12 B35 S	sig	-	+	-	-	+	-	-
OM12 B35 S b	sig	-	+	-	blocky	+	+	+

calcite in the center of the vein. Quartz often occurs within these reactivations. At vein margins, host rock inclusion bands often occur which are a sign of extensive cracking and resealing of the vein. Moreover, microveins are abundant within the host rock. Stylolites occur either as bedding parallel or as vein parallel stylolites. Vein parallel stylolites run subparallel to the host rock-vein interface or the reactivation-vein interface. Bedding parallel stylolites cut the vein-host rock interface. Many samples show solution structures, such as open voids or serrate grain boundaries, which are difficult to see under transmitted light. Reflected light under immersion oil, however, helps identifying solution due to its ability to display surface features at high detail. Cathodoluminescence microscopy shows no growth zonations of calcite crystals which have a dark red luminescence colour. Reactivations show only small or no difference in luminescense compared to the black impregnated part of the vein.

Natih B veins are often of high sinuosity with host rock clasts and calcite mud infill at the bottom. They might have been straight by the time of their formation and layer perpendicular shortening is assumed to have caused folding of the vein. This is assumed to cause high sinuosity Natih B veins. Loose material at the vein bottom is cemented with blocky calcite. Moreover, they have a syntaxial, competition of growth texture in the calcite cemented parts. The syntaxial growth starts at the vein bottom, the vein margins and around single clasts. Vein rims often consist of a zone between calcite cemented vein and pelagic host rock which is dark under transmitted light. Syntaxial calcite cement at the vein margin can reach deeper than mud vein infill at the bottom (sample OM12 B19). Therefore, a first calcite overgrowth of the open vein has occurred before sediment filled the bottom of the vein. Dolomite occurs in the center of all analysed big veins as a second phase after calcite cementation. Cathodoluminescense microscopy shows a chaotic luminescence distribution of dark red and red. The contact is wavy and does not indicate growth zonations. Dark luminescense occurs in the center of single crystals. Calcite cement between mud infill at the bottom of veins shows similar luminescence. Natih B veins can be reactivated by microveins and cross-cut by bedding parallel stylolites.

Fault samples consist of large blocky calcite crystals which are in some places highly deformed indicated by curved twins. Host rock inclusion bands as well as stylolites and reactivations occur. Cathodoluminescence microscopy of sample OM12 B28 shows clear growth zonations in calcite crystals. Moreover, colour zonations between black/grey and white in calcite rhombohedra, which are observed macroscopically, are also found as inclusion rich and inclusion poor areas which are separated by cleavage planes.

Solid bitumen in veins and faults

Different types of solid bitumen were distinguished. They have different optical properties, morphology and relations to the microstructure. All analysed solid bitumen particles do not show fluorescences under UV-light.

Solid bitumen trails consist of lined up intracrystal inclusions. Inclusions usually have a brown background colour under transmitted light and a negative crystal shape with solid bitumen as a coating of the inclusion, which is visible under reflected light. Large solid bitumen trails can be identified in reflected light overview images as black, elongated areas and in transmitted light overview images as black veinlets. Therefore, overlays of reflected and transmitted light overview images help identifying areas of interest. Black veinlets have not been found in fault samples. Solid bitumen trails are often straight along cleavage planes, but they are also curved in some places. The orientation of inclusion trails within one thin section can be uniform with preferred orientations parallel and/or perpendicular to the vein. This is not consistent as other veins show chaotic orientations of trails. Multiple trails can be oriented as a fan and meet in one point. Trails often end at grain boundaries, however, there are also trails which cut grain boundaries, interfaces between dolomite and calcite vein (foe Natih B veins) or vein- host rock interfaces. Moreover, solid bitumen trails also occur in Natih A and B host rocks in fossils. Solid bitumen trails occur in all vein samples. In fault samples, only one solid bitumen trail could be identified (sample OM12 B28), although, four more samples were prepared as blocks and analysed with reflected light.

Mosaic type solid bitumen occurs intracrystal and on grain boundaries in sample SV2010 002. It often occurs along or within reactivations and in calcites which lack solid bitumen trails. These reactivations can be very small and can not always be macroscopically visible. The particles have straight boundaries and can have a negative crystal shape. Mosaic type solid bitumen is found in all types of veins. Fault samples do not contain mosaic type solid bitumen.

Low reflective solid bitumen is always associated with solution structures. It usually occurs as angular particles at rims of solution structures and never occurs directly incorporated into twinned calcite crystals. Solution structures containing low reflective solid bitumen can often be identified as stylolites. Besides, they are found along serrate grain boundaries, host rock vein interfaces, microvein boundaries or fault-host rock interfaces which show solution. Low reflective solid bitumen occurs in both, vein and fault samples.

Cathodoluminescense does not show any difference in luminescence colours of solid bitumen rich areas (e.g. solid bitumen trail) and solid bitumen poor areas. Nevertheless, this method can help with the identification, because solid bitumen is non-luminescent.

4.2 Solid Bitumen Reflectance

Before measuring solid bitumen reflectance on highly polished thin sections, the methodology of polished thin section preparation had to be validated. This was done by comparison measurements which are shown in table 4.2.1 between polished blocks which were polished according to the standard procedure and highly polished thin sections which were made from the same sample. The number of measuring points was 49 or higher. The difference of all comparison measurements is lower than 0.05 % BR_r. With this, BR_r measurements on highly polished thin section are proven to be reliable.

Solid bitumen reflectance was measured on all polished thin sections of veins which contain a sufficient

Table 4.2.1: Bitumen reflectance comparison measurements between highly polished thin sections and polished blocks.

Sample	Thin section BR_r[%]	Block BR_r[%]	Difference BR_r[%]
OM12 B13	3.342	3.348	0.006
OM12 B31	0.863	0.894	0.031
OM12 B32	0.855	0.821	-0.034
OM12 SV 2010 02	3.611	3.582	-0.029

number of particles with a measurable size of at least 7 µm in diameter. These are eight thin sections from Natih A veins. The results are shown in fig 4.2.2. The measurements revealed two distinct groups of solid bitumen in veins which could be distinguished (fig. 4.30): (1) A low reflective group consisting of granular or homogeneous type solid bitumen and (2) a high reflective group consisting of mosaic type solid bitumen. The BR_r values for the low reflective solid bitumen range from BR_r = 0.86 - 0.97 % and for the high reflective group from BR_r = 3.40 - 3.76 %. The standard deviation for the low reflective group is low (0.05 - 0.15 %) whereas it is high (0.45 - 0.68 %) for the high reflective solid bitumen. The difference in the standard deviation is caused by the higher optical anisotropy of the mosaic type bitumen. Solid bitumen, or "migrabitumen" after Jacob (1989), can be classified as macerals dependent on their reflectivity. According to this, low reflective solid bitumen is classified as the maceral epi-impsonite and the mosaic type solid bitumen as cata-impsonite. Using the classification of Landis and Castaño (1995), who modified the older classification of Jacob (1989), both groups are classified as pyrobitumen.

On fault samples, it was tried two measure BR_r on two highly polished thin sections and four polished

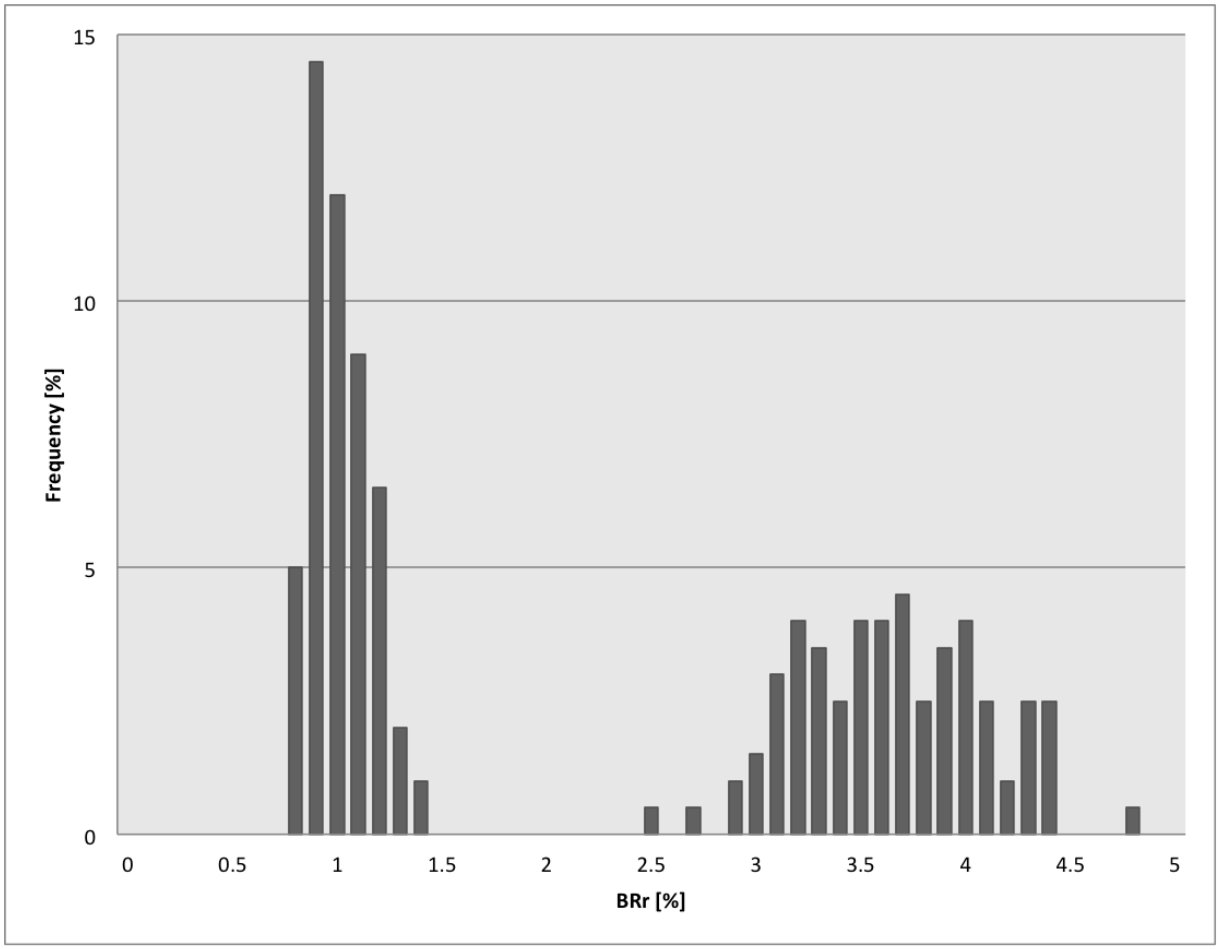


Figure 4.30: BR_r frequency distribution of sample OM12 B30S b. The BR_r measurements revealed two clearly separated groups of solid bitumen: A low reflective group with a low standard deviation and a high reflective group with a higher standard deviation due to the higher optical anisotropy of the high reflective mosaic type solid bitumen.

blocks. Unfortunately, fault samples do not contain a sufficient number of solid bitumen particles in a measurable size, therefore, it was not possible to obtain any BR_r values.

Natih B vein samples show a high variability in BR_r with chaotic distributions between BR_r = 0.7 - 4 % which were measured in the vein and the host rock. Therefore, average values over the whole sample are misleading when interpreting them as palaeotemperatures.

The Natih B source rock samples OM12 B11 - OM12 B13 were analysed under reflected light to obtain vitrinite reflectance data. Unfortunately, these samples do not contain measurable vitrinite particles. Therefore, solid bitumen reflectance was measured. The results are listed in table 4.2.3. OM 12 B11 has an average BR_r of 2.34 % with σ = 0.34 % and 100 counts. The values have a bimodal distribution with one peak maximum at 2.3 % and a second, lower peak with its maximum at BR_r = 3.2 %. Note that the high values were measured in fossils. OM12 B12 has a average BR_r

of 2.17 % with an unimodal distribution, σ = 0.26 % and 61 counts. BR_r values of OM12 B13 were measured only on bitumen veins in fossils. The average is BR_r = 3.34 % with σ = 0.10 % and 100 counts.

Table 4.2.2: Results of the BR_r measurements in vein samples from straight Natih A veins (svA) and sinistral en échelon sets (ee(s)). Shown values are grouped in high reflective and low reflective. Each group is normal distributed and the values are the average of all counts (cts.).

Thin section	Description	BR_r (low)	σ	cts	BR_r(high)	σ	cts
		[%]	[%]		[%]	[%]	
OM12 B23	svA				3.40	0.60	50
SV-2010-02	svA				3.61	0.45	100
OM12 B30 S	svA	0.87	0.14	33	3.62	0.60	31
OM12 B30 S b	svA	0.87	0.14	100	3.76	0.53	100
OM12 B31	svA	0.86	0.13	100	3.53	0.68	49
OM12 B03	ee(s)	0.86	0.05	50			
OM12 B32	ee(s)	0.86	0.15	50			
OM12 B14	ee(s)	0.92	0.10	50			

Table 4.2.3: Results of the BR_r measurements on Natih B host rock samples (hr). The values are the average of all counts (cts).

Thin section	Description	BR_r	σ	cts
		[%]	[%]	
OM12 B11	hr	2.34	0.34	100
OM12 B12	hr	2.17	0.26	61
OM12 B13	hr	3.34	0.10	100

4.3 Paleaotemperatures

VR_r values were calculated into BR_r values using equation (1.3.3).

For Natih A samples, calculated VR_r values were then calculated into palaeotemperatures with equation (1.3.4) for a hydrothermal setting. This leads to $T_{peak\ hydrothermal}$ = 163-169 °C for the low reflective solid bitumen and $T_{peak\ hydrothermal}$ = 317-325°C for the high reflective mosaic type solid bitumen.

Calculated VR_r for the Natih B source rocks are 2.4-3.6 % which corresponds to T_{burial} = 206-238 °C using equation 1.3.5.

4.4 Total Organic Carbon Content

TOC has been measured on a selection of samples including faults, straight veins from Natih A, veins from en échelon sets and the three Natih B host rock samples. Veins and fault samples have very low TOC contents (< 0.1 %), whereas the samples OM12 B11 and OM12 B13 from the shaly interval of Natih B have contents of 1.48 %. OM 12 B12, which is from a competent carbonate layer between the shaly layers, has a lower content of 0.20 %. The results are shown in table 4.4.1.

Table 4.4.1: Results of the TOC measurements from a selection of samples including faults (fa), veins from en échelon sets (ee(s), ee(d)), straight Natih A veins (svA) and Natih B source rocks (hr).

Sample	Position 40Q			TOC	Description
	East	*North*	*Locality*	[%]	
OM12 B05	0514747	2565679	Al Raheba	0.03	ee(s)
OM12 B25 S	0518928	2560834	Wadi Ghul	0.01	ee(d)
OM12 B06	0521277	2560369	Wadi Nakrh	0.03	fa
OM12 B10	0521277	2560369	Wadi Nakrh	0.03	fa
OM12 B11	0521277	2560369	Wadi Nakrh	1.48	hr
OM12 B12	0521277	2560369	Wadi Nakrh	0.20	hr
OM12 B13	0521277	2560369	Wadi Nakrh	1.48	hr
OM12 B31	0518450	2560921	Wadi Ghul	0.05	svA
OM12 B30 N	0518548	2560891	Wadi Ghul	0.09	svA

4.5 Rock-Eval Pyrolysis

Rock-Eval pyrograms of Natih B source rock samples OM12 B11-B13 and the standard are shown in figure 4.31. S_1 peaks of the samples are 0.1 $\frac{mg\ \ HC}{g\ \ rock}$ and S_2 peaks vary between 0.1 and 0.3 $\frac{mg\ \ HC}{g\ \ rock}$ (tab. 4.5.1). It was not possible to measure S_3 peaks. Hydrogen Index (HI) values range between 1 and 10 $\frac{mg\ \ HC}{g\ \ TOC}$ and production index (PI) values range between 0.25 and 0.5. T_{max} values range from 489 °C to 497°C. Due to the poor definition of S_1 and S_2 peaks, PI values are poorly reliable. Volatiles released by thermal desorption form the S_1 peak represent in situ produced hydrocarbons contained in the sample. Volatiles released from thermal cracking form the S_2 peak. The S_2 peak provides information on the overall hydrocarbon production potential. Hydrogen index is S_2 normalised with the TOC. Production Index (PI) provides information on the transformation of the kerogen into hydrocarbons and, therefore, information on the maturity. Generally, the low HIs (<150) and high T_{max} values (>460 °C) indicate that the Natih B source rock is thermally overmature and has passed the oil window (Espitalié et al., 1977).

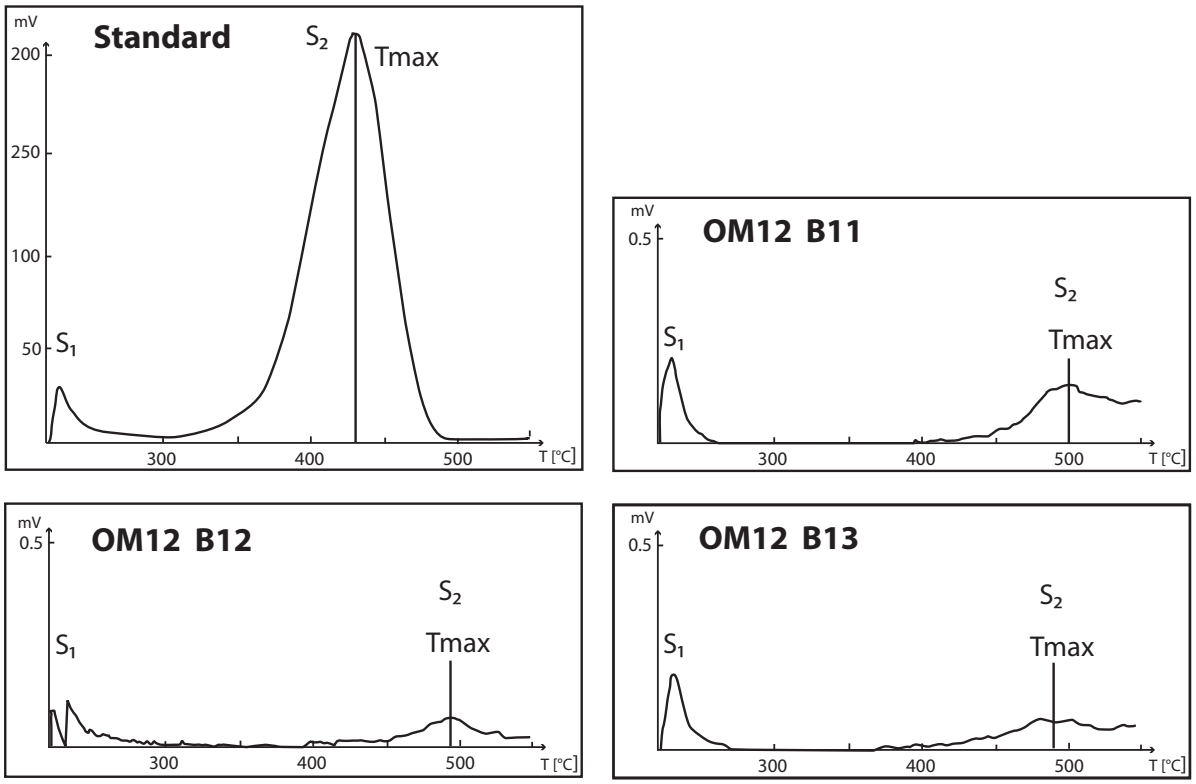


Figure 4.31: Rock-Eval pyrograms of OM12 B11-B13 and the measured standard. The T_{max} values were inserted manually and then corrected by 6 °C which is the difference between the measured and the given T_{max} of the standard. Y-axis of sample pyrograms are exaggerated 400 times compared to the standard pyrogram.

Table 4.5.1: Results of the Rock-Eval Pyrolysis of Natih B host rock samples. It was not possible to conduct Rock-Eval Pyrolysis on vein or fault samples because of their low TOC contents. HI is hydrogen index, PI is production index.

Sample	S_1 $[\frac{mgHC}{g\ \ rock}]$	S_2 $[\frac{mgHC}{g\ \ rock}]$	T_{max} [°C]	TOC [%]	HI $\frac{100 \cdot S_2}{TOC}$	PI $\frac{S_1+S_2}{S_2}$
OM12 B11	0.1	0.3	497	1.48	2	0.25
OM12 B12	0.1	0.2	492	0.20	10	0.33
OM12 B13	0.1	0.1	489	1.48	1	0.50

4.6 Residual Analysis with Scanning Electron Microscope

The amount and colour of residues on the filter prepared for the SEM differ significantly as shown in figure 4.32. With the scanning electron microscope (SEM) it is possible to take high resolution pictures in the nm range using SE and BSE detectors. Moreover, an EDX detector can identify the elemental distribution. The samples all show a high Si peak and lower peaks of O, Al, Mg, K, Fe and S with EDX overview images. Close examination of different particles show that the samples contain pyrite and quartz crystals (fig 4.33). The background signal with Si, O, Al, K and Mg is interpreted to originate from clay minerals which is supported by the SE images showing platy and sometimes idiomorphic hexagonal crystals which are typical for clay minerals. The background signal does not reflect the exact composition of the filter plates, because there is a high variation of Mg, K and Al peaks between the samples. Moreover, the filter crucible does not contain Mg.
Solid bitumen could not be identified, because there were no particles with a C peak. C detection with an EDX detector is very difficult and it is nevertheless possible that the residues do contain solid bitumen.

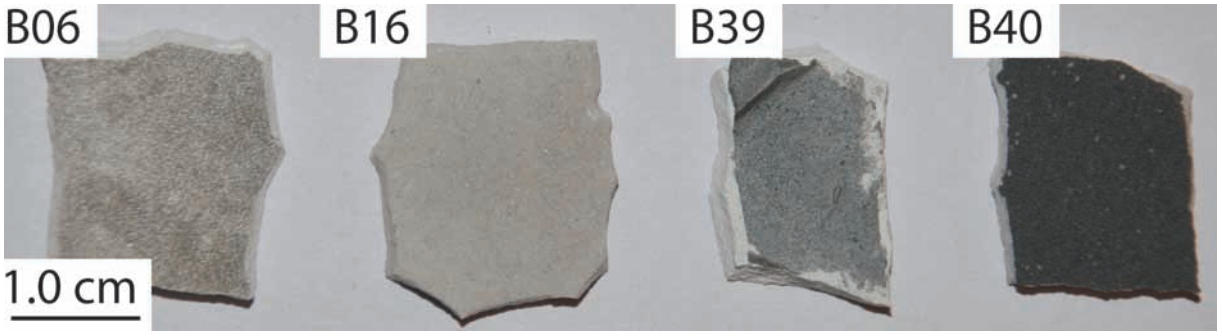
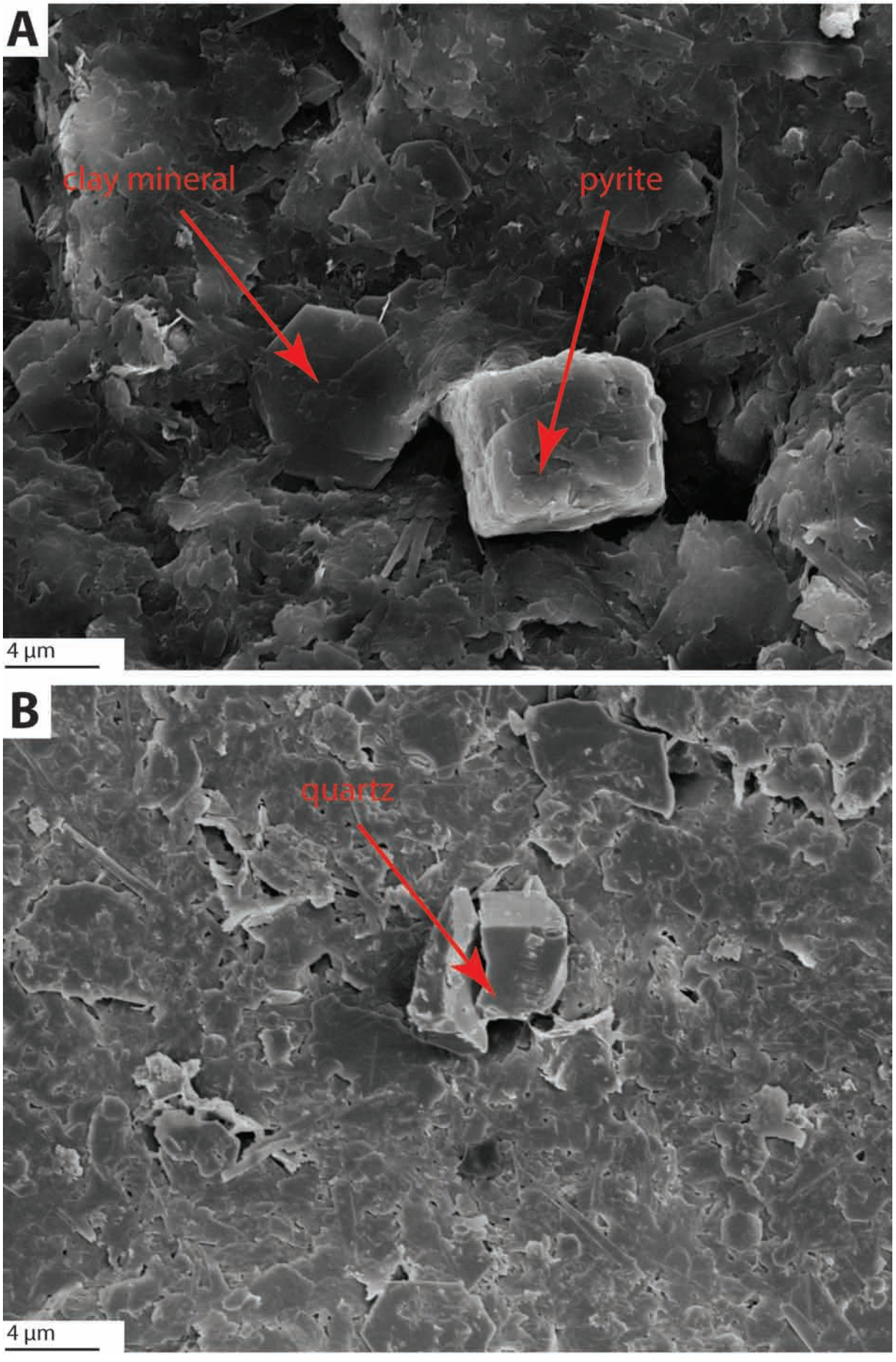


Figure 4.32: Photographs of the filter plates after filtration. The obtained residues on the filter plate have different colours from grey to black. Moreover, the amount of the residue differs significantly (between almost 0 and 10 mg).

Figure 4.33 ***(facing page)*****:** SEM images of residue from sample OM12 B40. ***A*****:** Cubic pyrite crystal and hexagonal clay mineral. SE inlens detector. ***B*****:** Quartz. SE inlens detector. The minerals in the background are part of the residue and not part of the filter.


A
clay mineral
pyrite
4 µm
B
quartz
4 µm

Chapter 5

Discussion

5.1 Palaeotemperatures

T_{burial} derived from BR_r measurements of homogeneous solid bitumen in source rocks indicate maximum burial temperature of the Natih A/B member on the southern flank of the Jebel Akhdar anticline, because the solid bitumen derived from the source rock itself and had to be formed before the peak temperature was reached. This is further supported by the Rock-Eval data. Small S_1 peaks, indicatig volatilisation of hydrocarbons in the rock, and small S_2 peaks, caused by cracking of kerogen during pyrolysis, characterize the organic matter as thermally overmature. Therefore, there is no more potential for hydrocarbon generation. Breton et al. (2004) give temperatures of <200° C for the Autochthonous units of the study area and an upper anchizone metamorphic facies which is less than the measured burial temperatures of 206-238 ° C from Natih B source rocks during this study. The thickness of the eroded overburden from maximum burial temperatures is difficult to estimate, because geothermal gradients during the obduction are assumed to be very complex. However, assuming a theoretical linear geothermal gradient of 30 $\frac{^\circ C}{km}$, 7 - 8 km of overburden are obtained.

The calculated temperatures of 317-325 °C derived from the mosaic type solid bitumen exceeds the burial temperature derived from host rock solid bitumen by approximately 100 °C. This indicates a hydrothermal event with elevated temperatures affecting only veins. Furthermore, this is supported by the mosaic texture which develops due to rapid thermal overprinting. Mosaic texture is well known from coke-structures which are often found in vitrinites close to magmatic intrusions (Khavari-Khorosani and Murchison, 1978). Holland et al. (2009b) measured temperatures of 134-221°C (pressure corrected) from quartz fluid inclusions in shear zones from the Sahtan Group approximately 1500m below the Natih. This is lower than the temperatures from mosaic type solid bitumen. Yet, temperatures from fluid inclusions may not reflect maximum temperatures, if they were trapped before or after peak

temperature.

Temperatures from low reflective solid bitumens are approximately 40-80 ° C lower than maximum burial temperatures. Using equation 1.3.5 for a burial setting (143-147 °C) instead of a hydrothermal setting (163-169 °C), the temperature difference would even increase to 60-80 °C. Therefore, low reflective solid bitumen formation is a late stage event postdating mosaic type solid bitumen formation and maximum burial.

5.2 Model for Vein Development

Results of the structural, microstructural and geochemical study show a complex, multiphase development of calcite veins from Natih outcrops. The key events affecting black impregnated vein development are shown in figure 5.1 and presented in the following.

1. Primary vein growth:

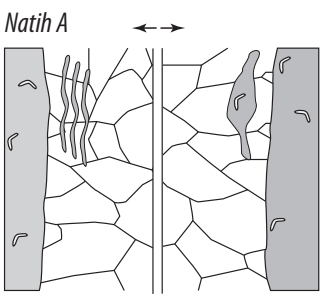
Natih A veins formed in a crack-seal mechanism (Ramsay, 1980) which is indicated by extensive host rock inclusion bands which are found in most veins. Cross-cut relationships in the field and at the micro-scale revealed that black impregnated veins from Natih A are older than all other Natih A veins they interact with.

Analysed Natih B veins are interpreted to have formed as syndepositional sediment-filled fractures, often referred as neptunian dikes. They can be identified by their sedimentary infill, host rock clasts derived from the wall and calcite cements covering the walls (Flügel, 2004). This indicates that they have opened in one increment. Neptunian dikes often form at platform margins and can be of tectonic origin (Frost and Kerans, 2009). Natih B veins are the oldest structures, because they are of synsedimentary origin. As a result they formed before hydrocarbon generation within the Natih B member. Primary solid bitumen inclusions can be identified under transmitted light by inclusion rich growth zonations (Goldstein, 2001). These growth zonations could not be identified in any vein. Thus, hydrocarbon migration along the veins during primary vein growth is not supported by the microscopy results.

2. Pressure solution:

Although having a different growth mechanism during vein opening, Natih A and B veins show a similar development. They have undergone pressure solution along bedding parallel stylolites which were clearly active after vein formation.

1. Primary vein growth

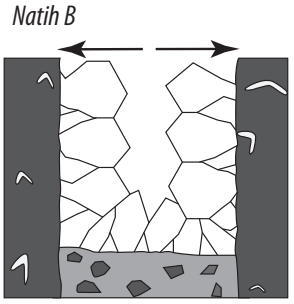


Opening and sealing of the vein in small increments indicated by host rock inclusions

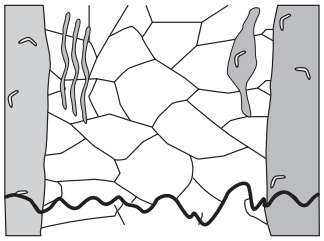
Blocky texture

Opening in one increment indicated by syn-sedimentary sediment infill

Competition of growth texture



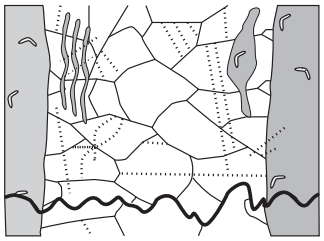
2. Pressure solution



Bedding parallel stylolites cross-cut vein-host rock interface

Natih B veins undergo steps 2-5 as Natih A veins

3. Solid bitumen trail formation in tectonic micro-cracks

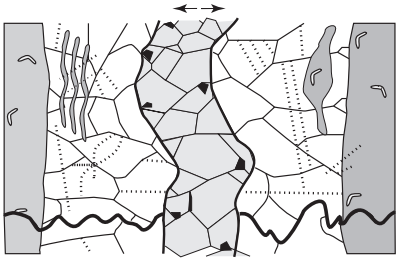


Intracrystal solid bitumen trails formed in tectonic microcracks

Solid bitumen trails may cross-cut grain boundaries, vein-host rock interface and host rock inclusions. They are curved or straight and often occur along cleavage planes in single crystals

Solid bitumen trails impregnate the calcite black

4. Mosaic solid bitumen formation in reactivations

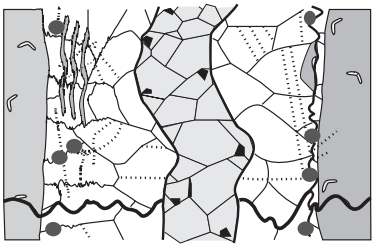


Mosaic type solid bitumen incorporation during reactivation

Reactivations appear white and are solid bitumen inclusion trail free

Stage 3 and 4 might have occurred simultaneously

5. Low reflective solid bitumen formation at solution sites



Vein parallel stylolites

Grain boundary solution indicated by serrate grain boundaries

Low reflective solid bitumen along solution structures

Legend:

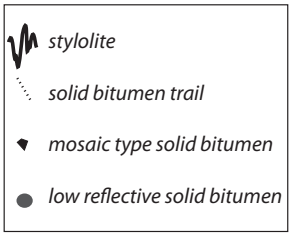


Figure 5.1: Black impregnated vein development model. 1. Primary growth of Natih A veins by a crack-seal mechanism and Natih B veins in one increment as neptunian dikes 2. Pressure solution along bedding parallel stylolites. 3. Solid bitumen trail formation due to microcracking of prior existing calcite crystals. 4. Mosaic type solid bitumen incorporation during reactivation. Step 3 and 4 might occur simultaneously. 5. Low reflective solid bitumen formation along solution structures.

Stylolites form with σ_1 perpendicular to the plane (Hancock, 1985). Therefore, σ_1 had to be perpendicular to bedding during stylolite formation. It is unclear how long bedding parallel stylolite were active, because there were no clear age relations to the following events.

3. Solid bitumen trail formation in tectonic micro-cracks:

All black impregnated veins get their colour by small solid bitumen inclusions, mostly lined up as trails. This has been shown by comparison of overview images from blocks and corresponding thin sections. Veins or calcites in veins with many solid bitumen trails appear black and veins with less trails are grey. Large trails are even visible macroscopically.

Analysing the orientation and the course of solid bitumen trails within the sample allows for conclusions on their formation processes. Solid bitumen trails cross-cut grain boundaries, fossils, dolomite-calcite interfaces host rock inclusion bands and even vein-host rock interfaces. Moreover, trails can be curved, fan out and are often found along cleavage planes of calcite. This indicates that crystals in the vein were tectonically micro-cracked which allowed for penetration of hydrocarbons forming secondary inclusions.

4. Mosaic solid bitumen formation in reactivations:

Mosaic type solid bitumen is usually found in inclusion poor calcite as particles and can be associated with white calcite reactivations. Therefore, the formation mechanism is different compared to solid bitumen trails. They may fill voids between growing crystals or are incorporated during crystal growth along reactivation margins. Within sample SV 2010 002b mosaic type solid bitumen is also found as aggregates along grain boundaries.

Mosaic type solid bitumen does not occur in the same structures as solid bitumen inclusion trails. They could have formed contemporary or after solid bitumen trails. Simultaneous formation of solid bitumen trails and mosaic type bitumen could have occurred during one event of hydrocarbon injection with solid bitumen trails filling micro cracks in existing structures and mosaic type bitumen filling voids between newly developing structures. This is supported by black halos around reactivations (sample OM12 B32 and OM12 B21). However, black halos and solid bitumen trails might have been formed before, due to an earlier solid bitumen injection.

There are also reactivations which clearly postdate the prior mentioned solid bitumen formation events. These reactivations cross-cut and separate solid bitumen trails and show little twinning. They do not contain any solid bitumen.

5. Low reflective solid bitumen formation at solution sites:

Low reflective solid bitumen formation clearly postdates all prior mentioned processes, because low reflective solid bitumen has a lower reflectance than mosaic type solid bitumen. Moreover, low reflective solid bitumen and only occurs associated with late stage solution features which even cross-cut

reactivations. These late stage solution features are often found at the interface of the vein and the host rock, between black impregnated vein and white calcite reactivation or randomly oriented along grain boundaries. Organic material is often enriched along stylolites, because it is not affected by pressure solution. This is often found in the Natih host rocks with fine solid bitumen particles being enriched along stylolites. Low reflective solid bitumen particles in veins, however, were not enriched along stylolites, because there were no solid bitumen particles found in the vein calcite. Therefore, a late stage hydrocarbon migration event occurred along stylolites and other solution features. It is very likely that this event affected other white veins and even the host rock.

5.3 Faults

The southern flank of the Jebel Akhdar anticline is cut by hundreds of normal faults striking 100 ° (Holland et al., 2009a). Black impregnated calcite of some of these faults from different stratigraphic levels and a thrust fault from Ghul ramps have been analysed. They differ from veins and could not be included into the development model.

No mosaic type solid bitumen has been found in faults and only one single solid bitumen trail was clearly identified. Moreover, the clear colour zonations often found along cleavage planes indicate a different style of solid bitumen entrapment, assuming the dark colour is derived from solid bitumen inclusions.

The staining of fault calcite can have different origins such as small host rock inclusions which were dragged into the cemented fault gouge during fault movement or authigenic clay minerals which were precipitated during calcite cementation. Residual analysis of dissolved fault calcite using SEM showed that there are pyrite, quartz and clay minerals within the cemented fault zone. Unfortunately, it is not possible to identify very small organic particles, as they might occur in fault zones, with reflected light. Therefore, the chosen methodology does not work for this type of very small inclusions. Using cathodoluminescence, many inclusions which are black under plane-polarised light, disappear and some stay black as a non-luminescent phase. It is very likely that these represent solid bitumen, because in vein samples, the identified solid bitumen was found to be non-luminescent. Applying this, some more solid bitumen inclusions arranged as trails could be identified.

Growth zonations identified with cathodoluminescence give evidence for migration of fluids with different chemical properties. Hydrocarbon migration might have occurred during a short period of fault development. Later reactivations with deformation of the calcite cemented fault core might lead to a solid bitumen dilution effect.

5.4 Kinematics of Natih A Vein Formation

Brittle fractures are subdivided into tensile fractures, hybrid or mixed mode fractures and shear fractures (fig. 5.2). Mode I dilatant opening veins form at low differential stress and lithostatic fluid pressure with σ_3 ideally developed perpendicular to the opening direction. Hybrid fractures form at slightly higher differential stress and a high fluid pressure close to lithostatic. Shear fractures which do

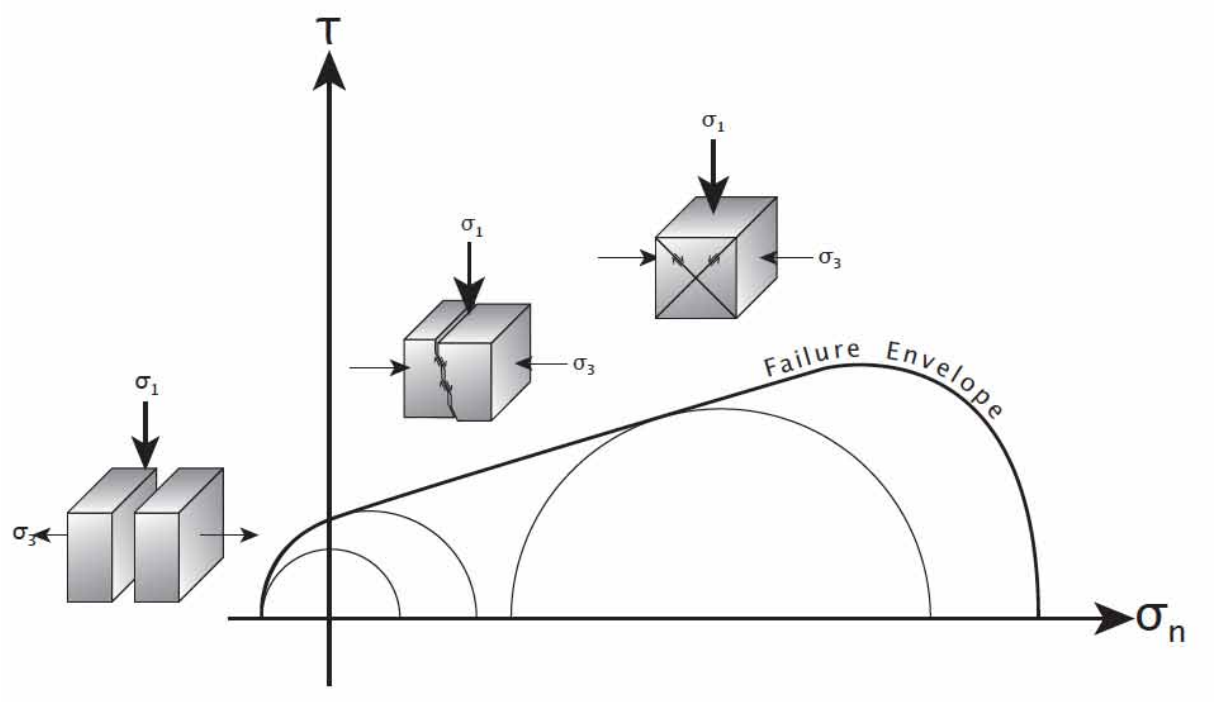


Figure 5.2: Mohr diagram illustrating stresses for extensional, hybrid and shear failure from left to right (Virgo and Arndt, 2010).

not have an opening component form at high differential stress and low fluid pressure. They develop at an angle of 20-30° to σ_1.

All black impregnated Natih A veins can be classified either as tensile or hybrid fractures. They are oriented in a steep angle to bedding, close to 90° with strike directions of veins from straight Natih A veins clustering around 115°. Therefore maximum compressive stress σ_1 is normal to bedding and minimum compressive stress σ_3 is parallel to bedding and its direction is 25°. Most en échelon veins show sinistral shear. Even some straight veins show a sinistral shear component in thin section and at the outcrop scale. Moreover, no conjugate sets of en échelon veins have been found which could be used for palaeostress analysis. Black impregnated veins are thought to have been formed in an extensional regime (σ_1 is vertical) with a sinistral slip component. This could have happened before the obduc-

tion by bending of the Arabian plate towards the newly created subduction zone (Glennie et al., 1974).

5.5 Palaeotemperatures During Regional Fracture Network Evolution

Holland et al. (2009b) identified four fracture sets. The oldest set strikes N-S and the following represent an anticlockwise rotation of 135°. This contradicts the observations made during this study. The analysed fracture set, which is the oldest set observed during field work, strikes WNW-ESE . Therefore, black impregnated veins are older than N-S striking veins or they are part of the WNW-ESE striking set (fig. 5.3) and cross-cut relationships with N-S striking veins have not been found during this study.

Mosaic type solid bitumen formation occurred by vein reactivation during later veining stages. Maturation of mosaic type solid bitumen is interpreted to have occurred locally by external hot fluids which migrated through open fractures. Fluid inclusion data of Holland et al. (2009b) from bedding parallel veins show temperatures close to maximum burial which should have occurred during thrust stacking before normal fault developement which was followed by uplift during which low reflective solid bitumen was formed.

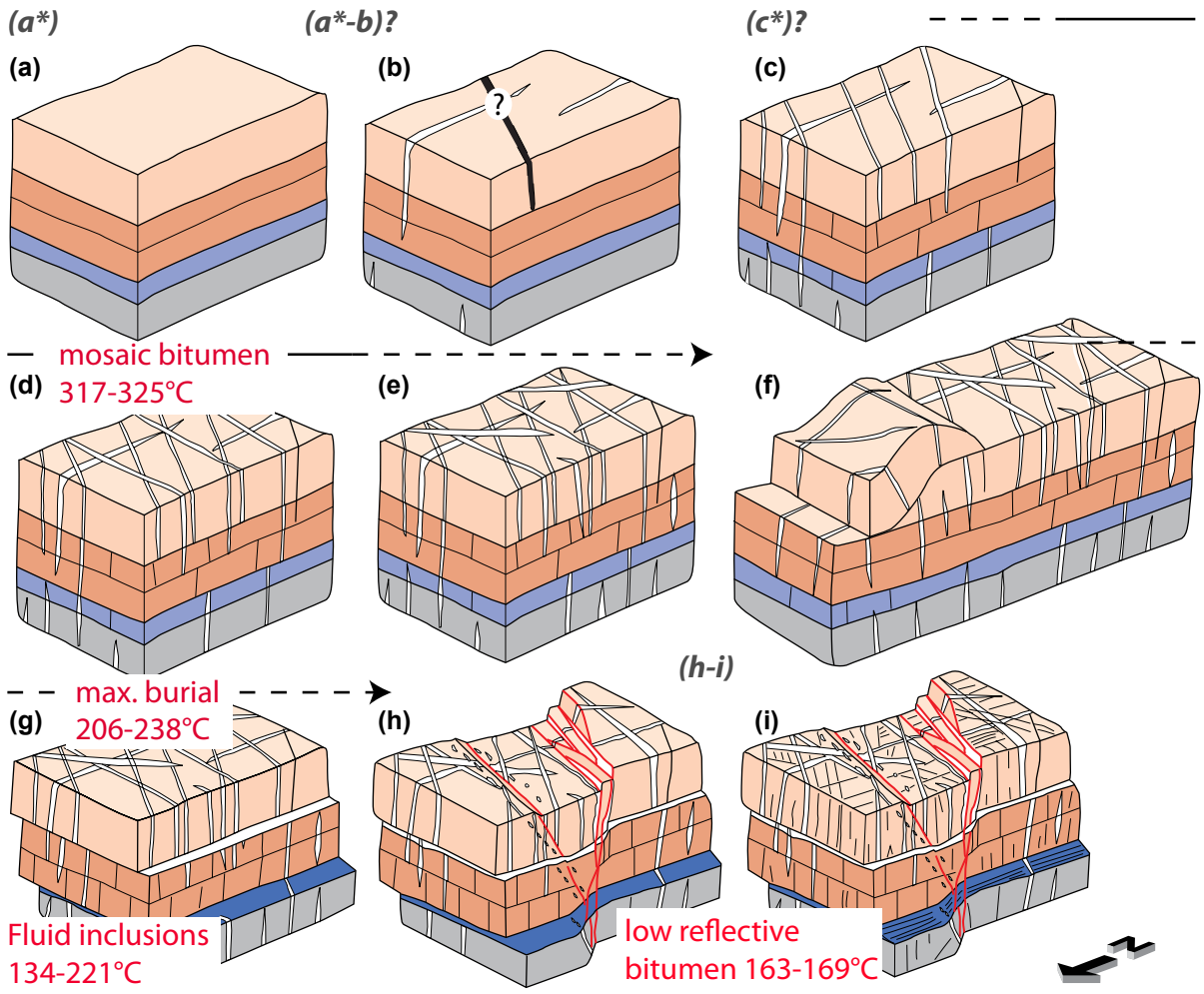


Figure 5.3: Evolution of the regional fracture network after Holland et al. (2009b) with additional information on palaeotemperatures and black impregnated vein formation (grey letters): ***(a*)*** Formation of Natih B synsedimentary veins during deposition of the carbonate rocks ***(a)***. Black impregnated Natih A veins formed either before N-S striking bedding-normal veins ***(b)*** as an independent set ***(a*-b)*** or as part of the white calcite NW-SE striking bedding-normal vein set ***(c, c*)***. Neither ***(a*)*** nor ***(c*)*** could be ruled out, because no overprinting relationships between black impregnated and N-S striking veins were found. E-W ***(d)*** and NE-SW ***(e)*** striking bedding-normal vein sets overprint black impregnated Natih A veins. Mosaic type solid bitumen formed before the ramp structures ***(f)*** and while or after vein set ***(c)***. Mosaic type bitumen was most likely maturated by external hot fluids migrating locally through open fractures of stages ***(c-e)***. Fluid inclusion data Holland et al. (2009b) from bedding parallel veins ***(g)*** show temperatures in the range of maximum burial. Normal fault development ***(h)*** was followed by uplift during which low reflective solid bitumen was formed ***(h-i)***. ***(i)*** Exhumation leads to the opening of joints. (simplified sketch, arrow points to north, not to scale).

5.6 Natih B Bedding Confined Veins

Natih B bedding confined veins which were described by Holland et al. (2009b) have a white colour and occur only in the competent Natih B layers (compare fig.1.4). They are thought to form during burial due to layer parallel extension. Moreover, they are younger than the ramp structures at Ghul ramps described by Hilgers et al. (2006), because they are bent together with the bedding. Neptunian dikes in the same competent Natih B layers which were found in close proximity to bedding confined veins are impregnated by solid bitumen. If bedding confined veins formed before hydrocarbon generation, they should be impregnated, too. Therefore, bedding confined Natih B veins are assumed to have developed after or while hydrocarbon generation.

Cracked fossils containing solid bitumen veins from sample OM12 B13 (see section 4.1.2) within the less competent more shaly Natih B layers could have formed similar to bedding confined veins by layer parallel extension. This leads to cracking and separation of the more brittle fossil fragments allowing hydrocarbons to flow into the newly formed cracks.

5.7 Hydrocarbon Migration Pathways

Secondary hydrocarbon migration (from the source rock to the reservoir rock) is a buoyancy driven process. Petroleum migration usually occurs along fractures, faults or through the pore space. Solid bitumen as a remnant of migrated hydrocarbons might give evidence of the migration pathway.

Within the Natih A solid bitumen was found in the host rock of sample SV 2010 002b as a coating of grains, but not in the calcite cement. Some examples of solid bitumen in cracks within fossils have also been found. This might give evidence for migration through the pore space. However, the solid bitumen coating could also be a residue from organic rich micritic envelops instead of a remnant of migrated hydrocarbons. Today, the carbonates have lost almost all porosity due to pressure solution with corresponding calcite cementation.

The role of faults during hydrocarbon migration stays unclear. They could act as a hydrocarbon migration pathway from Natih E or Shuiba source rocks which would extend the system vertically.

Secondary solid bitumen trails in non-reactivated veins indicate that hydrocarbons migrated into or along micro-cracks. Micro-cracks may form before failure of the vein which is then cemented as a white calcite reactivation. Hydrocarbon migration along the reactivation may lead to the invasion of the prior formed micro-cracks. This is not supported for Natih B neptunian dikes, because most secondary solid bitumen trails are oriented bedding parallel, indicating an impregnation from the surrounding producing Natih B source rocks. Bedding parallel veins are common in source rocks with high fluid overpressures (Parnell et al., 2000). Stylolites and solution structures form hydrocarbon migration

pathways as shown in section 5.2. Fluid flow along stylolites should be preferred after rotation of σ_1, because this releases stress from the stylolite's plane. The maturity of low reflective solid bitumen is lower than the maturity of the Natih B source rock. Therefore, it is very unlikely that low reflective solid bitumen originates from any source rock in the Jebel Akhdar. Late stage lateral migration, during uplift of the Oman mountains in the Tertiary, from the active Natih oil kitchen located approximately 50 km SW (Terken, 1999) could explain the occurrence of low reflective solid bitumen in the Jebel Akhdar.

In summary, hydrocarbon migration from the Natih B source rock through the Natih A is interpreted to have taken place within reactivations induced by later veining stages. Migration through the pore space of the Natih A is assumed to have played a minor role, because early stage pressure solution with corresponding calcite cementation should have reduced porosity and permeability during burial. During uplift of the Jebel Akhdar, hydrocarbon migration occurred along stylolites and solution sites. Stylolites and solution sites can be found in any structure, therefore, late stage hydrocarbon migration is assumed to have affected the whole Natih A member.

5.8 Outlook

This is the first overview study on solid bitumen in calcite veins in the Oman Mountains. Therefore, it is far from being complete and is seen as preliminary.

More work is required to test and develop the presented model of vein development. This can be done by fluid inclusion studies. They give information on formation temperatures of the impregnated and reactivated parts of the veins which is helpful to understand the role of vein reactivations during hydrocarbon migration in the Natih. The same could be applied for fault samples.

The natural "staining" of the veins makes reactivation structures visible. This can be used to study vein growth and cracking mechanism in the vein.

Working with solid bitumen in calcite veins, it is very helpful to make overview images of the polished block during thin section preparation before gluing the sample on the object slide. With this, it is possible to make exact overlays of the block and the thin section micrographs. This should be applied in the future during thin section preparation. Thus, it might be possible to study fracture mechanisms and cementation of existing veins. Sample SV2010 002 b for example contains angular black impregnated calcite fragments within the white reactivation which might be caused by shearing. However, without precise overlays, it is difficult to map them.

Folk (1987) introduced a method using a white card to detect organic matter in carbonate rocks. This can be applied in the future to map secondary inclusion trails, because other disturbing features

such as twins, aqueous fluid inclusions and grain boundaries almost disappear. Transmitted light overview images which were made during this study with an ordinary photo-scanner are similar to Folk's method. However, the resolution is not sufficient.

It is also possible to make automated reflected light overview images under immersion oil at the LEK. This is usually applied for coal and shale blocks, but it might work for carbonate thin section, as well.

More field work should be done to understand the spatial distribution of black impregnated veins and their relationships to faults, reactivations, sedimentary layers etc. The field work focused on Natih A/B outcrops. The overlaying Muti formation and underlaying Natih members and Shuiba formation might as well contain solid bitumen in calcite veins.

The presented work gives an idea of white veins possibly playing an important role during hydrocarbon migration. Therefore, veins reactivating black impregnated veins should be sampled to better understand relative timing of hydrocarbon migration. Moreover, Natih B bedding confined veins could also have acted as pathways connecting shaly layers within the source rock interval and, therefore, may contain solid bitumen. This should be tested with reflected light.

The hypothesis that low reflective solid bitumen formation is not restricted to black impregnated veins should be tested by analysing white Natih A veins or other structures with reflected light.

Chapter 6

Conclusions

- Calcite veins which contain solid bitumen can be found in various Natih outcrops at the southern flank of the Al Jabal al Akhdar anticline.
- Highly polished thin sections, which were prepared for reflected and transmitted light microscopy simultaneously, allow for the identification of solid bitumen types while studying their microstructural relationships. This is a powerful tool which can be applied in other organo-microstructural studies.
- The Natih B source rock interval is classified as thermally overmature with maximum burial temperatures of 206 - 238 °C. Therefore, it has passed the oil window and is the most likely source of solid bitumen.
- Black impregnated Natih A veins formed before white Natih A veins. Moreover, black impregnated Natih B veins formed synsedimentary as neptunian dikes. Solid bitumen inclusion trails which impregnate veins black formed after vein growth due to migration of hydrocarbons into micro-cracks.
- Mosaic type solid bitumen gives evidence for a hydrothermal event overprinting black impregnated veins with temperatures of 317 - 325 °C.
- Hydrocarbon migration along solution structures occurred as the latest event after maximum burial. This may affect the whole Natih sequence and is a highly underestimated fluid migration pathway. It is most likely, that migration happened during uplift of the Oman mountains in the late Tertiary from producing Natih source rocks in the foreland basin.
- Faults do not contain mosaic type solid bitumen, but might contain very small solid bitumen inclusions. Their role as hydrocarbon pathways stays unclear.

Acknowledgements

Janos L. Urai is sincerely thanked for supervising this thesis. He launched this thesis in a short-term decision and within a single week I was on the plane to the Oman Mountains. The thesis greatly benefited from his ideas and review.

Ralf Littke co-supervised this thesis. He is thanked for lending me two expensive oil objectives, letting me use the equipment at the LEK and his interest, especially during solid bitumen classification.

Special thanks go to Simon Virgo. He is the one who first thought about hydrocarbon migration in the Jebel Akhdar and started this project. We went together to the field trip in Oman. There, he guided me and I benefited from his geological and his great knowledge of the area. Moreover, I thank him for his help during fruitful discussions and corrections.

Max Arndt is thanked for his great support and the planning of the field trip together with Alexander Raith. His great interest and suggestions during discussions at al stages of the thesis highly improved this work.

Werner Kraus and Donka Macherey are acknowledged for preparation of thin sections and polished blocks and for helping me developing the polishing of thin sections.

For the spontaneous XRD measurement and the discussion on the synsedimentary formation of Natih B veins, thanks go to Lars Reuning. Uwe Wollenberg is thanked for coating samples and Ben Laurich for his help during SEM residual analysis.

Bibliography

Barker, C., Pawlewicz, M., 1994. Calculation of vitrinite reflectance from thermal histories and peak temperatures. A comparison of methods. In: Mukhopadhyay, P.K., Dow, W.G. (Eds.), Vitrinite reflectance as a maturity parameter: applications and limitations. ACS Symposium series 570 , 216–229.

Beurrier, M., Bechennec, F., Rabu, R., Hutin, G., 1986. Geological map of Rustaq, Sheet NF 40-3D, Geological map of Oman (1:100 000). Oman MInistry of Petroleum and Minerals, Directorate General of Minerals .

Breton, J.P., Béchennec, B., Le Métour, J., Moen-Maurel, L., Razin, P., 2004. Eoalpine (Cretaceous) evolution of the Oman Tethyan continental margin : insights from a structural field study in Jabal Akhdar (Oman Mountains). Geoarabia 9, 41–58.

van Buchem, F.S.P., Eschard, R., Desaubliaux, G.M.J., Razin, P., Platel, J.P., Roger, J., Homewood, P.W., Boisseau, T., Leduc, J.P., Labourdette, R., Cantaloube, S., Philip, J.M., Eberli, G.P., 1996. High resolution sequence stratigraphy of the Natih formation (Cenomanian/Turonian) in northern Oman: distribution of source rocks and reservoir facies. GeoArabia 1, 65–91.

van Buchem, F.S.P., Razin, P., Homewood, P.W., Oterdoom, W.H., Philip, J., 2002. Stratigraphic organization of carbonate ramps and organic-rich Intrashelf basins: Natih formation (Middle Cretaceous) of northern Oman. AAPG Bulletin 86, 21–53.

Clarke, M.H., 1988. Stratigraphy and rock unit nomenclature in the oil-producing area of interior Oman. Journal of Petroleum Geology 11, 5–60.

Droste, H., 2010. High-resolution seismic stratigraphy of the Shu'aiba and Natih formations in the Sultanate of Oman: implications for Cretaceous epeiric carbonate platform systems. Geological Society, London, Special Publications 329, 145–162.

Espitalié, J., La Porte, J., Madec, M., Marquis, F., Le Plat, P., Paulet, J., Boutefeu, A., 1977. Rapid method for source rocks characterization and for determination of petroleum potential and degree

of evolution. Oil and Gas Science and Technology - Revue de l'Institute Francais du Pétrole 32, 23–42.

Filbrandt, J.B., Al-Dhahab, S., Al-Habsy, A., Harris, K., Keating, J., Al-Mahruqi, S., Ozkaya, S.I., Richard, P.D., Robertson, T., 2006. Kinematic interpretation and structural evolution of North Oman , Block 6 , since the Late Cretaceous and implications for timing of hydrocarbon migration into Cretaceous reservoirs. GeoArabia 11, 97–115.

Flügel, E., 2004. Microfacies of Carbonate Rocks. Springer, Berlin.

Folk, R.L., 1987. Detection of organic matter in thin-sections of carbonate rocks using a white card. Sedimentary Geology 54, 193–200.

Frost, E.L., Kerans, C., 2009. Platform-margin trajectory as a control on syndepositional fracture patterns, Canning Basin, Western Australia. Journal of Sedimentary Research 79, 44–55.

Glennie, K.W., Boeuf, M., Clark, M., Moody-Stuart, M., Pilaar, W., Reinhardt, B.M., 1974. Geology of the Oman Mountains. volume 31. Verhandelingen Koninklijk Nederlands Geologie en Mijnbouw Genootschap.

Goldstein, R.H., 2001. Fluid inclusions in sedimentary and diagenetic systems. Lithos 55, 159–193.

Gomez-Riveras, E., Bons, B.D., Koehn, D., Urai, J.L., Arndt, M., Virgo, S., Laurich, B., Zeeb, L., Blum, P., unpuplished. The Jabal Akhdar Dome in the Oman Mountains: a case study of a highly tectonized and overpressured dynamic system. In preparation.

Goodarzi, F., Eckstrand, O., Snowdon, L., Williamson, B., Stasiuk, L.D., 1992. Thermal metamorphism of bitumen in archean rocks by ultramafic volcanic flows. International Journal of Coal Geology 20, 165–178.

Grélaud, C., Razin, P., Homewood, P.W., Schwab, A.M., 2006. Development of incisions on a periodically emergent carbonate platform (Natih formation, Late Cretaceous, Oman). Journal of Sedimentary Research 76, 647–669.

Hancock, P.L., 1985. Brittle microtectonics: principles and practice. Journal of Structural Geology 7, 437–457.

Hilgers, C., Kirschner, D.L., Breton, J.P., Urai, J.L., 2006. Fracture sealing and fluid overpressures in limestones of the Jabal Akhdar dome, Oman mountains. Geofluids 6, 168–184.

Holland, M., Saxena, N., Urai, J.L., 2009a. Evolution of fractures in a highly dynamic thermal, hydraulic, and mechanical system - (II) Remote sensing fracture analysis, Jabal Shams, Oman Mountains. GeoArabia 14, 163–194.

Holland, M., Urai, J.L., 2010. Evolution of anastomosing crack-seal vein networks in limestones: Insight from an exhumed high-pressure cell, Jabal Shams, Oman Mountains. Journal of Structural Geology 32, 1279–1290.

Holland, M., Urai, J.L., Muchez, P., Willemse, E.J.M., 2009b. Evolution of fractures in a highly dynamic thermal, hydraulic, and mechanical system - (I) Field observations in Mesozoic carbonates, Jabal Shams, Oman Mountains. GeoArabia 14, 57–110.

Homewood, P., Razin, P., Grélaud, C., Droste, H., Vahrenkamp, V., Mettraux, M., Mattner, J., 2008. Outcrop sedimentology of the Natih Formation, northern Oman: A field guide to selected outcrops in the Adam Foothills and Al Jabal al Akhdar areas. GeoArabia 13, 39–120.

Hwang, R., Teerman, S., Carlson, R., 1998. Geochemical comparison of reservoir solid bitumens with diverse origins. Organic Geochemistry 29, 505–517.

Jacob, H., 1989. Classification, structure, genesis and practical importance of natural solid oil bitumen ("migrabitumen"). International Journal of Coal Geology 11, 65–79.

Khavari-Khorosani, G., Murchison, D.G., 1978. Thermally metamorphosed bitumen from Windy Knoll, Derbyshire, England. Chemical Geology 22, 91 – 105.

Landis, C.R., Castaño, J.R., 1995. Maturation and bulk chemical properties of a suite of solid hydrocarbons. Organic Geochemistry 22, 137–149.

Littke, R., Urai, J.L., Uffmann, A.K., Risvanis, F., 2012. Reflectance of dispersed vitrinite in Palaeozoic rocks with and without cleavage: Implications for burial and thermal history modeling in the Devonian of Rursee area, northern Rhenish Massif, Germany. International Journal of Coal Geology 89, 41 – 50.

Loosveld, R.J., Bell, A., Terken, J.J., 1996. The tectonic evolution of interior Oman. GeoArabia 1, 18–51.

Parnell, J., Honghan, C., Middleton, D., Haggan, T., Carey, P., 2000. Significance of fibrous mineral veins in hydrocarbon migration: fluid inclusion studies. Journal of Geochemical Exploration 69-70, 623–627.

Ramsay, J.G., 1980. The crack-seal mechanism of rock deformation. Nature 284, 135–139.

Reuning, L., 2012. Personal communication .

Robertson, A., 1987. The transition from a passive margin to an Upper Cretaceous foreland basin related to ophiolite emplacement in the Oman Mountains. Geological Society of America Bulletin 99, 633–653.

Schoenherr, J., Littke, R., Urai, J.L., Kukla, P.A., Rawahi, Z., 2007. Polyphase thermal evolution in the Infra-Cambrian Ara Group (South Oman Salt Basin) as deduced by maturity of solid reservoir bitumen. Organic Geochemistry 38, 1293 – 1318.

Searle, M.P., 2007. Structural geometry, style and timing of deformation in the Hawasina Window, Al Jabal al Akhdar and Saih Hatat culminations, Oman Mountains. GeoArabia 12, 99–130.

Terken, J.M.J., 1999. The Natih petroleum system of North Oman. Geoarabia 4, 157–180.

Terken, J.M.J., Frewin, N.L., Indrelid, S.L., 2001. Petroleum systems of Oman: charge timing and risks. AAPG Bulletin 85, 1817–1845.

Virgo, S., 2012. Personal communication .

Virgo, S., Arndt, M., 2010. Evolution of a crack-seal calcite vein network in limestone: a high resoluti on structural, microstructural and geochemical study from the Jebel Akhdar high pressure cell, Oman Mountains. Diplomarbeit, RWTH Aachen .

Virgo, S., Arndt, M., Sobisch, Z., Urai, J.L., unpuplished. Development of fault and vein networks in a carbonate sequence near Hayl al Shaz, Oman Mountains .

Appendix

Table .0.1: List of samples

Description: *fa* fault; *hr* host rock; *svA* straight vein Natih A; *svB* straight vein Natih B; *ee(s;d)* en echelon array of veins (sinistrale; dextrale); *sig* sigmoidal vein. Sample SV2010 002 was sampled in 2010.

Sample	Position 40Q			Description
	East	*North*	*Locality*	
OM12 B01	0518475	2560988	Wadi Ghul	svA
OM12 B02	0522725	2560284	Ghul ramps	fa
OM12 B03	0514747	2565679	Al Raheba	ee(s)
OM12 B04	0514747	2565679	Al Raheba	ee(s)
OM12 B05	0514747	2565679	Al Raheba	ee(s)
OM12 B06	0521277	2560369	Wadi Nakrh	fa
OM12 B07	0521277	2560369	Wadi Nakrh	fa
OM12 B08	0521277	2560369	Wadi Nakrh	fa
OM12 B09	0521277	2560369	Wadi Nakrh	fa
OM12 B10	0521277	2560369	Wadi Nakrh	fa
OM12 B11	0521277	2560369	Wadi Nakrh	hr
OM12 B12	0521277	2560369	Wadi Nakrh	hr
OM12 B13	0521277	2560369	Wadi Nakrh	hr
OM12 B14	0514821	2565991	Al Raheba	ee(s)
OM12 B15	0522563	2559951	Ghul ramps	svB
OM12 B16	0522725	2560284	Ghul ramps	fa
OM12 B17	0522536	2559960	Ghul ramps	svB
OM12 B18	0522536	2559960	Ghul ramps	svB
OM12 B19	0522536	2559960	Ghul ramps	svB
OM12 B20 N	0522536	2559960	Ghul ramps	svB
OM12 B20 S	0522536	2559960	Ghul ramps	svB
OM12 B21	0522525	2559914	Ghul ramps	svB
OM12 B22	0522525	2559914	Ghul ramps	svB
OM12 B23	0518921	2560780	Wadi Ghul	svA
OM12 B24	0518921	2560780	Wadi Ghul	svA
OM12 B25 N	0518928	2560834	Wadi Ghul	ee(d)

OM12 B25 S	0518928	2560834	Wadi Ghul	ee(d)
OM12 B26	0521277	2560369	Wadi Nakrh	fa
OM12 B27	0521277	2560369	Wadi Nakrh	fa
OM12 B28	0521215	2560289	Wadi Nakrh	fa
OM12 B29	0518611	2560854	Wadi Ghul	svA
OM12 B30 N	0518548	2560891	Wadi Ghul	svA
OM12 B30 S	0518548	2560891	Wadi Ghul	svA
OM12 B31	0518450	2560921	Wadi Ghul	svA
OM12 B32	0518479	1560997	Wadi Ghul	ee(s)
OM12 B33	0518478	2561024	Wadi Ghul	ee(s)
OM12 B34	0518476	2561043	Wadi Ghul	ee(s)
OM12 B35 N	0518543	2561031	Wadi Ghul	svA
OM12 B35 S	0518543	2561031	Wadi Ghul	sig
OM12 B36	0514818	2565876	Al Raheba	ee(s)
OM12 B37	0514821	2565878	Al Raheba	ee(s)
OM12 B38	0522725	2560284	Ghul ramps	fa
OM12 B39	0521783	2566156	Wadi Nakrh	fa
OM12 B40	0527517	2562496	Hayl Al Shaz	fa
OM12 B41 A	0522558	2559955	Ghul ramps	svB
OM12 B41 B	0522558	2559955	Ghul ramps	hr
SV2010 002	0518456	2561021	Ghul ramps	svA

Table .0.2: List of thin sections

Description: *fa* fault; *hr* host rock; *svA* straight vein Natih A; *svB* straight vein Natih B; *ee(s;d)* en echelon array of veins (sinistrale; dextrale); *sig* sigmoidal vein.

Sample	GED-number	Location	Description
OM12 B09	2057	Wadi Nakrh	fa
OM12 B28	2156	Wadi Nakrh	fa
OM12 B13	2152	Wadi Nakrh	hr
OM12 B41 B	2120	Ghul ramps	hr
OM12 B15	2058	Ghul ramps	svB
OM12 B19	2059	Ghul ramps	svB
OM12 B21	2119	Ghul ramps	svB
OM12 B21 b	2155	Ghul ramps	svB
OM12 B23	2154	Wadi Ghul	svA
SV 002b	0993	Wadi Ghul	svA
SV-2010-02	2114	Wadi Ghul	svA
OM12 B30 S	2062	Wadi Ghul	svA
OM12 B30 S b	2153	Wadi Ghul	svA
OM12 B35 N	2063	Wadi Ghul	svA
OM12 B31	2064	Wadi Ghul	svA
OM12 B29	2118	Wadi Ghul	svA
OM12 B01	2115	Wadi Ghul	ee(s)
OM12 B03	2157	Al Raheba	ee(s)
OM12 B04	2060	Al Raheba	ee(s)
OM12 B37	2158	Al Raheba	ee(s)
OM12 B32	2061	Wadi Ghul	ee(s)
OM12 B14	2116	Al Raheba	ee(s)
OM12 B25 N	2117	Wadi Ghul	ee(d)
OM12 B35 S	2159	Wadi Ghul	sig
OM12 B35 S b	2160	Wadi Ghul	sig

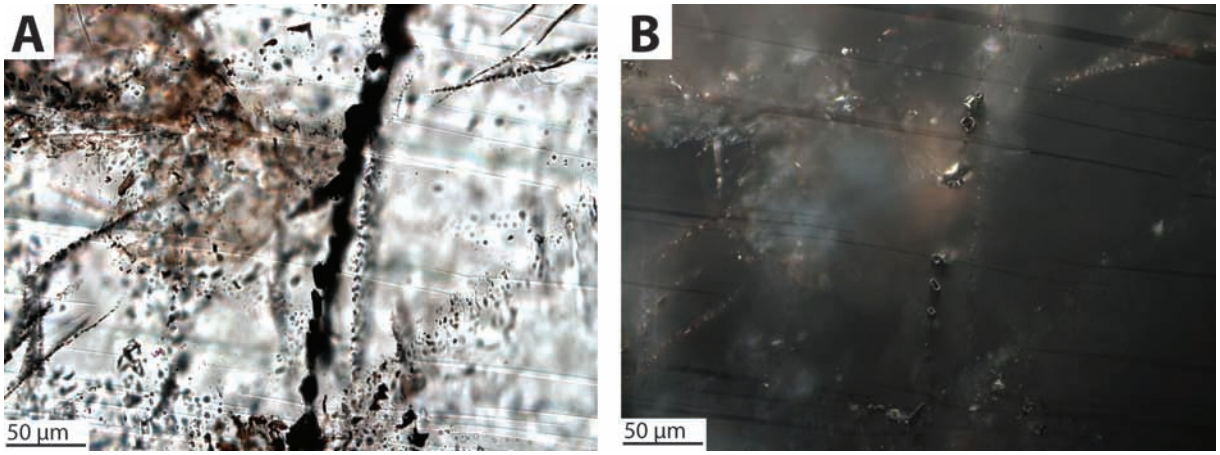


Figure 1: Micrographs of thin section SV 2010 002b showing the same section in transmitted, plane-polarised light (A) and reflected light under immersion oil (B). ***A*:** Intracrystal solid bitumen inclusion trail running perpendicular to cleavage planes. ***B*:** Single inclusions have a solid bitumen rim with a negative crystal shape.

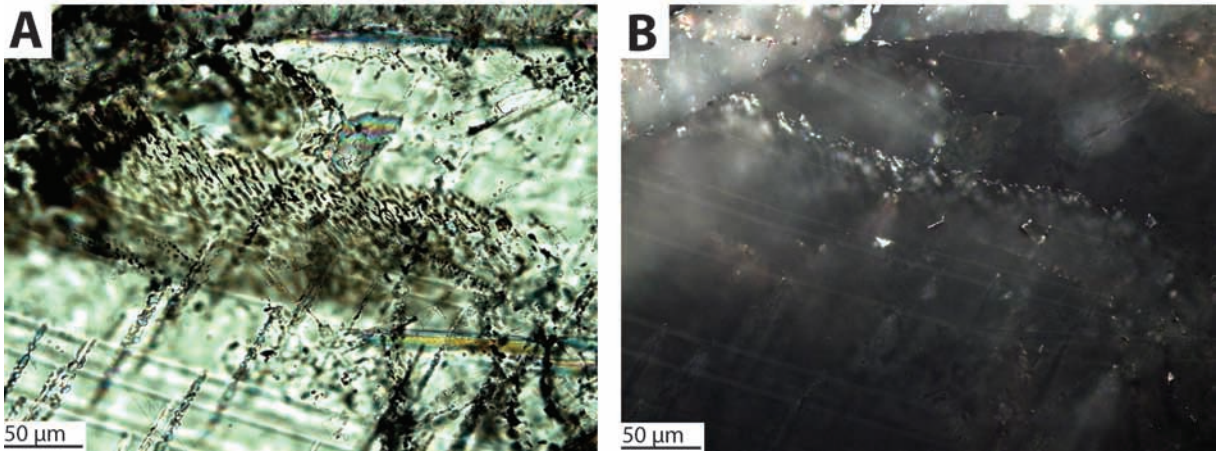
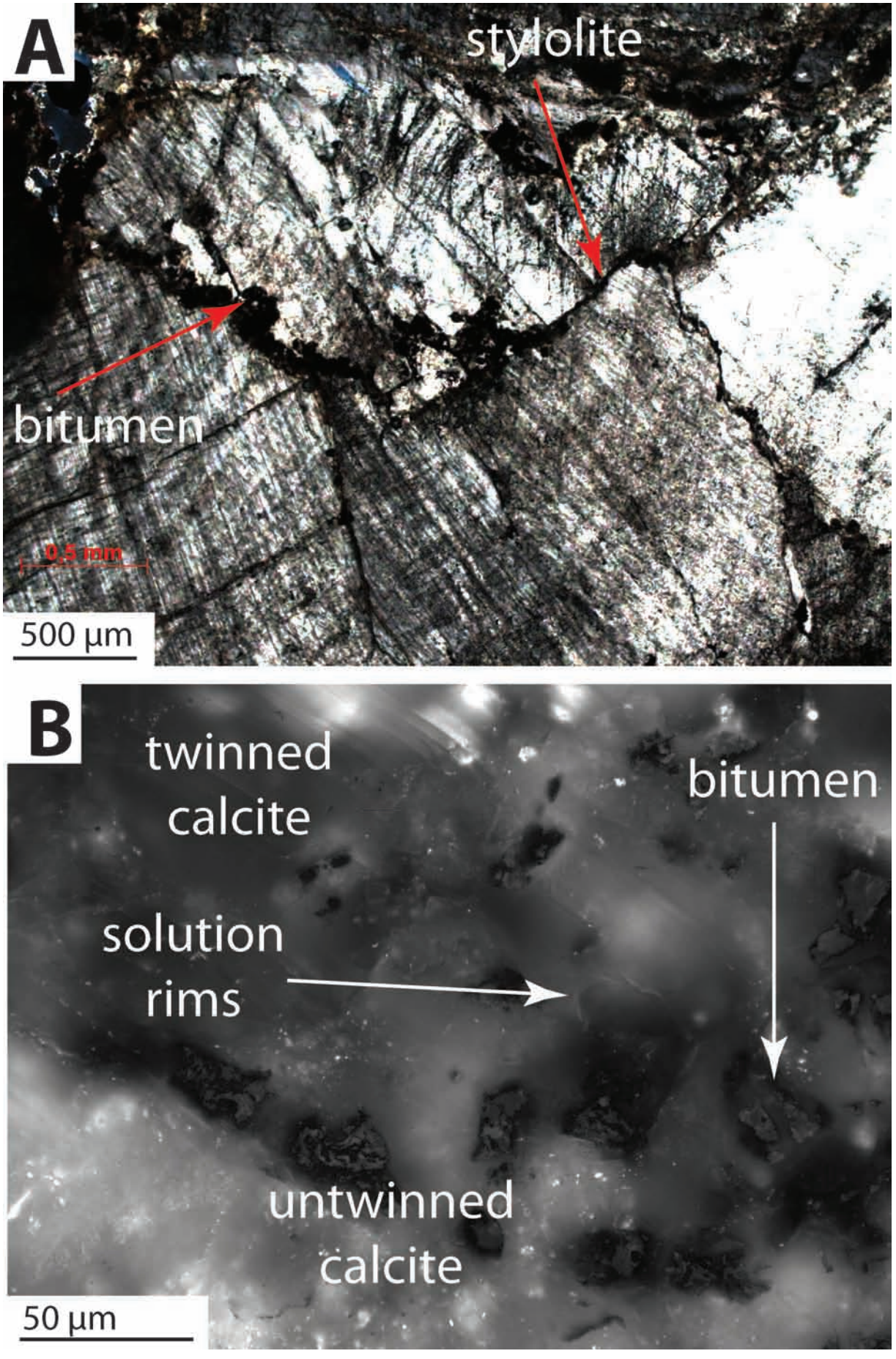


Figure 2: Micrographs of thin section SV 2010 002b showing the same section in transmitted, plane-polarised light (A) and reflected light under immersion oil (B). ***A*:** Crack on cleavage plane filled by brown solid bitumen inclusions with a worm-like shape. ***B*:** Inclusions are visible as elongated bright shining lines.

Figure 3 ***(facing page)*:** Microphotographs showing low reflective solid bitumen along stylolite with transmitted, plane-polarised light (A) and reflected light under immersion oil (B). Sample OM 12 B30 S. ***A*:** Stylolite forms boundary between twinned calcite crystal. Along the stylolite occur low reflective solid bitumen particles. ***B*:** Solid bitumen particles are only incorporated in untwinned calcite. The structure shows solution features. The boundary between twinned and untwinned calcite is wavy.


A
stylolite
bitumen
0.5 mm
500 µm
B
twinned
calcite
bitumen
solution
rims
untwinned
calcite
50 µm

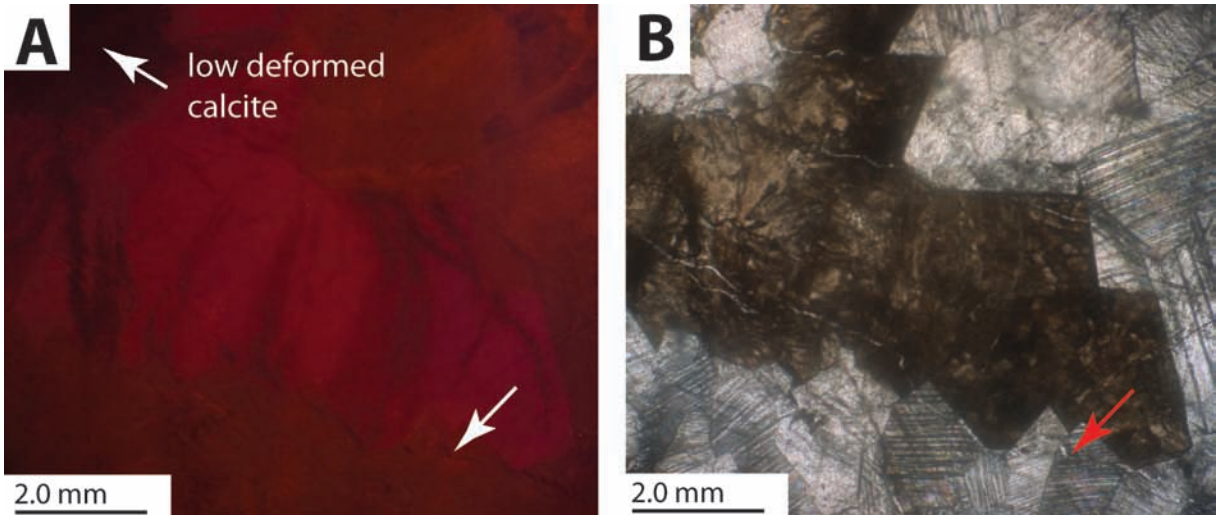
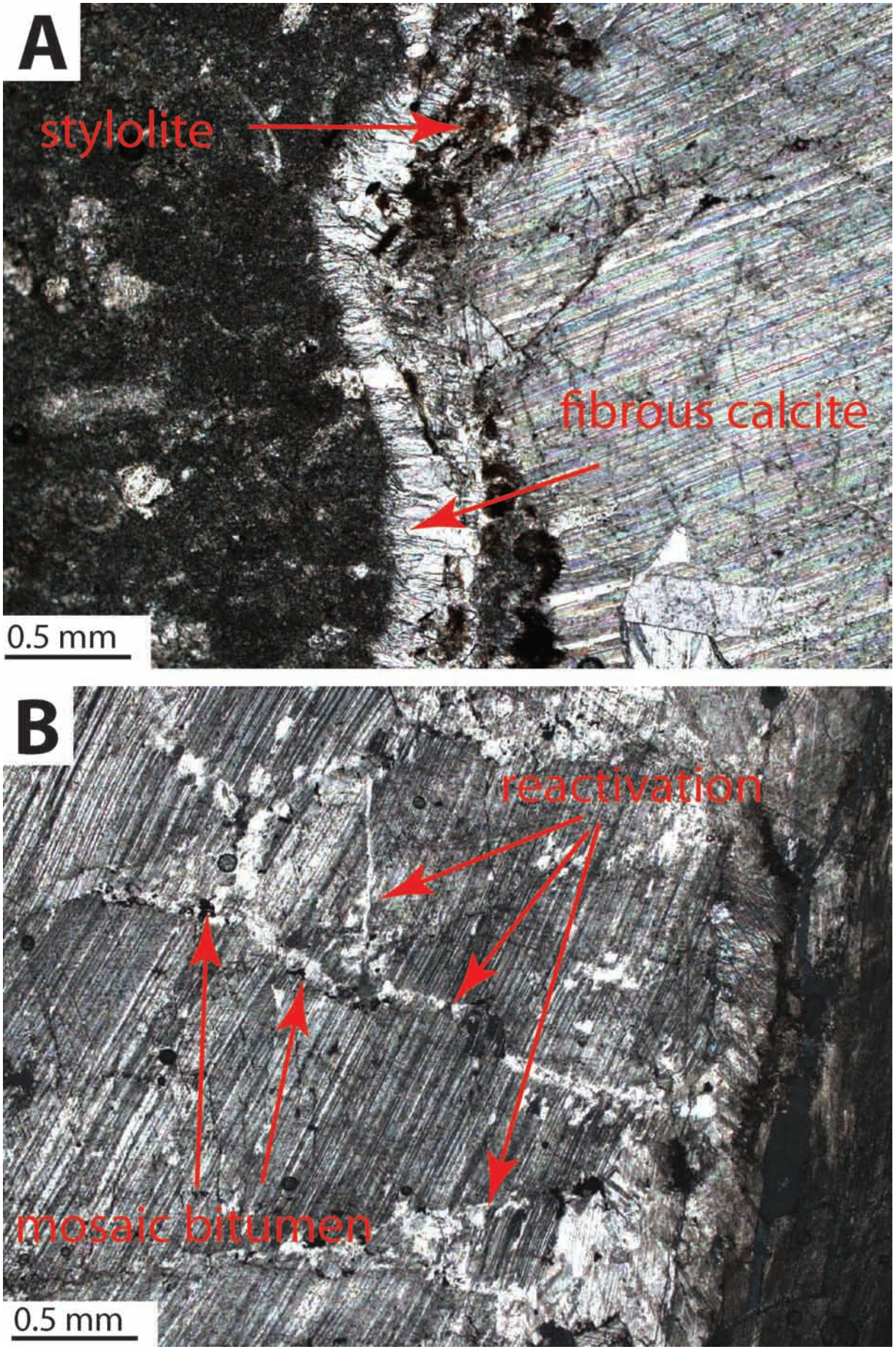


Figure 4: Micrographs of the same section from thin section OM12 B21 b with cathodoluminescences (***A***) and transmitted, plane-polarised light (***B***). Dolomite has a pink luminescence colour. Low deformed calcite within the dolomite (position of mosaic type solid bitumen) is non luminescent as well as microrovein reactivations (younger than dolomite) which are indicated with white and red arrows.

Figure 5 ***(facing page)*****:** Mirophotographs of sample OM12 B30 S b. ***A*****:** Stylolite at the vein margin with fibrous calcite crystals arranged as a band running subparallel to it. Transmitted, plane-polarised light. ***B*****:** Reactivations, which contain mosaic type solid bitumen, run through calcite crystals within the black impregnated area. Transmitted, crossed-polarised light.


A
stylolite
fibrous calcite
0.5 mm
B
reactivation
mosaic bitumen
0.5 mm

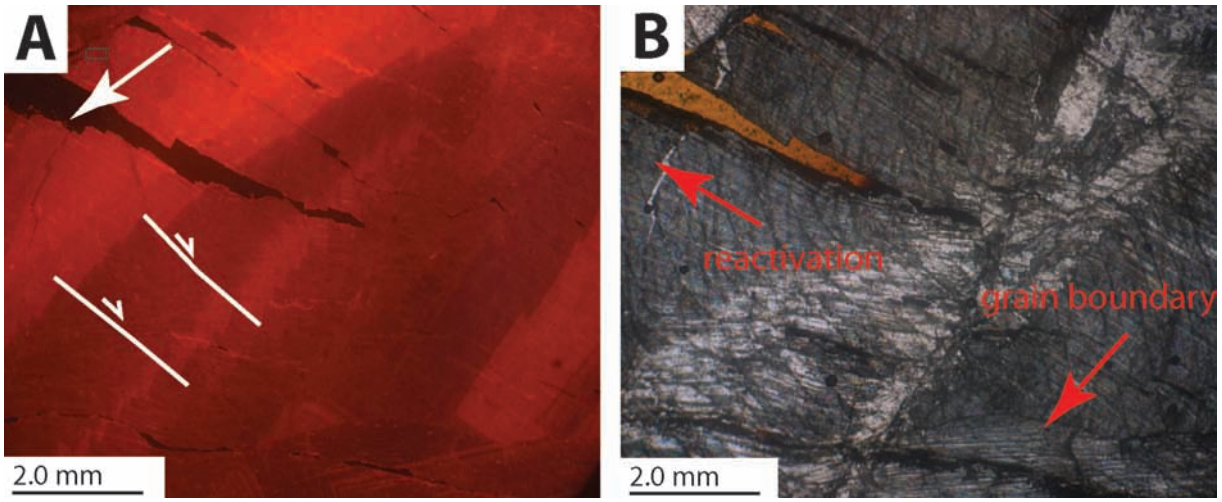
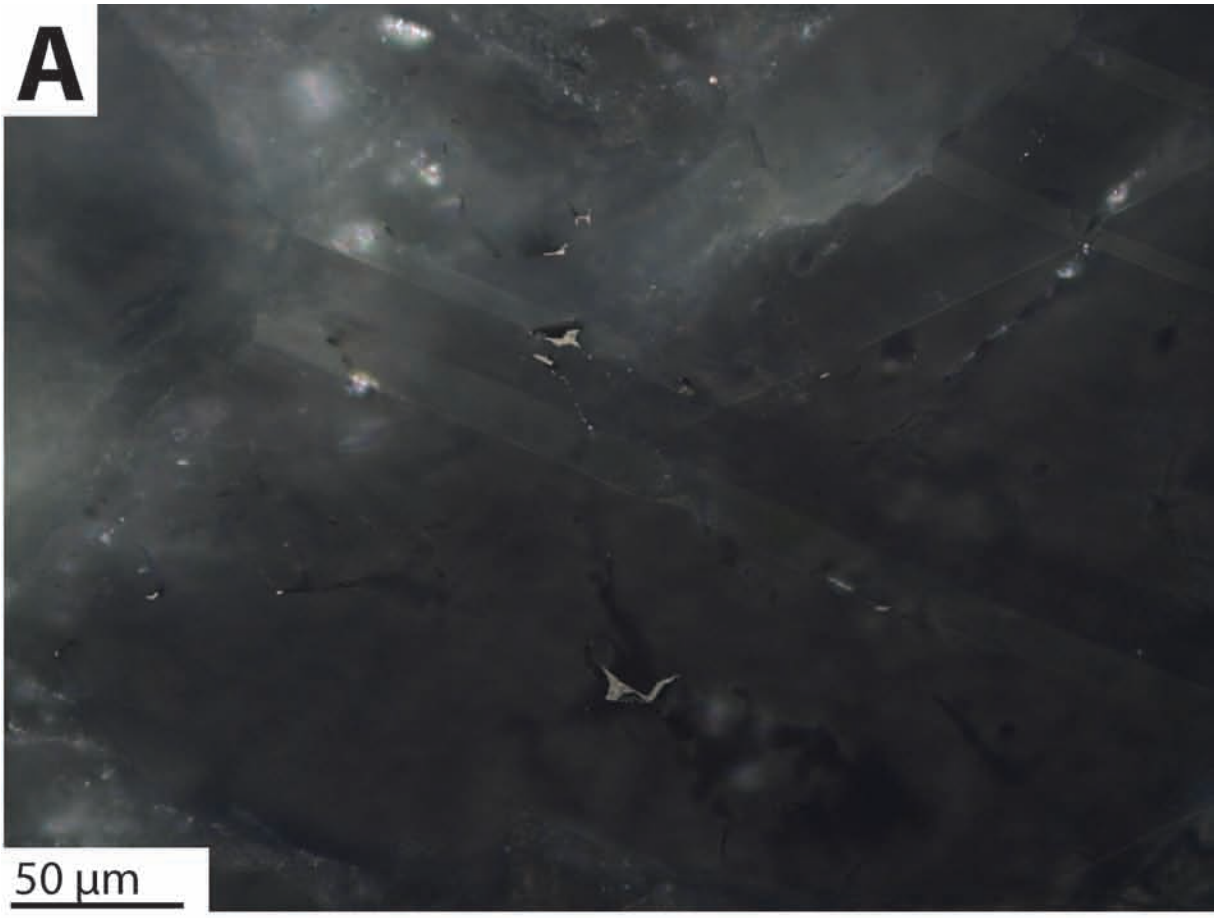
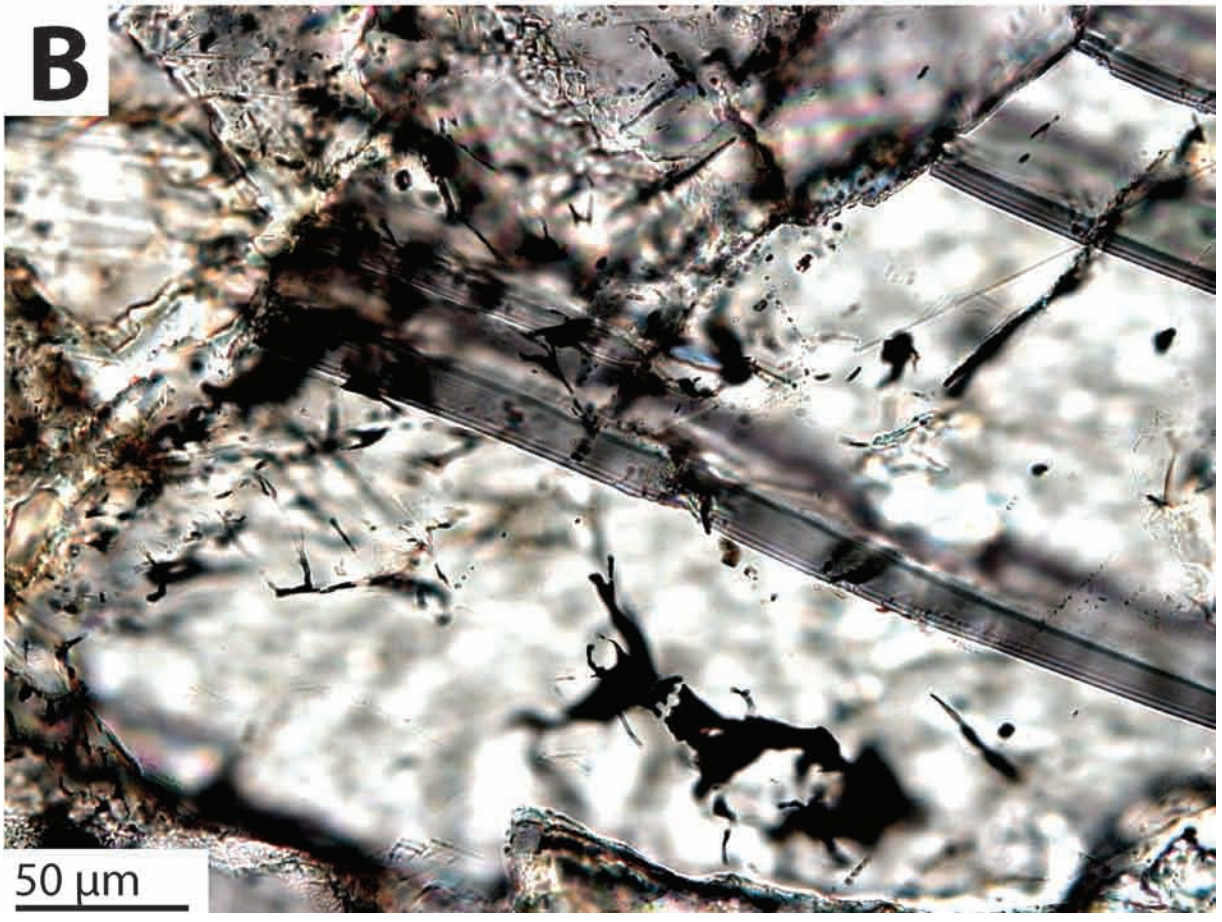


Figure 6: Micrographs of the same section from thin section OM12 B28 with cathodoluminescences (***A***) and transmitted, plane-polarised light (***B***). Deformation of crystals can be identified by slip oblique to growth zonations. White arrow indicates hole. Microvein reactivation indicated by red arrow is non-luminescent.

Figure 7 ***(facing page)*****:** Micrographs of thin section OM12 B35 S b showing the same section in transmitted, plane-polarised light (***A***) and reflected light under immersion oil (***B***). Mosaic type bitumen particles having a wing like shape within a calcite crystal.


A
50 µm


B
50 µm

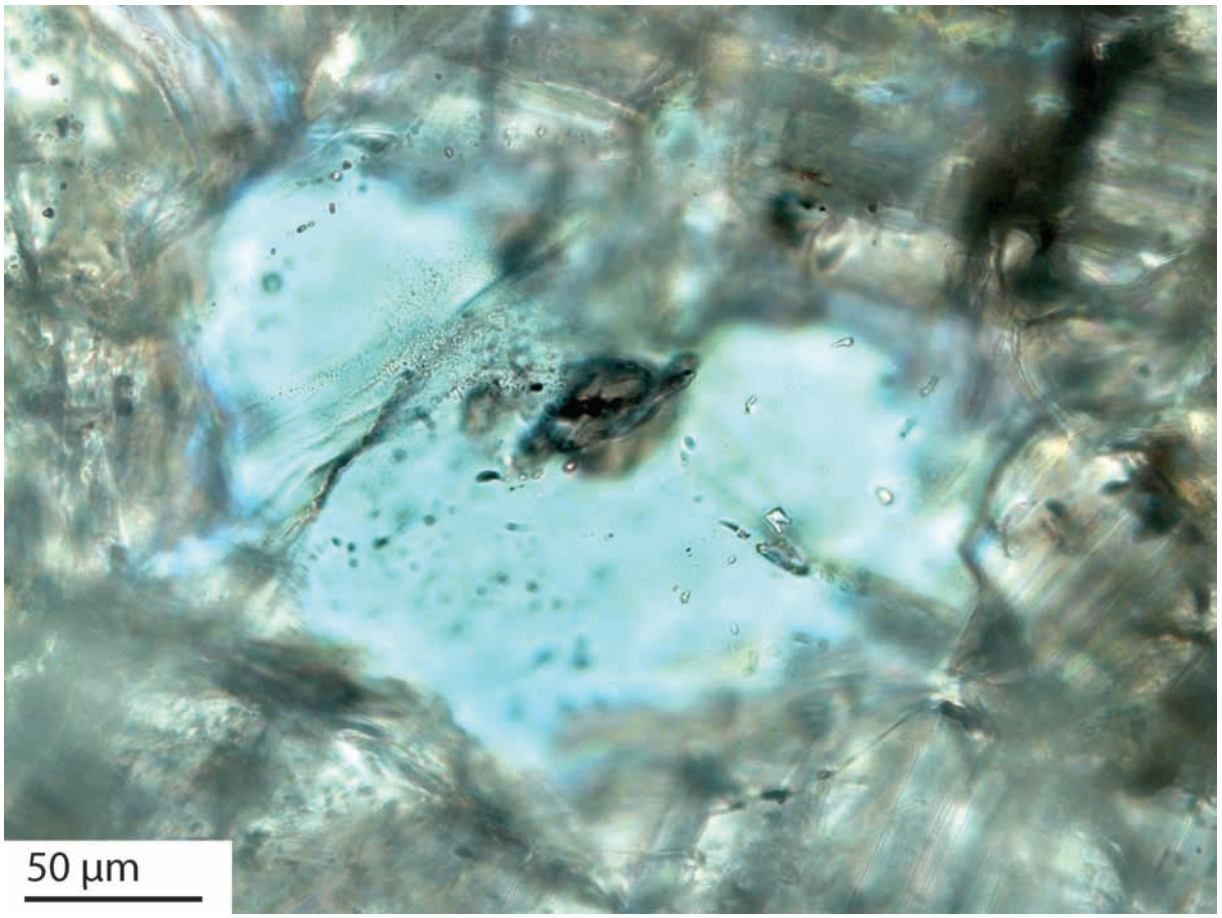


Figure 8: Mirophotograph of sample OM12 B32. Quartz crystal with solid bitumen inclusion. Transmitted, plane-polarised light.